THE PATTERNS OF POLAR NEAR-SURFACE OZONE ASSOCIATED WITH VARIOUS ATMOSPHERIC CONDITIONS

A Dissertation
Presented to
The Academic Faculty

by

Ja-Ho Koo

In Partial Fulfillment
of the Requirements for the Degree
Doctor of Philosophy in the
School of Earth and Atmospheric Sciences

Georgia Institute of Technology
May 2014

THE PATTERNS OF POLAR NEAR-SURFACE OZONE
ASSOCIATED WITH VARIOUS ATMOSPHERIC CONDITIONS

Approved by:

Dr.Yuhang Wang, Advisor
School of Earth and Atmospheric Sciences
Georgia Institute of Technology

Dr. Yi Deng
School of Earth and Atmospheric Sciences
Georgia Institute of Technology

Dr. Athanasios Nenes
School of Earth and Atmospheric Sciences
Georgia Institute of Technology

Dr. Armistread (Ted) Russell
School of Civil and Environmental Engineering & School of Earth and Atmospheric Sciences
Georgia Institute of Technology

Dr. Rodney Weber
School of Earth and Atmospheric Sciences
Georgia Institute of Technology

Date Approved: 10 February 2014

To my family and all my friends

ACKNOWLEDGEMENTS

First, I would appreciate my advisor, Dr. Yuhang Wang. He basically leads my doctoral research here with promising working topics. In the working area, I have learned his earnest attitude in front of research and passion for the discussion. Outside the office, he encouraged me when I was depressed and also taught for how the students better plan their future. All his advises now become the fundamentals in mind, which I always consider first in front of walls. I would thank him to help me complete this long race that I have never experienced before.

I would like to thank my Ph. D. thesis committee members, Drs. Yi Deng, Rodney Weber, Athanasios Nenes, and Ted Russell for their attention to my research. I have learned a lot of important knowledge from their lectures and enhanced my research capability with all their precious comments and advices. Based on your guidance, now I can move a step of mine forward to be a real scientist. I would say thank you again.

I thank all the current members and alumni of Yuhang Wang's group, especially Dasa Gu, Charles Smeltzer, Yongjia Song, Yuzhong Zhang, Yufei Zou, Ruixiang Zhang, Hang Qu, Ziming Ke, Burton Gray, Drs. Yunsoo Choi, Tao Zeng, Chun Zhao, Zhen Liu and Qing Yang. I was happy with them together to have many interesting discussions for our research and great events for the refreshment. I also thank all my good friends in the EAS, especially Dr. Taewon Park, Boryoung Shin, and Zheng Lu.

I also would like to thank the persons working for the ARCTAS, ARCPAC, and ARCIONS Experiment science team, especially Dr. Greg Huey, Anne Thompson, Kelly

Chance, Thomas Kurosu, Andreas Richter, and Jin Liao. I also thank Dr. Samuel Oltmans in NOAA ESRL, Mike Shaw in Environment Canada, and Sverre Solber in NILU to let me use their data. Drs. Yi Deng and Tianyu Jiang collaborated with me for the storm track calculation, and Drs. Yongjia Song and Taewon Park help me for CAM5 modeling data processing of global reanalysis data. I appreciate their contribution to my research.

Finally I would appreciate my family. My father and mother have believed my decision at each significant moment of life and encouraged me to do what I wish to do. I am and will be trying to do my best to reward their love. My younger brother, Ja-Hyun, is also a graduate student with studying philosophy. I would support his decision to walk a tough road now, which however will be brightened in the future. Definitely it will be.

This study has been supported by the NASA International Polar Year (IPY) program and Atmospheric Chemistry Modeling and Analysis Program (ACMAP).

TABLE OF CONTENTS

LIST OF FIGURES

Page

LIST OF SYMBOLS AND ABBREVIATIONS

Symbols

a	mean distance between the sun and earth
dT/dz	vertical temperature lapse rate
hν	solar radiation for photochemistry
r	instantaneous distance between the sun and earth
H	half day
Q	total daily solar intensity
R	Pearson's linear correlation coefficient
S	solar constant
δ	solar inclination angle
φ	latitude
ρ	Spearman's Rank correlation coefficient
σ	Standard deviation

Abbreviation

1-D	one-dimentional
3-D	three-dimentional
AC&C/SPARC	Atmospheric Chemistry and Climate / Stratospheric Processes and their Role in Climate
AMF	air mass factor
AMIP	Atmospheric Model Intercomparison Project
ANTCI	Antarctic Tropospheric Chemical Investigation

ARCIONS	ARCtic Intensive Ozonesonde Network Study
ARCPAC	Aerosol, Radiation, and Cloud Processes affecting Arctic Climate
ARCTAS	Arctic Research of the Composition of the Troposphere from Aircraft and Satellites
AO	Arctic Oscillation
AMDE	Atmospheric Mercury Deposition Event
Br2	bromine molecule
BrO	bromine monoxide
$BrNO_3$	bromine nitrate
CAM 5	Version 5 of the Community Atmosphere Model
CAPMoN	Canadian Air and Precipitation Monitoring Network
CIMS	Chemical Ionization Mass Spectrometer
CTM	Chemical Transport Model
DIAL	DIfferential Absorption Lidar
DMS	dimethylsulfide
DOE	Department of Energy
DOY	Day of Year
ECC	Electrochemical Concentration Cell
ENSO	El Niño/Southern Oscillation
DOAS	Differential Optical Absorption Spectroscopy
EOF	Empirical Orthogonal Function
ESRL	Earth System Research Laboratory
FNL	global final analysis

GEM	Gas-phase Elemental Mercury
GOME-2	Global Ozone Monitoring Experiment-2
HBr	hydrogen bromide
HCl	hydrogen chloride
HOBr	hypobromous acid
JISAO	Joint Institute for the Study of the Atmosphere and Ocean
MM5	PSU/NCAR mesoscale model
MOZART	Model for OZone And Related chemical Tracers
NAO	North Atlantic Oscillation
NCAR	National Center for Atmospheric Research
NCDC	National Climatic Data Center
NCEP	Natonal Centers for Environmental Prediction
NDR2	NCEP-DOE reanalysis 2 data
NILU	Norwegian Institute for Air Research
NOAA	National Oceanic and Atmospheric Administration
NO_x	Nitrogen Oxides ($NO + NO_2$)
NSIDC	National Snow and Ice Data Center
ODE	Ozone Depletion Event
ODS	Ozone Depletion Season
OMI	Ozone Monitoring Instrument
OI	optium interpolation
Pa	Pascal
PDO	Pacific Decadal Oscillation

PNA	Pacific North America
RAQMS	Regional Air Quality Modeling System
RGM	reactive gaseous mercury
RPCA	Rotated Principal Component Analysis
ppbv	part per billion by volume
SAM	Southern Annular Mode
SCD	slant column density
SCIAMACHY	SCanning Imaging Absorption spectrometer for Atmospheric CHartographY
SLP	Sea Level Pressure
SMMR	Scanning Multichannel Microwave Radiometer
STE	Stratosphere-Troposphere Exchange
TOPSE	Tropospheric Ozone Production about the Spring Equinox
UV	ultraviolet
VCD	Vertical Column Density
VOC	Volatile Organic Carbon
WDCGG	World Data Centre for Greenhouse gases
WMO	World Meteorological Organization
WP	Western Pacific
ZPL	Zeppelinfjellet

SUMMARY

Understanding the spatiotemporal pattern of near-surface ozone is the key part of polar atmospheric environment. Locally the near-surface ozone can be depleted by the catalytic halogen (mainly bromine) chemistry in the heterogeneous (gas and particle) phase but produced due to the snow photochemistry of NO_x. In addition to the local chemistry, ozone pattern is also affected by regional meteorology and air-mass transport. Since the polar region is quite sensitive to the climate change, these conditions can be also affected by climate change and variability. Based on the analysis of large amount of dataset combined with in-situ observations, satellite measurements, model simulations, and global reanalysis data, the characteristics of polar ozone pattern and relation to the regional and large-scale atmospheric situations were investigated. This study will also be useful to understand and diagnose other polar environmental issues related to the polar near-surface ozone (e.g., atmospheric mercury deposition on the surface, the extent of atmospheric oxidation, and radiative forcing budget in the polar troposphere).

This work is composed of two large issues, near-surface ozone depletion in the Arctic spring and the trend of surface background ozone at South Pole in the Antarctica. At first, the characteristics of tropospheric ozone depletion in the Arctic spring are examined using the measurements during ARCTAS, ARCPAC, and ARCIONS campaign in April 2008 with tropospheric BrO columns retrieved from satellite measurements and back trajectory calculations. Time-lagged correlation analysis and aircraft observations indicate that the ODEs are due to either local halogen-driven ozone loss or short-range (1~2 day) transport from adjacent high-BrO regions such as Chukchi

Sea or Canadian archipelago. The vertical extent of local ozone loss is surprisingly deep at Resolute and Churchill, different from ODEs at Barrow. Particularly the unstable boundary layer during ODEs at Churchill seems potentially provide a source of free-tropospheric BrO through convective transport. Continually the influences of various atmospheric patterns to the Arctic surface ODE are investigated. In years with frequent ODEs at Barrow and Alert, the WP teleconnection pattern is usually in its negative phase, during which the Pacific jet is strengthened but the storm track from western Pacific is weakened. Both factors tend to reduce the transport of ozone-rich airmass from mid-latitudes to the Arctic, creating a favorable environment for the Arctic ODEs. The impact of WP patterns seems become stronger in recent decade to cover ODEs in broader Arctic regions. Comparison between two Arctic sites, Barrow and Alert, shows the initiation of ODS in spring is decided by the solar intensity and the termination is by the ambient surface air temperature. Monthly mean frequency of ODEs at Both sites also indicate the wind strength from the Arctic Ocean is largely influential to the extent of local ODEs, and this wind pattern depends on the regional atmospheric variability, which are the anomaly of Beaufort Sea High or the Katabatic flow in the Greenland. Finally the long-term trend of surface ozone at South Pole is analyzed. In spite of more pristine than the Arctic, the surface ozone production in summer is detected due to the NO_x snow photochemistry. The surface ozone trend in three decades is a clearly year-round reversal trend and lower-tropospheric potential temperature shows a consistent trend. Their strong correlation reveals the possibility of large meridional mixing, which enhances the background level of ozone and NO_x at South Pole.

CHAPTER 1

INTRODUCTION

1.1 Statement of problem

1.1.1 The characteristics of near-surface ozone depletion in the Arctic spring

Near-surface ozone often decreases during the springtime in the polar region resulting in what are called ozone depletion events (ODEs) [Simpson et al., 2007a]. Local ODEs occur by the catalytic process of halogen (mainly bromine) chemistry in the gas and particle phase [Fan and Jacob, 1992], or by the transport of ozone-poor air masses from a source region such as the Arctic Ocean [Bottenheim and Chan, 2006]. To characterize local ODEs, understanding the source of bromine is essential. The most effective particle phase release of bromine is recycling amplification called bromine explosion [Wennberg, 1999]. Generally the first-year sea ice (FYI) area is widely believed to be a source region for high atmospheric bromine and ozone-poor air masses [e.g., Simpson et al., 2007b]. Satellite observations can be used to identify these regions. NIMBUS-7 SMMR DMSP has measured sea ice information [Cavalieri et al., 1996], and OMI [Kurosu and Chance, 2011] and GOME-2 [e.g., Begoin et al., 2010] have monitored the total BrO VCDs. Recently, several retrieval methods were applied to estimate tropospheric BrO VCDs [e.g., Choi et al., 2012]. Whether or not these tropospheric BrO VCDs can explain the variation of local ODEs will be examined.

Backtrajectory analysis has been frequently used to find the source region of local ODEs. Previous backtrajectory calculations simply traced the pathway of air mass

transport based on the level of local ozone or analyzed selected cases [e.g., Bottenheim and Chan, 2006; Oltmans et al., 2012]. Combining this backtrajectory analysis with the above mentioned satellite measurements, will be a better approach to detect the source region. Further, including the time scale of air mass transport in the backtrajectory calculations enables us to consider the variation of source conditions, resulting in a more accurate diagnosis of the source effect.

Since the near-surface ODEs are catalytic chemical processes, vertical stability of the local atmosphere has been supposed as a prerequisite condition [e.g., Lehrer et al., 2004]. However, recent field measurements also detected ODE cases in unstable conditions, even near a storm [Begoin et al., 2010; Jones et al., 2010; Frieß et al., 2011]. This is a clue that blowing snow is also an appropriate particle condition for bromine chemistry [e.g., Liao et al., 2012a]. Vertical structures of ODEs have only been partly investigated [Tarasick and Bottenheim, 2002; Jacobi et al., 2006]. Using backtrajectory calculations for each vertical height combined with satellite BrO VCDs, analysis for differences in the transport effect will be feasible, providing regional characteristics that relate vertical stability to the extent of ODEs.

1.1.2 The role of ambient conditions for the polar surface ozone

Since the sea ice surface is one of the sources for ODEs, it has been believed that cold temperature relates to low ozone [Tarasick and Bottenheim, 2002; Seabrook et al., 2011] and high BrO [Zeng et al., 2003; Pöhler et al., 2010], but this relationship was not found for all measurements [Neuman et al., 2010; Halfacre et al., 2013] and is still an issue for debate. In this study, ozone and temperature measured simultaneously at several regions in April 2008 will be compared. To avoid the possibility that natural variability

has a larger scale than the physically meaningful signal, both ozone and temperature will be detrended before analysis.

Since the extent of ODEs can be affected by air mass transport, the analysis of regional wind patterns in the polar region will be necessary. Generally the wind from the ocean or coastal region will intensify the local ODEs [Morin et al., 2005; Zeng et al., 2006; Van Dam et al., 2013]. As expected, the transport pattern is also associated with the synoptic pressure pattern over the Arctic, showing the dominant effect of the Beaufort High on local ODEs [Zhao et al., 2008]. Therefore, spatial pattern analysis based on the combined information of wind and sea level pressure will provide useful insights for the frequency of ODEs.

Once the atmospheric bromine and particle existence are guaranteed, theoretically the ozone depletion can be maintained by the continuous recycling of bromine. Nonetheless, the initialization and the termination processes of ODEs are still uncertain [Simpson et al., 2007a]. Previously it was thought that the Br_2 could pre-exist from the reaction between atmospheric ozone and sea ice particle in dark conditions [Oum et al., 1998]. Thus, a small amount of sunlight, even twilight, [Spicer et al., 2002] seems the only prerequisite to have ODEs. This hypothesis, however, does not explain the real patterns of measured ozone well. For understanding the termination process, several analyses examine mixing with an ozone-rich air mass [Strong et al., 2002; Jacobi et al., 2010, Hu et al., 2011], but these mechanisms only work for episodic termination of ODEs. The relevant condition of final ODEs in a year has not been clearly identified. As shown, the effective conditions affecting the beginning and end of ODEs are not well established

at the present time. More information about these will improve the model simulation of ODEs.

1.1.3 Influence of large-scale atmospheric patterns to the polar surface ozone.

The polar atmosphere is strongly affected by global climate patterns. Thus the polar surface ozone also appears highly associated with climate variability. In fact, previous studies have shown that climate variability (i.e., teleconnection) relates to the variation of local chemistry in terms of AMDEs [Cole and Steffen, 2010] and to the transport of CO [Eckhardt et al., 2003], CO_2 [Murayama et al., 2004] and aerosols [Di Pierro et al., 2011]. Therefore in a similar manner, how climate variability relates to polar surface ozone will be examined. Within that analysis, stratospheric ozone variation will also be discussed because its effect, related to the SAM [Thompson et al., 2011], seems important for understanding the Antarctic surface pattern (e.g., temperature) [Son et al., 2009]. Recently, stratospheric ozone loss also occurred over the Arctic area [Manney et al., 2011], implying that the stratospheric effect should be evaluated first in the analysis of surface pattern change in the polar region. At least, stratospheric ozone variation changes the UV flux from space and, therefore, influences the photolysis rate of surface ozone [Schnell et al., 1991].

1.2 Specialty of atmospheric chemistry in the polar region

1.2.1 Photochemical activity relevant to snow and ice conditions

Polar atmospheric chemistry shows peculiar chemistry events that are attributed to processes in the particle phase as well as processes in the gas phase. In particular, the

polar region possesses snow and ice particles, which do not appear in the tropic or mid-latitude regions. Thus the photochemistry related to the snow/ice particles becomes a dominant factor in determining the polar chemical environment. There are two main relevant events, which are the ozone depletion events (ODEs) [e.g., Barrie et al., 1988], and the atmospheric mercury deposition events (AMDEs) [e.g., Schroeder et al., 1998].

Mainly in the springtime, surface ozone often falls to zero ppbv and sometimes maintains a low level for several days. This ODE is basically the catalytic process due to the halogen photochemistry in the heterogeneous phase [Simpson et al., 2007a]. Since the polar ocean is the source of bromine, various kinds of particles have been considered as a source of airborne bromine such as frost flowers [e.g., Kaleschke et al., 2004], snowpack [e.g., Michalowski et al., 2000], FYI [e.g., Simpson et al., 2007b], and blowing snow [e.g., Jones et al., 2010]. For example, satellite observations illustrate that high bromine monoxide (BrO) resides over the FYI regions (Figure 1.1) These particle phases capture an airborne bromine atom and return two bromine atoms back to the air during the bromine explosion identified above [Wennberg, 1999]. The rate of bromine explosion depends on the particle acidity (R8) and the type of precipitate in the ocean [Sander et al., 2006; Morin et al., 2008]. Relative to other particles, the contribution of many common aerosols (e.g., sulfate) to the bromine activation seems small but still influential. These various kinds of particle phases enable to have the most efficient environment for strong ODEs with bromine chemistry in the polar region.

Atmospheric mercury is a strong toxic chemical that efficiently reacts with airborne bromine radicals such as Br and BrO. Since gaseous elemental mercury has a relatively long lifetime, it can be transported into the polar region where the active

bromine chemistry leading to ozone depletion occurs. Reaction of mercury with bromine is also prominent in the polar region [Steffen et al., 2008]. Once mercury reacts with bromine, it becomes quite reactive and is readily deposited to particle surfaces such as snow and ice, which are then easily scavenged from the air and accumulate onto the land or ocean surface. This process threatens the quality of polar ecosystem and the fishery biology.

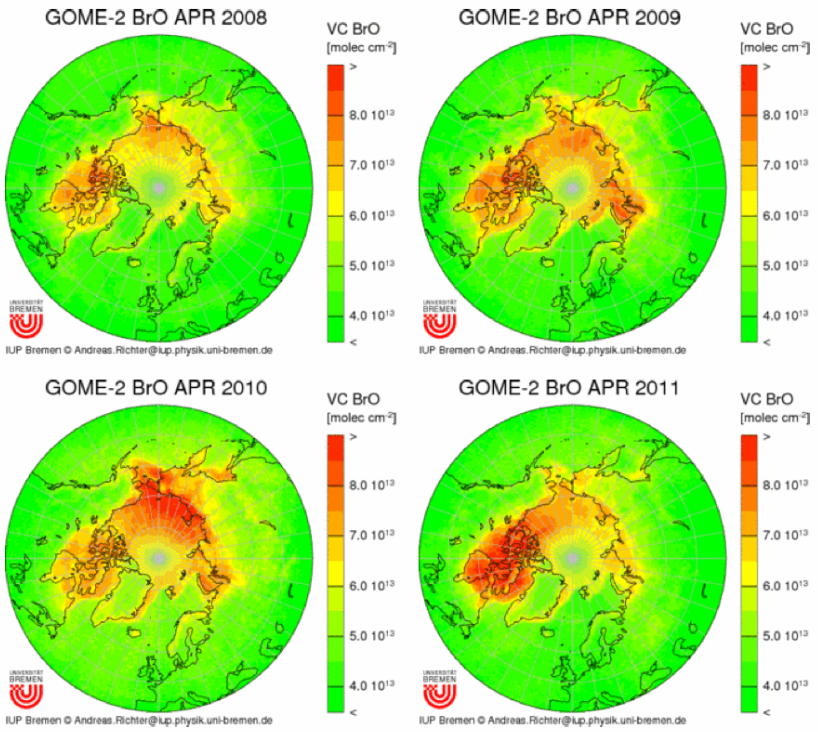

Figure 1.1 The spatial distribution of April mean total vertical column BrO VCDs by GOME-2 satellite measurements from 2008 to 2011. Data were processed from the University of Bremen (http://www.doas-bremen.de/scia_data_browser.htm)

1.2.2 Sensitivity to the global climate change and variability

Polar atmospheric environment is quite sensitive to global climate patterns [Solomon et al., 2007; Min et al., 2008]. The well-known features are the increase of sea ice melting and decrease of perennial sea ice extent in the Arctic due to the global warming [Nghiem et al., 2007; Howell et al., 2009]. Figure 1.2 shows the decadal change

of the Arctic sea ice concentration in September (the largest melting season). Compared to the 1980s (left), sea ice concentrations are significantly decreased in the 2000s, especially over the Chukchi Sea, Kara Sea, Barents Sea, and Canadian archipelago. Strong ice melting contributes to an increase of FYI and a decrease in sea ice thickness, which presumably increases the area of open leads and polynyas. This also affects the amount of bromine release into the air and, therefore, modifies the activity of ODEs and AMDEs. Also, varied sea ice conditions change the surface albedo associated with the global radiation budget. In Antarctica, surface temperature patterns appear connected to sea surface temperature (SST) in the tropical ocean [Ding et al., 2011], which also shows recent global climate change. Thus, it will be considered if the increasing trend of SST (Figure 1.3) is relevant to the temporal pattern of Antarctic surface chemistry.

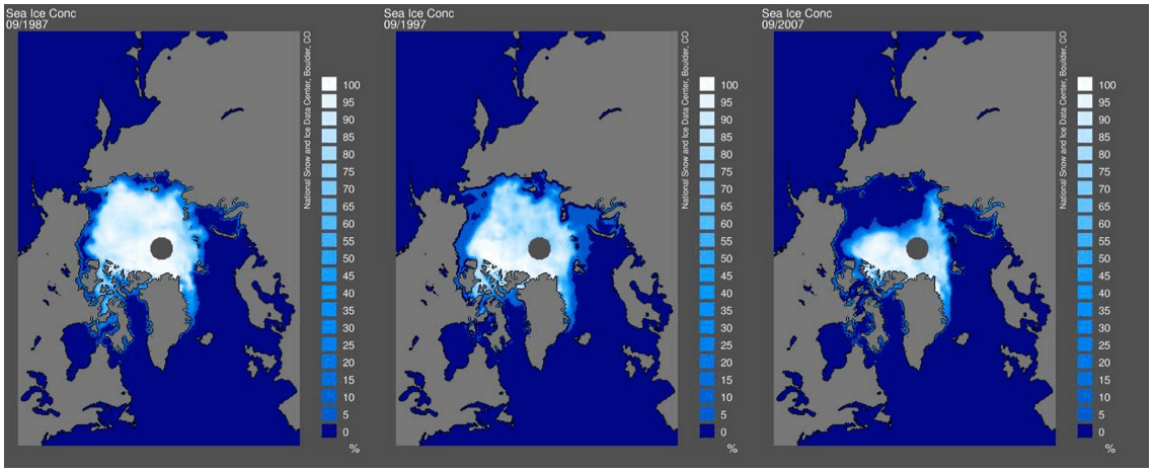

Figure 1.2 The monthly mean pattern of sea ice concentration in the Arctic region for September in 1987 (left), 1997 (middle), and 2007 (right). Images are taken from the NSIDC data archive.

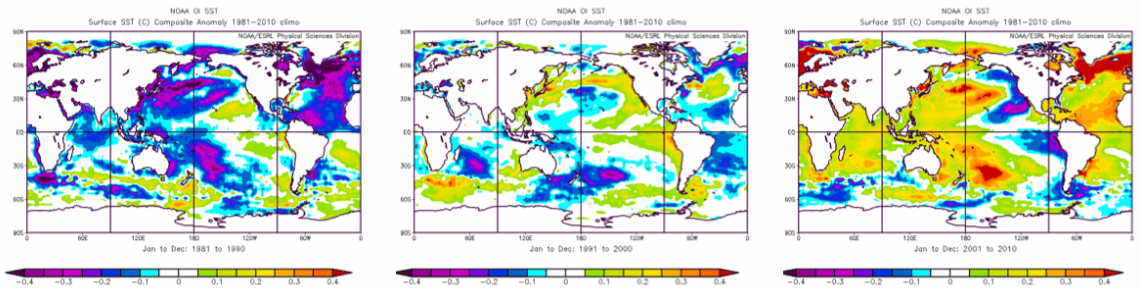

Figure 1.3 The decadal mean anomaly pattern of global SST in the 1980s (left), 1990s (middle), and 2000s (right), obtained from the NOAA/OI SST version 2.

Large-scale atmospheric modulations and climate variability are expressed by teleconnection indices. These indices are generated by statistical methods such as EOF [e.g., Thompson and Wallace, 1998] and principal component analysis [e.g., Wallace and Gutzler, 1981]. Figure 1.4 shows the long-term variation of some teleconnection indices in the northern hemisphere. Typically they show strong inter-annual variations and sometimes even decadal variations (e.g., PDO). In accordance with phase changes in these teleconnections, regional and large-scale atmospheric dynamic (e.g., jet stream and storm track) and meteorological (e.g., temperature) patterns show variations resulting in oscillation of the Arctic atmospheric pattern. Also, the spatiotemporal features of long-range transport from the mid-latitude to the Arctic region sometimes have been explained by these climate variabilities [Eckhardt et al., 2003; Murayama et al., 2004; Di Pierro et al., 2011]. In Antarctica, the Southern Annular Mode (SAM) is quite influential in describing the Antarctic atmospheric pattern. The oscillation of SAM depends on the variation of stratospheric ozone [Thompson et al., 2011] and has been used to explain the surface and tropospheric the temperature trend in the Antarctic [Son et al., 2009, 2010]. The analysis of large-scale atmospheric patterns, consequently, will be essential for the

interpretation of long-term variation in polar chemical environments and relevant features.

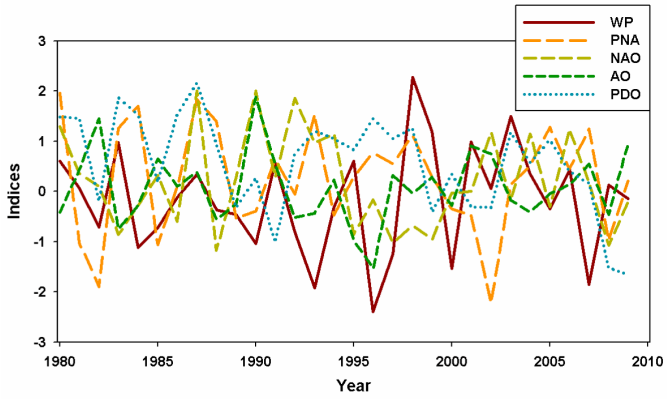

Figure 1.4 Annual variation of April mean index of 5 teleconnections in the northern hemisphere such as WP, PNA, NAO, AO, and PDO.

1.2.3 Increasing trend of Arctic pollution

In the Arctic winter and spring, severe pollution happens annually, called Arctic haze [Shaw 1995; Quinn et al., 2009]. Generally the wild fire and anthropogenic emissions from Eurasia and Northern America are factors inducing this event [Streets et al., 2013]. As global emission increases, this Arctic haze will likely be more frequent. If ODEs become more frequent due to the large area of FYI, as mentioned, the oxidation potential of the Arctic atmosphere also become weaker and more serious haze events will occur. Larger global emission will also likely enhance polar chemistry such as AMDEs and snow NO_x photochemistry. Figure 1.5 shows the annual variation of monthly mean surface ozone for three monitoring stations in Antarctica. As shown, surface ozone production in the austral summer was found at South Pole. This higher ozone in summer has been supposed because of larger nitrogen transport from mid-latitude source areas enhancing the NO_x accumulation in the snowpack of east Antarctic plateau [Davis et al.,

2004, 2008]. The possibility of higher pollution in the polar region and its implication to global climate should be considered in future studies.

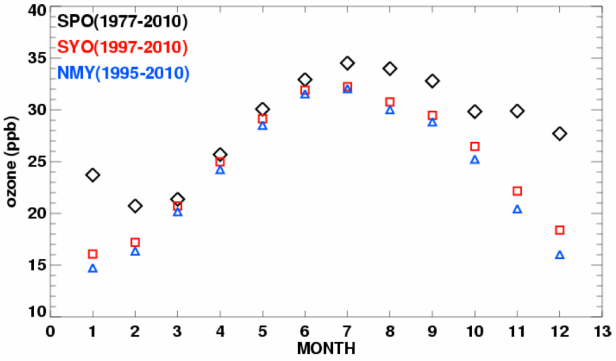

Figure 1.5 Monthly mean variation of surface ozone measured at South Pole (SPO, average for 1977-2010), Syowa (SYO, average for 1997-2010), and Neumayer (NMY, average for 1995-2010) stations in the Antarctica. All data were obtained from the WDCGG data archive.

1.3 Background of polar ozone chemistry

1.3.1 Key reactions of surface ozone depletion

Bromine radical (Br) is usually generated by the photolysis of inorganic bromine molecules (R1), and Br and BrO are then related to ozone depletion (R2, R3). In this process BrO determines the extent of ozone depletion. Two bromine atoms are regenerated by the self-reaction of BrO (R2). In the reaction R2, 20% Br_2 and 80% two Br are produced. BrO reacts with chlorine oxides (ClO) to produce bromine monochloride (BrCl) (R4), which subsequently produces two halogen radicals by photolysis.

$$Br_2 + h\nu \rightarrow 2Br \quad \text{(R1)}$$

$$Br + O_3 \rightarrow BrO + O_2 \quad \text{(R2)}$$

$$BrO + BrO \rightarrow Br_2 + O_2 \quad \text{(R3)}$$

$$\rightarrow 2Br + O_2$$

$$BrO + ClO \rightarrow BrCl + O_2 \quad (R4)$$

Br and BrO (hereafter BrO_x) are well oxidized by the hydroperoxy radical (HO_2). HO_2 reacts with BrO_x and produces hypobromous acid (HOBr) (R5) and hydrogen bromide (HBr). CH_2O and NO_x also participate in halogen chemistry. CH_2O reacts with Br and BrO to produce HBr and HOBr, and also contributes to the production of HO_2. NO_2 reacts with BrO and produces bromine nitrate ($BrONO_2$) (R6). $BrONO_2$ then produces HOBr by hydrolysis (R7) [Tang and McConnell, 1996; Sander et al., 1999]. HBr, HOBr, and $BrONO_2$ are called 'reservoir' species for reactive bromine.

$$BrO + HO_2 \rightarrow HOBr + O_2 \quad (R5)$$

$$BrO + NO_2 + M \rightarrow BrONO_2 \quad (R6)$$

$$BrONO_2 + H_2O \rightarrow HOBr + HNO_3 \quad (R7)$$

ODEs can be explained using only the three dominant reactions R1 to R3 [Zeng et al., 2003]. However, these reactions do not explain the supply of bromine necessary to carry out ODE because the concentration of reactive bromine species (BrO_x) does not increase as result of these three reactions alone. Previous research showed that bromine species are released from aerosols or snow pack auto-catalytically, and this supports the continuation of ODE. This is the process called 'bromine explosion' [Fan and Jacob, 1992; Tang and McConnell, 1996; Wennberg, 1999].

$$HOBr + Br^- + H^+ \rightarrow Br_2 + H_2O \quad (R8)$$

$$HOBr + Cl^- + H^+ \rightarrow BrCl + H_2O \quad (R9)$$

$$BrCl + Br^- \leftrightarrow Br_2Cl^- \quad (R10)$$

$$Br_2Cl^- \leftrightarrow Br_2 + Cl^- \quad (R11)$$

In a bromine explosion, one bromine atom goes into the particle phase, but two bromine atoms are transferred from particle into atmosphere as a result of reaction with bromide (Br^-) in the particle phase. Some bromine reservoir species are soluble, therefore, will efficiently transfer into the particle phase. For example, HBr rapidly converts to bromide and $BrONO_2$ converts to HOBr in the particle phase. R8 is the main reaction of bromine explosion. Because chloride concentrations are usually greater than bromide [Hara et al., 2002; Simpson et al., 2005], HOBr also reacts with chloride and produces BrCl (R9) [Vogt et al., 1996], which can be converted to Br_2 by equilibrium reactions in the particle phase (R10, R11) [Wang et al., 1994]. Finally, Br_2 and BrCl transfer to the atmosphere again because they are insoluble. Foster et al. (2001) detected a peak in Br_2 and BrCl during ODE period, confirming the mentioned bromine explosion actually occurs.

1.3.2 Atmospheric mercury deposition

ODEs are also related to the atmosphere mercury deposition events (AMDEs) [Schroeder et al., 1998], because bromine actively reacts with mercury. While mercury has some natural sources such as forest fire and ocean emissions, generally it comes from anthropogenic sources such as coal-fired power plants, medical activities, and some electric devices [Simpson et al., 2007a]. Gas elemental mercury (GEM, Hg^0) can have a long transport lifetime and becomes reactive gaseous mercury (RGM) by oxidation with bromine radicals (R12, R13, R14, R15).

$$Br + Hg^0 \rightarrow HgBr \quad \text{(R12)}$$

$$BrO + Hg^0 \rightarrow HgO + Br \quad \text{(R13)}$$

$$BrO + Hg^0 \rightarrow HgBrO \quad \text{(R14)}$$

$$BrO + Hg^0 \rightarrow HgBr + O \quad \text{(R15)}$$

RGM is more reactive than GEM, and easily deposits to snow, ice, or other particles able to be taken by snow and ice surfaces. These mercury-included particles are scavenged from the air and deposit onto the surfaces.

1.3.3 Snow NO_x chemistry

Snow surface is known as an important sink of NO_x in the polar region [e.g., Slusher et al., 2002]. In general, the lifetime of tropospheric NO_x is controlled by the reaction with OH radical (R16). However, NO_x lifetime at South Pole is determined by reactions with both OH and HO_2 radicals (R16, R17). The reason is that the temperature at South Pole area is so sufficiently low that the thermal decomposition of HO_2NO_2 is too slow. Also HNO_3, HO_2NO_2 at South Pole is readily deposited to the snowpack (R19) [Slusher et al., 2002].

$$OH + NO_2 + M \rightarrow HNO_3 \quad \text{(R16)}$$

$$HO_2 + NO_2 + M \rightarrow OH + NO_2 \quad \text{(R17)}$$

$$HO_2 + NO + M \rightarrow OH + NO_2 \quad \text{(R18)}$$

$$HNO_3, HO_2NO_2 \rightarrow \text{surface deposition} \quad \text{(R19)}$$

Once the NO_x level increases, however, OH becomes more dominant again due to the reaction between NO and HO_2 (R18), which is one of pathways for tropospheric ozone production. At South Pole, ozone production is only associated with the NO_x chemistry because other pathways such as VOCs are absent in pristine Antarctica. Therefore, ozone production at South Pole is mostly determined by the R18 reaction as background NO_x

level increases. Once NO_x goes into the snow surface, it will be emitted again by the snowpack cycling processes [Davis et al., 2008].

1.4 Data and Method

1.4.1 In situ Measurements

Surface measurements

Ozone data was collected by surface, ozonesonde, and aircraft measurements. Long-term surface ozone data at fixed sites were useful to see the temporal trend of ozone levels. Surface ozone is measured by an optical technique using its strong UV absorption band, usually 254 nm. In this study, surface ozone data from three continuous measurement sites were selected in the Arctic area: Barrow, Alaska (71.3°N, 156.8°W), Alert, Canada (82.5°N, 62.3°W), and Zepplinfjellet (ZPL, 78.9°N, 11.88°E). Continuous surface ozone monitoring has been conducted by NOAA ESRL at Barrow [Oltmans and Levy, 1994], CAPMoN in Environment Canada at Alert [Anauf et al., 1994], and NILU at ZPL stations [Solberg et al., 1996] (Figure 1.6). In Antarctica, continuous measurements of surface ozone at South Pole were used, obtained from the WMO world data center for greenhouse gases (WDCGG). Qualified data (evaluated with the process of quality control and assurance) were provided for all sites and all data were processed for hourly mean first for this study. The uncertainty is only in the range of 0.5 to 2 ppbv [Helmig et al., 2007], which is acceptable for general data analysis. The meteorological data such as temperature and wind information used in this study were obtained from the NOAA NCDC data archive. For the NO_x measurements at South Pole (See Appendix B.3), the commercial chemiluminescence NO_x-NO instrument (Thermo Environmental

Instruments Model 42S) was used [Davis et al., 2004]. The clear OD Teflon line was used for sampling ambient air.

Ozonesonde measurements

Vertical profiles of ozone were measured by ozonesonde using Electronical Concentration Cell (ECC). In 2008, intensive ozonesonde measurements were made by the Arctic Intensive Ozonesonde Network Study (ARCIONS) campaign (http://croc.gsfc.nasa.gov/arcions) from April 1 to 20 2008 [Thompson et al., 2011]. Related to the objective of this study, ozone data for Barrow, Churchill (58.7°N, 94.1°W), and Resolute (74.7°N, 95.0°W) were used (Figure 1.6). All data were reprocessed with a 100 m interval from the surface, as were temperature measurements.

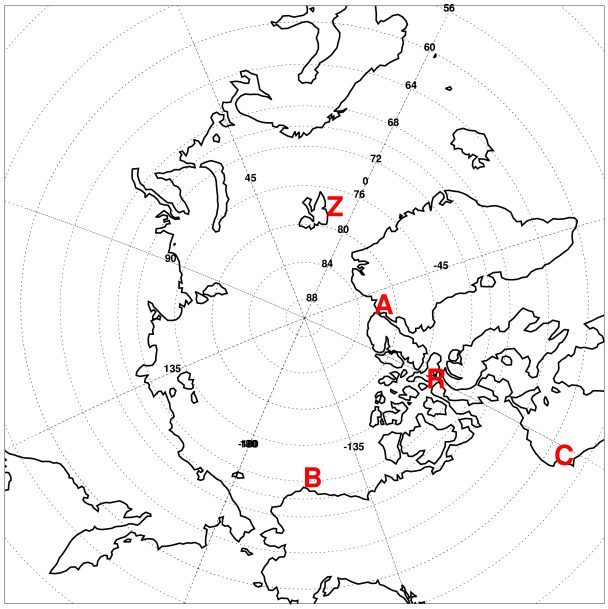

Figure 1.6 The location of Arctic stations for surface ozone measurements, which are Alert (A), Barrow (B), Churchill (C), Resolute (R), and ZPL (Z). Alert, Barrow, and ZPL are the stations for continuous surface ozone measurements; Churchill and Resolute are for ozonesonde observations.

Aircraft measurements

Aircraft measurements are also important in that they collect data over a wider spatial coverage. In April 2008, various chemical species were measured by NASA DC-8 aircraft for the ARCTAS and NOAA WP-3D aircraft for the ARCPAC campaign. The vertical patterns of ozone level were detected by on-board lidar (UV-DIAL). In this study, one minute merged data were used for analysis. Aircraft measurements of bromine species (Br_2, BrO, and soluble bromide) were conducted during the ARCTAS and ARCPAC periods. The quality of these was assured with comparison to the ground DOAS measurements and satellite BrO VCDs [Choi et al., 2012; Liao et al., 2012b].

1.4.2 Satellite Data: OMI and GOME-2 framework

Tropospheric BrO VCDs

BrO is used as a tracer to show where ozone is depleted (referring to R1−R3). BrO VCDs have been monitored by satellite remote sensing. Ozone Monitoring Instrument (OMI, Aura satellite) and Global Ozone Monitoring Experiment-2 (GOME-2, MetOp satellite) observation have produced the total slant column density (SCD) of BrO and this data was converted to total vertical column density (VCD) of BrO using the air mass factor (AMF). To get a tropospheric BrO VCDs, the amount of stratospheric BrO VCDs must be estimated. Several hypotheses were used to calculate the amount of stratospheric BrO VCDs; Stratospheric BrO VCDs are estimated by considering as the 20th percentile of vertical column BrO VCDs (20th percentile method), by using the simulated amount of stratospheric bromine species from Regional Air Quality Modeling System scaled by the latitudinal 20th percentiles (RAQMS method), and by using the second fitting extrapolation based on SCIAMACHY measurement (SCIA2ND method) More details are described in Chapter 2. Then, tropospheric BrO VCDs were retrieved by

subtracting assumed stratospheric BrO VCDs from the total BrO VCDs. Data verification using in situ measurements [Choi et al., 2012] shows six estimates of tropospheric BrO VCDs can be used in this study: three from the OMI applied 20th percentile method, the RAQMS method, and the SCIA2ND method (hereafter, OMI-20th, OMI-RAQMS, OMI-SCIA2ND), and also three from the GOME-2 applied same methods (hereafter, GOME-2-20th, GOME-2-RAQMS, and GOME-2-SCIA2ND). All processed data are daily representatives with a few missed dates generated by interpolation. Retrieved BrO VCDs in the high latitudinal region have large uncertainty because the data quality of BrO SCDs becomes poor when solar zenith angle becomes large. Therefore, data are not used for regions where latitude is higher than 85°N.

Sea ice information

Sea ice concentration is generated using the brightness temperature retrieved from the measurements of the NIMBUS-7 Scanning Multichannel Microwave Radiometer (SMMR), the Defense Meteorological Satellite Program (DMSP) and Special Sensor Microwave/Imagers (SSM/Is), and the DMSP Special Sensor Microwave Imager/Sounder (SSMIS) [Cavalieri et al., 1996]. The data is produced with 25 km resolution grids on the polar stereographic projection. Estimated sea ice concentrations used the NASA Team algorithm developed by the Oceans and Ice Branch, Laboratory for Hydrospheric Processes at NASA Goddard Space Flight Center (GSFC). The dataset used in this study was obtained from the NSIDC data archive. An estimation of first-year sea ice (FYI) is necessary for this study. There are several methods to retrieve FYI (e.g., using the difference of brightness temperature of sea ice), but in this study we simply

estimated FYI using the difference of sea ice existence between September (a season showing the largest melting) and April (a season showing the largest freezing).

1.4.3 Model experiments

Backtrajectory calculation

Backtrajectory information is useful to estimate the source and pathway of the transported air mass for the specified regions. Ozone-poor air mass transport can be recognized using BrO distribution. Based on the polar version of MM5, a simple kinematic model was developed to calculate the backtrajectory [Zeng et al., 2006; Arimoto et al., 2008]. MM5 meteorological field was simulated based on the initial constraint of the NCEP global final analysis (FNL) grid data and ARCTAS DC-8 measurements. Five-day backtrajectories were calculated for surface monitoring sites (Barrow, Alert, and ZPL), ozonesonde launching sites (Barrow, Churchill and Resolute) and the locations of ODEs detected by the aircraft (DC-8 and WP-3D) measurements. Generally the transport pattern is comparable to the results produced by the NOAA Hybrid Single Particle Lagrangian Integrated Trajectory (HYSPLIT) 4.0 model [Draxler and Hess, 1998], but the model in this study considers the meteorology with finer resolution. Also in this study, backtrajectory data were analyzed by considering time lag of air mass transport (Figure 1.7). This provides better insight into the transport effect from the source regions. For more details see Chapter 2.

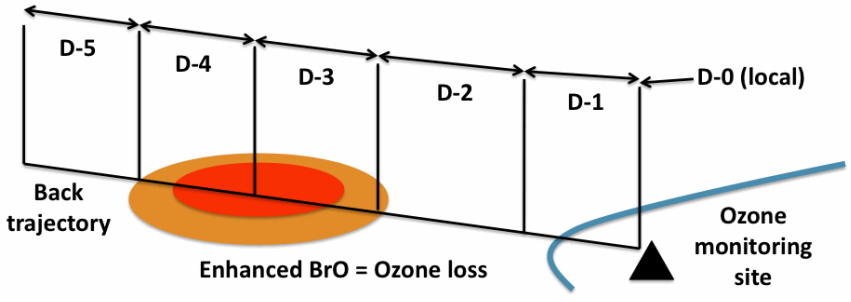

Figure 1.7 Description of backtrajectory analysis of this study with considering time lag of air mass transport.

Global model simulations

To investigate how stratospheric ozone variations influence tropospheric and surface ozone in Antarctica, the NCAR Community Atmospheric Model version 5.0 (CAM5) [Neale et al., 2008] was used in this study. The default settings are based on F component set, 1.9 × 2.5 resolution, and 30 vertical levels from the surface to the top of atmosphere. The prescribed or initial conditions for model experiments described later are: Meteorology information from the Atmospheric Model Intercomparison Project (AMIP), natural surface emission from the fourth version of Model for Ozone and Related chemical Tracers 4 (MOZART 4), sea surface temperature (SST) and sea ice concentration (SIC) from the merged Hadley-NOAA/OI SST and SIC [Reynolds et al., 2002]. Stratospheric ozone information is obtained from the AC&C/SPARC ozone database.

Box model simulations

Halogen chemistry related to ODEs was investigated by box model simulation. The model was developed based on the REAM 1-D model [e.g. Zeng et al., 2003, 2006], with halogen (iodine excluded) chemistry updated based on several previous model studies [Michalowski et al., 2000; Evans et al., 2003; Piot and von Glasow, 2008]. This model considers the heterogeneous reactions between gas and particle phases. The mass transfer process between phases was expressed using the method of Dahnake [Seinfeld and Pandis, 1998]. The aerosol surface area and volume information was that of Evans et al., (2003). In total, 110 gas-phase reactions, 10 mass-transfer reactions, and 16 aqueous-phase reactions were included in this model. Meteorological field data was considered in

the model based on polar MM5 simulation [Bromwich et al., 2001]. We ran the model for several days with repeating daily meteorology. ODE simulations were executed based on the measured concentration for some of chemical species, and the concentration of bromide in particle phase was changed to control ODE. The results of these simulations were compared to field measurements.

1.4.4 Climate data

To see the impact of climate variability on local surface ozone in the polar area, several teleconnection indices and large-scale meteorology data were used in this study. In the northern hemisphere, five indices, WP, PNA, AO, NAO, and PDO were selected for correlation and composite analysis with surface ozone (for more details refer to chapter 3). WP, PNA, AO, and NAO indices were obtained from NOAA's Climate Prediction Center (CPC) and PDO from the JISAO in the University of Washington. Southern Annular Mode (SAM) was also used for the analysis of surface ozone at South Pole, and was provided by Gareth Marshall in the British Antarctic Survey (http://www.nerc-bas.ac.uk/icd/gjma/sam.html). Global meteorology used in the data analysis was obtained from the NCEP/NCAR reanalysis 1 [Kalnay et al., 1996] and NCEP/DOE reanalysis 2 dataset [Kanamitsu et al., 2002]. Global storm track information (used in chapter 3) is estimated based on the methodology of Cressman (1959) and Hoskins and Hodges (2002).

1.5 Preliminary studies

Time series of surface ozone mixing ratios (ppbv) at Barrow, Alert, and ZPL in April 2008 were compared first. All three sites show several ODE cases (< 20 ppbv) and

Barrow shows the most frequent ODEs compared to other sites. In this study two ODEs are defined based on ozone level, which are a strong ODE (SODE, ozone less than 10 ppb), and partial ODE (PODE, ozone between 10 and 20 ppbv). Time series of ozone in April 2008 show that SODEs usually have longer duration than PODEs, probably implying that there are some additionally required conditions to have SODEs. Around 15 April, all three sites show the strong decrease of ozone, falling below 10 ppbv. This may be related to the wide impact of large-scale atmospheric patterns. Diurnal patterns of ozone mixing ratios are consistent with the daily pattern of solar elevation.

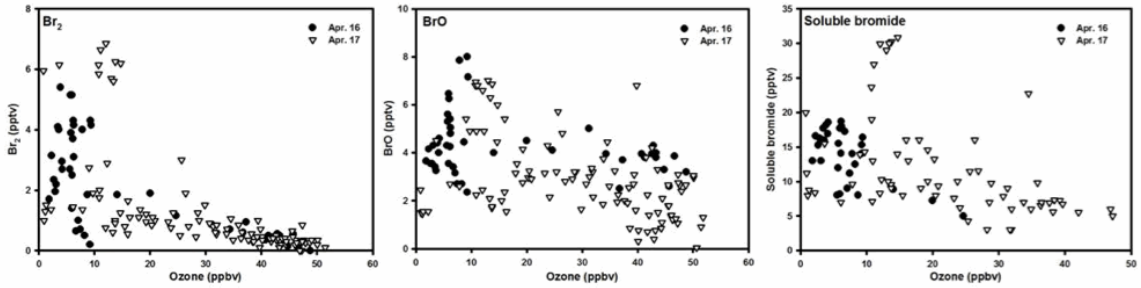

Figure 1.8 Comparison of ozone with Br_2 (left), BrO, and soluble bromide measured by the NASA DC-8 aircraft on 16 (black dots) and 17 (white triangle) April, 2008, which are periods in the ARCTAS campaign.

In-situ measured ozone and bromine species measured by NASA DC-8 missions were compared to each other (Figure 1.8). In the ARCTAS period, DC-8 aircraft measured bromine species (Br_2, BrO, and soluble bromide) only on April 16 and 17. For these two days, simultaneous ozone and bromine measurements in the troposphere (height below 1 km) were selected and analyzed. Generally, ozone shows negative correlations with bromine species, meaning high concentrations of bromine contribute to tropospheric ozone depletion. Between the two days, the April 17 case shows better anti-relationship. The DC-8 flight track (http://www-air.larc.nasa.gov/missions/arctas/flight_tracks.htm) on April 16 covered only overland

regions in northern Alaska, while on April 17 the DC-8 flew from Alaska to the North Pole. The two-day difference is presumed because April 17 flew over the Arctic Ocean with an implied more efficient and stronger bromine chemistry with ozone depletion. This result also illustrates that satellite BrO VCD will be useful for the ODE analysis.

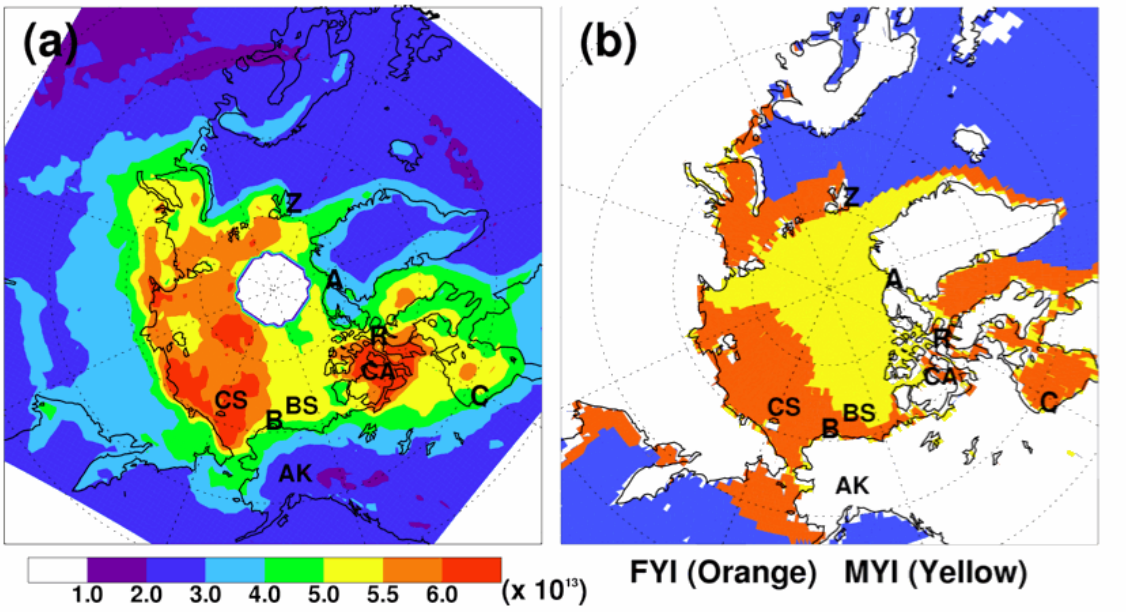

Figure 1.9 (a) Monthly mean tropospheric BrO vertical column density (VCD, molecules/cm2) and (b) the sea ice distribution in April 2008. "A" denotes the location of Alert, "B" for Barrow, "C" for Churchill, "R" for Resolute, and "Z" for Zeppelinfjellet (ZPL), "CA" for Canadian Archipelago, "CS" for Chukchi Sea, "BS" for Beaufort Sea, and AK for Alaska. In (b), the yellow area is covered by multi-year sea ice (MYI), and the orange area is covered by the first-year sea ice (FYI). The GOME-2-SCIA2ND results are shown in (a).

The source regions of ozone-poor air masses were first estimated then backtrajectory analysis used to define the transport patterns. Since BrO enhancements indicate local ozone losses [e.g., Zeng et al., 2003], tropospheric BrO VCDs from satellite measurements were used for April 2008 (Figure 1.9). Two high-BrO regions are clearly indentified over the Chukchi Sea and the Canadian archipelago. Sea ice conditions, which are influential to the bromine release, were also compared with the

pattern of tropospheric BrO VCDs. Interestingly we also find that FYI and high BrO VCDs tend to be collocated particularly over the Chukchi Sea. This indicates the FYI region likely plays a role as a source of bromine release and recent increases of sea ice melting may enhance and broaden the spatiotemporal range of ODEs. Additionally, the large area of FYI over the Hudson Bay (Figure 1.9b) explains high BrO VCDs despite the location having relatively lower latitude.

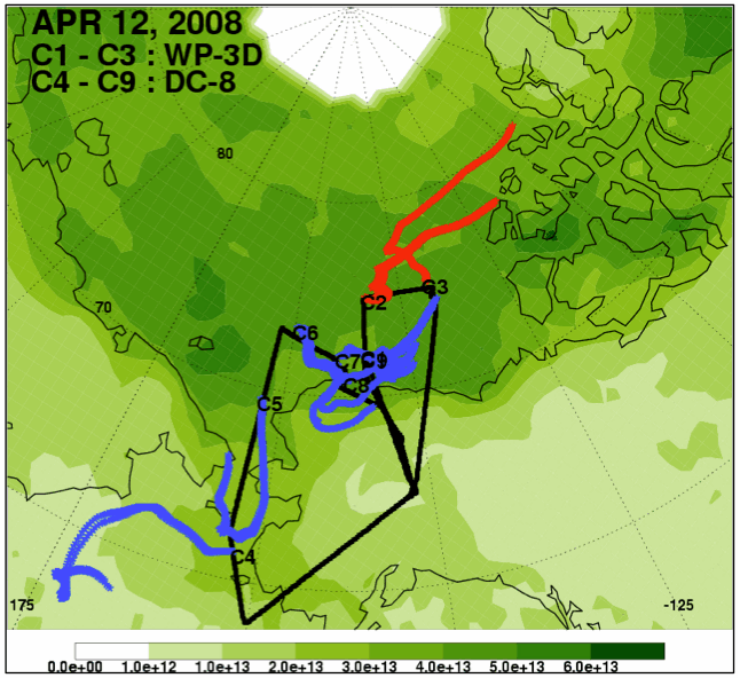

Figure 1.10 The ODE cases in 12 April 2008, which is the only day when NOAA WP-3D (ARCPAC campaign, C1-C3) and NASA DC-8 (ARCTAS campaign, C4-C9) aircraft measured ozone together. ODEs were detected by WP-3D but not by DC-8. 48-hour backtrajectory shows that the difference of air mass transport may be a main reason. Red lines are backtrajectories for ODE cases, and blue lines for non-ODE cases. The shading of green color indicates the daily mean BrO VCDs.

The effect of air mass transport can be investigated by combining the tropospheric ozone measurements, tropospheric BrO VCDs retrieved from the satellite (OMI and GOME-2) observations, and backtrajectory calculations. Figure 1.10 is a good example to depict the contrast of air mass transport according to the extent of ozone depletion.

Backtrajectory analysis provided the source region from which ozone-poor air mass comes [e.g., Bottenheim and Chan, 2006; Oltmans et al., 2012], and they suggested that the ozone-poor air mass generally comes from the Arctic Ocean. Morin et al. (2005) also presented a case showing the clear contrast of ozone and bromine in accordance with the change of local wind direction.

Figure 1.11 shows the simulation result of ozone, Br_2, BrO and bromide. First, ozone decreases during the daytime and does not change during the nighttime. This decreasing pattern continues day by day until ozone falls to almost zero after about 6-7 days. The pattern and time duration of simulated ozone depletion is similar to the previous results [Evans et al., 2003; Piot and von Glasow, 2008]. As ozone starts to decrease after sunrise, Br_2 decreases and produces BrO. Br_2 is rapidly photolyzed and BrO increases during the daytime. As the sun sets, BrO starts decreasing rapidly and Br_2 is accumulated at night. This diurnal pattern is repeated until ozone becomes zero. Bromide in the model usually decreases rapidly only in a day, as shown in other modeling studies [Sander et al., 1999; Piot and von Glasow, 2009]. These preliminary model results show that the model includes many limitations obscuring the reproduction of observed patterns, which require further investigation of ODE features.

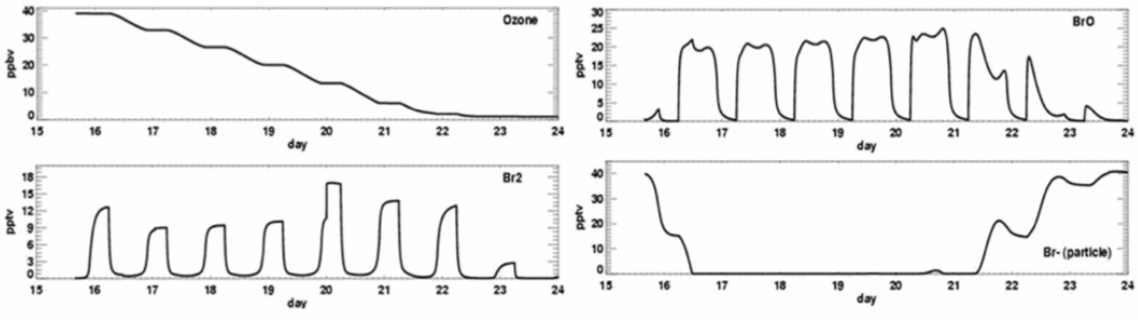

Figure 1.11 Examples of REAM 1-D model simulations (at surface layer) for ozone, Br_2. BrO, and Br^- with starting at noontime in 15 April 2008.

In addition to the local halogen chemistry, the ambient conditions also seem very important to explain the spatiotemporal pattern of ODEs. Figure 1.12 is an example of the relationship between ozone and atmospheric pattern, showing the spatial distribution of correlations between surface ozone and surface level pressures over the Arctic (for April 2008). Surface ozone at both sites shows the similar correlation pattern with surface pressures and seems affected by same regional or large-scale atmospheric modulations. This interesting feature, which has not been investigated before, presumably reveals the possibility of hidden atmospheric influence to control the extent of local ODEs.

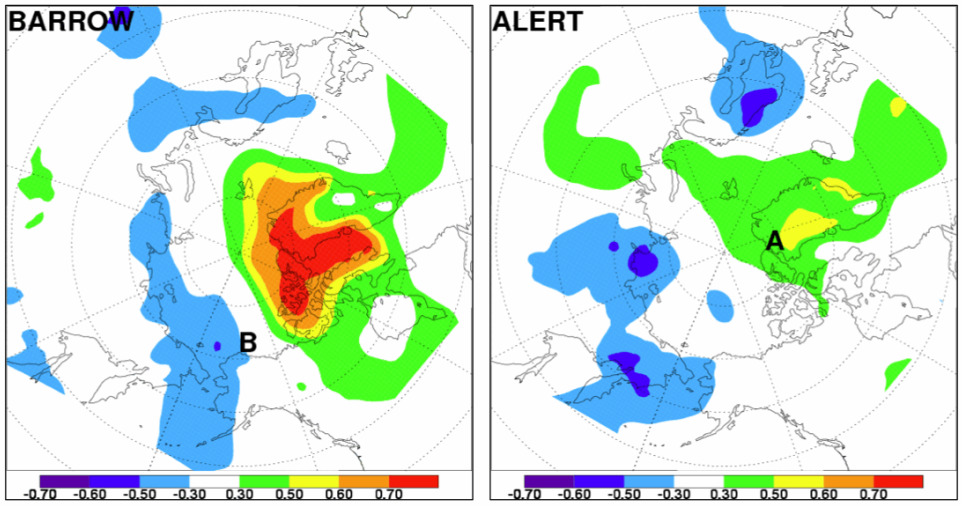

Figure 1.12 Correlations of surface observed ozone at Barrow (left) and Alert (right) with the MM5 surface level pressure for the each grid of the Arctic. Daily mean values for April 2008 was used.

1.6 Scope of this work

This dissertation looks into how sensitive near-surface polar ozone is to the ambient environment. With a combined dataset of in-situ (surface, ozonesonde, and aircraft) measurements, satellite observations, model simulations, and global reanalysis data, this dissertation specifically examines (1) the horizontal and vertical range of near-

surface ozone depletion in the polar region, (2) influence of atmospheric conditions to spatiotemporal characteristics, and (3) the relationship to the large-scale atmospheric variability and climate change. All the findings in this work will provide useful direction to better understand ODEs, which to date are not perfectly interpreted with only the limited scope and insight of local halogen chemistry.

In detail, the following chapters are organized as follows.

Chapter 2, "Characteristics of tropospheric ozone depletion events in the Arctic spring: analysis of the ARCTAS, ARCPAC, and ARCIONS measurements and satellite BrO observations," describes the features of ODE structures in the Arctic spring. The analysis of large combination of data collected for April 2008 evaluates the driving forces of local ODEs: local chemistry versus the transport of ozone-poor air masses, and also compares the regional differences of vertical structure of ODEs. Comparison of ODEs at three surface stations reveals that ODEs at Barrow is more associated with the transport of ozone-poor air mass, whereas ODEs at Alert seems affected the local chemistry more. Particularly the backtrajectory analysis with considering time lag of air mass transport provides that the effective time scale of transport is less than 3 days. Satellite measurements of tropospheric BrO VCDs indicate the feasible source regions in the Arctic, which are the Chukchi Sea and Canadian archipelago. Detrending process in this study supports the existence of positive correlation between ozone and temperature, which is still one of debating issues related to the ODE. Ozonesonde data analysis shows that some ODEs occur in a stable boundary layer, similar to the previous expectation. But also several ODEs exist showing deep vertical structure of ODEs. Especially ODEs at Churchill occurs in unstable situation

showing vertical convection, consistent with the recent hypothesis that blowing snow may an important condition providing the heterogeneous phase of ODEs. All these findings indicate that the more analysis of ambient air pattern and synoptic conditions will be required for interpretation of measured ODEs.

Chapter 3, "Influence of climate variability on near-surface ozone depletion events in the Arctic spring," starts from the large inter-annual variation of monthly (April) ODE frequencies at all surface monitoring sites, which does not seem affected by the activity of local halogen chemistry. Among several teleconnections, WP pattern shows the strongest relationship to the ODE frequency at Barrow and Alert. They are negatively correlated, i.e., the year with negative phase of WP pattern shows the relatively more frequent ODEs. Pacific jet stream and storm track intensity that have been known related to the phase change of WP pattern [e.g., Rivière, 2010] also show the large contrast between the years of weak and strong ODE occurrences. Based on this feature, it is supposed that the phase change of WP pattern controls the extent of meridional mixing, resulting in the variation of airmass inflow from mid-latitude to the Arctic. Therefore it looks that WP pattern can be used to diagnose the extent of ODEs in the Arctic spring. ODE frequency at ZPL, located far away from the Pacific, is only related to the WP pattern in the 2000s, not in the 1990s. This may allude that the impact of WP pattern to the Arctic is getting higher. The results in this chapter are first tried in this working field therefore will broaden our views for the impact of climate variability to the local surface.

Chapter 4, "Significant factors influencing the spatiotemporal variation of surface ozone depletion: The onset, progression, and termination," addresses the role of several ambient conditions affecting the initiation, progression, and termination of

Arctic surface ozone depletion in the springtime. Comparison of onset dates between Barrow and Alert shows that the role of solar radiation is not limited just to start the catalytic process of ozone depletion, but extended to have enough depletion of ozone. Wind strength from the Arctic Ocean was also compared to interpret the monthly difference of ODE frequencies, and the termination of springtime ozone depletion in the Arctic is explained with the temperature. The finding here provide useful information for how to improve the model simulation of ODEs. In other words, it shows that the ambient environmental conditions as well as halogen chemistry should be treated carefully in the future model. In fact, the level of HO_2 (R5) is so sensitive to the diurnal solar pattern that reaction with BrO (R5) is highly variable, and temperature changes the snow conditions that should be considered as a particle phase of ODEs in the model.

Chapter 5, "The year-round pattern of surface ozone at South Pole: a reversal trend in recent three decades," interprets a unique reversal trend of surface ozone measured during three decades at South Pole. This reversal trend happens year around implying that there are slow and steady forcing factors. Previous studies generally mentioned the role of stratospheric ozone variation and SAM to the surface. However the result in this chapter shows weak effect of those to the surface ozone trend. Instead, it was found that the lower-tropospheric potential temperatures from the NCEP/NCAR reanalysis shows quite similar year-round reversal trend over the east Antarctic plateau. As similar to Chapter 3, here the extent of meridional mixing is discussed as a reason to explain a long-term variation of surface ozone at South Pole. Findings in this chapter show how global climate change and emission increase possibly influences to the polar surface environment.

Chapter 6, "Conclusions and future work," summarizes all findings in Chapter 2 – 5 and provides several key points and remained questions for future study to improve our knowledge of polar near-surface chemistry in terms of global climate change.

CHAPTER 2

CHARACTERISTICS OF TROPOSPHERIC OZONE DEPLETION EVENTS IN THE ARCTIC SPRING: ANALYSIS OF THE ARCTAS, ARCPAC, AND ARCIONS MEASUREMENTS AND SATELLITE BrO OBSERVATIONS

2.1 Introduction

Tropospheric ozone depletion events (ODEs) in the Arctic spring were first found in the early 1980s [Oltmans et al., 1981], and Barrie et al. (1988) showed that the ODEs were associated with high particulate bromide concentrations. Catalytic ozone loss processes involving halogens, especially heterogeneous bromine chemistry, are believed to be the main cause of the ODEs [e.g., Fan and Jacob, 1992; Sander and Crutzen, 1996; Tang and McConnell, 1996]. During these events, aqueous-phase reactions involving soluble species such as HOBr, $BrNO_3$, HBr and HCl play important roles in the conversion of the gas and aqueous phase reservoir species into reactive bromine radicals [e.g., Vogt et al., 1996; Sander et al., 1999; Foster et al., 2001]. In addition to aerosols, potentially important medias for heterogeneous reactions include snowpack [Michalowski et al., 2000; Simpson et al., 2005; Toyota et al., 2011], frost flower [Kaleschke et al., 2004; Kalnajs and Avallone, 2006; Piot and von Glasow, 2008], and first-year sea ice [Simpson et al., 2007]. Recently, blowing snow was also suggested to be a source of bromine [Jones et al., 2009; Yang et al., 2010].

Transport of ozone-poor air mass is another important factor contributing to the observed ODEs. The transport pattern during ODE periods was investigated using the analysis of synoptic-scale meteorology patterns [Hopper et al., 1998; Strong et al., 2002; Zhao et al., 2008]. Back trajectory analysis is often useful to identify and quantify the potential source regions of ozone-poor air mass [Bottenheim and Chan, 2006]. The rate-limiting step of bromine-driven ozone depletion is mostly through the self-reaction of bromine monoxide (BrO) [e.g., Hausmann and Platt, 1994; Zeng et al., 2006]. Analyses of satellite measurements of BrO, sea ice conditions, and back trajectories suggest that the ozone-poor air mass is usually transported from high-BrO regions [Zeng et al., 2003, 2006; Kaleschke et al., 2004; Simpson et al., 2007; Bottenheim et al., 2009; Gilman et al., 2010; Nghiem et al., 2012; Oltmans et al., 2012]. Not all ODEs can be explained by the transport effect [Jacobi et al., 2006], implying the importance of in situ chemistry.

The characteristics of ODEs are affected by ambient conditions. Although high BrO enhancements can be related to cold temperature [Pöhler et al., 2010, Nghiem et al., 2012], ODEs occur in a wide range of temperature [Zeng et al., 2003, 2006; Bottenheim et al., 2009; Neuman et al., 2010]. Atmospheric stability affects the vertical profile of ODEs [Bottenheim et al., 2002; Tarasick and Bottenheim, 2002; Jacobi et al., 2006]. Generally ODEs occur in a stable layer, which effectively isolates depleted ozone air mass from mixing with ozone-rich air mass above [Lehrer et al., 2004; Bottenheim et al., 2009; Jacobi et al., 2010]. However, ODEs also occur when there is vertical mixing from the surface [McElroy et al., 1999; Jones et al., 2010].

The Arctic Research of the Composition of the Troposphere from Aircraft and Satellites (ARCTAS), the Aerosol, Radiation, and Cloud Processes affecting Arctic

Climate (ARCPAC), and the Arctic Intensive Ozonesonde Network Study (ARCIONS) experiments in April 2008 made extensive aircraft and ozonesonde measurements. We combine these measurements with surface and satellite observations and back trajectory calculations to analyze the spatiotemporal characteristics of ODEs. Following Tarasick and Bottenheim (2002), we define two categories of ODEs, strong ODEs (ozone mixing ratio < 10 ppbv) and partial ODEs (ozone mixing ratio between 10 to 20 ppbv). We focus on two aspects of the ODE characteristics: the relative importance of in situ chemistry compared to transport of ozone-poor air mass, and the impacts of tropospheric BrO distributions on ODEs in the Arctic. Available in situ BrO observations are too limited [e.g., Neuman et al., 2010; Liao et al., 2012b] to be applied directly to analyze ODE characteristics. The retrievals of tropospheric BrO columns from satellite measurements are problematic [e.g., Choi et al., 2012], but can potentially provide useful information on tropospheric BrO distributions [e.g., Zeng et al., 2003; 2006]. A particular challenge in this work was to define how useful information on ODE characteristics could be obtained from careful analysis of satellite BrO products while taking into account the uncertainties in these products. We describe the in situ measurement data, the retrievals of tropospheric BrO columns from satellite observations, and meteorological and back trajectory simulations in Section 2. Detailed analyses of these data are presented in Section 3. We discuss in Section 4 the feasibility of using available in situ BrO measurements to validate satellite column BrO products and the implications of our analysis results for satellite BrO product validation. Conclusions are given in Section 5.

2.2 Data description

2.2.1 In situ measurements: ozone and temperature

We used surface ozone measurements at three monitoring stations in the Arctic located in Barrow (71.3°N, 156.8°W), Alaska in the US [Oltmans and Levy, 1994] and Alert (82.5°N, 62.3°W), Nunavut in Canada [Anlauf et al., 1994], and Zeppelin mountain (78.9°N, 11.9°E) at Spitsbergen, Norway [Solberg et al., 1996]. All three sites are in coastal regions. The Barrow site (near the sea level) is located along the northern coast of Alaska and surrounded by the Chukchi Sea to the west and the Beaufort Sea to the north. The station, operated by the NOAA Earth System Research Laboratory (ESRL), has observed surface ozone since the 1970s. The Alert site (at 200 m above the sea level) is located on the northeastern tip of Ellesmere Island close to Greenland. The Canadian Air and Precipitation Monitoring Network (CAPMoN) of Environment Canada has collected surface ozone observations at this site from the 1990s. The Zeppelin (ZPL) mountain site is located at a fjord on a mountain ridge of 474 m altitude close to Ny-Ålesund, which is on the island Spitsbergen in the Norwegian Arctic Ocean. The Norwegian Institute for Air Research (NILU) started surface ozone measurements at this site in the 1989 and ODEs were often detected [Solberg et al., 1996; Bottenheim and Chan, 2006]. The optical technique using the strong UV absorption band [e.g., Oltmans et al., 2012] was used to measure ozone at all three sites. Hourly averaged ozone data were used in this study. The accuracy of ozone dataset is in the range of 0.5-2 ppbv [Helmig et al., 2007], adequate for the study. Surface temperature measurements at Barrow and Alert were obtained from the NOAA National Climatic Data Center (NCDC), and temperature measurements at ZPL were obtained from NILU.

Ozonesonde measurements were made during the ARCIONS campaign for April 1-20, 2008 [Thompson et al., 2011]. Balloons carrying the Electrochemical Concentration Cell (ECC) instrument were launched daily around local noontime at Barrow, Alaska in the US (71.3°N, 156.8°W), Resolute, Nunavut in Canada (74.7°N, 95.0°W), and Churchill, Manitoba in Canada (58.7°N, 94.1°W).

In spring 2008, aircraft measurements were made during two extensive field campaigns, the ARCTAS and ARCPAC experiments. Ozone was measured in situ by the chemiluminescence method on the NASA DC-8 [Jacob et al., 2010] and NOAA WP-3D [Brock et al., 2010] aircraft missions. Ozone and potential temperature data used in this study are from 7 DC-8 flights (on April 4, 5, 8, 9, 12, 16, and 17) and 5 WP-3D flights (on April 12, 15, 18, 19, and 21). The vertical distribution of ozone was also measured using the ultraviolet Differential Absorption Lidar (UV-DIAL) on DC-8 [Fenn et al., 1999; Browell et al., 2003]. The high-resolution (151 layers) UV-DIAL profiles of ozone provided additional cases of ODEs not detected by the in situ measurements. We analyze in situ and DIAL aircraft observations below 1 km where ODEs usually occurred.

2.2.2 In situ measurements: Bromine species

In situ bromine measurements from aircraft during the ARCTAS and ARCPAC experiments were used for the comparison with satellite-derived tropospheric BrO columns. We used in situ observations of BrO, soluble bromide, and Br_2+HOBr [Neuman et al., 2010; Liao et al., 2012b] in the lowest 2 km. BrO and Br_2+HOBr were measured by a chemical ionization mass spectrometer (CIMS) and soluble bromide by a mist chamber [Dibb et al., 2010]. Soluble bromide includes ~ 100 % of Br_2, HOBr, and HBr and 40% for BrO [Liao et al., 2012b]. The uncertainty of measurements is ±40 % with

detection limits of 2-5 pptv for BrO, ±15 %+0.5pptv for soluble bromide, and 15 %+2pptv for Br_2+HOBr [Neuman et al., 2010; Liao et al., 2012b].

2.2.3 Satellite measurements: Tropospheric BrO vertical column

Tropospheric BrO columns from satellite observations are good indicators of ODEs [e.g., Zeng et al., 2003; 2006]. We use the residual method [e.g., Zeng et al., 2003; Theys et al., 2011; Choi et al., 2012] to derive tropospheric vertical columns of BrO. In this method, we need the total vertical BrO columns retrieved from satellite sensors, estimates of the stratospheric BrO columns, and stratospheric and tropospheric air mass factors (ratio of the slant column to the vertical column at a given vertical range) calculated from a radiative transfer model. Tropospheric vertical columns of BrO are obtained by subtracting the estimated stratospheric columns from the satellite total vertical BrO columns, followed by air mass factor correction. We used the total vertical columns of BrO from two satellite instruments, the Ozone Monitoring Instrument (OMI, Aura satellite) [Kurosu and Chance, 2011] and the Global Ozone Monitoring Experiment 2 (GOME-2, MetOp satellite) [Begoin et al., 2010]. We did not use tropospheric BrO columns at latitudes higher than 85° north since the uncertainty of retrieval is very large due to large solar zenith angles [Richter et al., 1998; Zeng et al., 2003; Choi et al., 2012].

Retrievals of tropospheric BrO columns from satellite measurements are quite uncertain, particularly in the estimate of stratospheric BrO columns [e.g., Choi et al., 2012]. During our analysis period, in situ BrO observations are too limited and they do not provide enough quantitative constraints to validate satellite tropospheric BrO column products (the details will be discussed in Section 4). This lack of quantitative validation, however, does not imply that satellite BrO measurements do not provide useful

information in the analysis of the ODE characteristics. For example, if ODEs were driven by BrO chemistry, we expect that the air mass of an ODE had encountered high BrO previously. The question to analyze is, therefore, whether or not there is an enhancement of BrO along the back trajectory of the ODE air mass. A key point here is that the enhancement can be relative to BrO measurements in other regions. We do not necessarily need the absolute magnitude of BrO column or concentration. The appropriate statistical method is correlation analysis between BrO along the air mass back trajectory and ozone. In correlation analysis, it is the variation not absolute magnitude that matters.

In order to take into account the uncertainties in the estimates of stratospheric BrO vertical columns, we use three different estimate methods. These methods give different estimates of latitudinal/longitudinal variations in stratospheric BrO column and consequently in tropospheric BrO column. Most importantly, the estimated stratospheric BrO columns using these methods are independent from one another and should not introduce an unphysical correlation with tropospheric ozone. Consequently the uncertainty in the retrieval method can reduce or even eliminate the (anti)correlations between ozone and BrO, but it should not produce false correlations consistently.

If we can establish consistent (anti)correlations between ozone and time-lagged tropospheric BrO, we should be able to learn characteristics of ODEs from the correlation information without the need to know if the magnitudes of tropospheric BrO columns are correct. In fact, even the values of (anti)correlations between ozone and BrO are not that important. It is the change of the (anti)correlation between ozone and BrO with time or

altitude that provides useful information on the importance of in situ chemistry relative to transport and on the vertical extent of bromine-driven ozone loss.

The three methods we chose in this study to estimate stratospheric BrO columns from satellite measurements are as follows. The first one is the 20th percentile method, in which we assume that the lowest 20th percentile among all total BrO vertical columns of each 80-km latitude bin is the stratospheric BrO column. In this estimate, the longitudinal variations of satellite observed BrO columns are assumed to reside all in the troposphere. In the other two estimates, we include longitudinal variations of stratospheric BrO columns. In the second estimate, we derive stratospheric BrO columns using BrO profiles from limb measurements of the SCanning Image Absorption Spectrometer for Atmospheric Cartography (SCIAMACHY) measurements [Sinnhuber et al., 2005; Rozanov et al., 2011]. Here, the stratospheric BrO data of version 3.2 provided by the Institute of Environmental Physics, University of Bremen [Rozanov et al., 2011] are used. The averaging kernels imply that the BrO profile measurements from SCIAMACHY are sensitive down to about 15 km altitude. Therefore, we estimate stratospheric BrO profile below 15 km by extrapolation as follows: Since the SCIAMACHY limb sounding is sparse we use the mean BrO profile for latitude bins of 10 degrees. We assume the stratospheric BrO mixing ratio profile to be a second-order polynomial function of altitude. We then extrapolate the polynomial fit obtained between 15 and 33 km to the tropopause. We integrate the obtained BrO profile from the tropopause to the upper limit of SCIAMACHY BrO profile (33 km). We use the reanalysis data from the National Center for Environmental Prediction/National Center for Atmospheric Research (NCEP/NCAR) [Kalnay et al., 1996] to calculate the

tropopause height. Hereafter, we refer to these stratospheric BrO columns as the SCIA2ND method. In the third approach, we estimate the stratospheric BrO columns calculated by the Regional Air Quality Modeling System (RAQMS) by zonal scaling such that the zonal mean values match the estimates from the 20th percentile method since RAQMS estimated stratospheric columns are too low compared to the previous two methods. By subtracting 3 sets of stratospheric column estimates from the total columns of OMI and GOME-2, we obtain 6 sets of tropospheric BrO columns (OMI-20th, OMI-SCIA2ND, OMI-RAQMS, GOME-2-20th, GOME-2-SCIA2ND, and GOME-2-RAQMS).

The in situ aircraft observations of BrO, Br_2+HOBr, and soluble bromide are used to investigate to what extent satellite products capture the distributions of lower tropospheric BrO. To correlate with tropospheric BrO columns, we integrate in situ aircraft observations of BrO, Br_2+HOBr, and soluble bromide from the surface to 7 altitude levels (100, 300, 500, 750, 1000, 1500, and 2000 m), respectively. The vertical profile of correlation coefficients between these integrated concentrations of bromine compounds and retrieved tropospheric BrO columns are calculated (see the Appendix A).

The analysis does not quantify the uncertainties in the derived tropospheric BrO columns, but the large separation of correlation coefficients indicates that the products have different characteristics. As discussed previously, the uncertainty of satellite retrievals can affect the (anti)correlations between ozone and BrO. The six products generally show reasonably good consistency in the correlations between ozone and BrO as we will discuss in Section 2.3. For simplicity, we show in the paper only the analysis results using the GOME-2-SCIA2ND product, which has the highest correlations with in

situ measurements of bromine compounds used in this study. The analysis results using the other five products are shown in the Supplement.

2.2.4 Back trajectory simulations

We used back trajectory calculations to investigate transport patterns for ODE regions. Back trajectories were computed using a kinematic model [Arimoto et al., 2008] based on meteorological simulations by the polar version of PSU/NCAR mesoscale model (MM5) [Bromwich et al., 2001], which was constrained by the NCEP global final analysis (FNL) grid data and DC-8 aircraft measurements. The details of polar MM5 model setup were described in Zeng et al. (2006). 5-day back trajectories were calculated every 10 minutes at the surface sites (10 m above the ground) and at the altitudes of ozonesonde and aircraft measurements.

2.3 Results and discussions

2.3.1 Diurnal ozone cycle

Observed ODEs can occur due to in situ bromine chemistry or transport of air mass with depleted ozone from another region. We first investigate the surface ozone observations at Barrow, Alert, and ZPL, which have better temporal coverage than ozonesonde or aircraft measurements.

Figure 2.1 shows the time series of surface ozone mixing ratios at Barrow, Alert, and ZPL in April 2008. All three sites have several ODEs during the analysis period, but ODEs at Barrow are the most frequent. To illustrate how the diurnal cycles of ODEs may differ from non-ODE days, we show the diurnal patterns of the 10th, 25th, 50th (median),

75th, and 90th percentile of hourly ozone at the sites. Also shown is the diurnal solar elevation. For ozone above the 50th percentile, we see no clear diurnal patterns. For 25th percentile and particularly 10th percentile ozone, there is an increasingly clear diurnal pattern at Alert, lower at high solar elevations and higher at night. While more detailed bromine chemistry simulation is needed to understand the particular shape of the diurnal pattern, it is consistent with daytime bromine-driven ozone loss and nighttime recovery (by transport). In contrast, the diurnal patterns of 10th and 25th percentile ozone at Barrow are similar to those of higher-percentile ozone, which do not show a clear diurnal cycle. The 10th and 25th percentile ozone at ZPL shows larger diurnal variations than the higher-percentile ozone, but they are not as distinct as at Alert. These results indicate that in situ chemistry is more important at Alert and potentially so at ZPL but transport of ozone-poor air is more important at Barrow. We examine how transport patterns at the three sites differ.

2.3.2 Transport patterns and BrO distributions

We use back trajectory analysis to define the transport patterns. However, we also need information on the source regions of ozone-poor air masses. Since BrO enhancements indicate local ozone losses [Zeng et al., 2003; 2006], tropospheric BrO vertical columns from satellite measurements were used to estimate the source region of ozone-poor air mass in the Arctic. Figure 2.2 shows the monthly mean distribution of tropospheric BrO columns in April 2008. We can identify two high-BrO regions over the Chukchi Sea and the Canadian archipelago. Transport of ozone-poor air mass from these two regions could contribute to the observed ODEs.

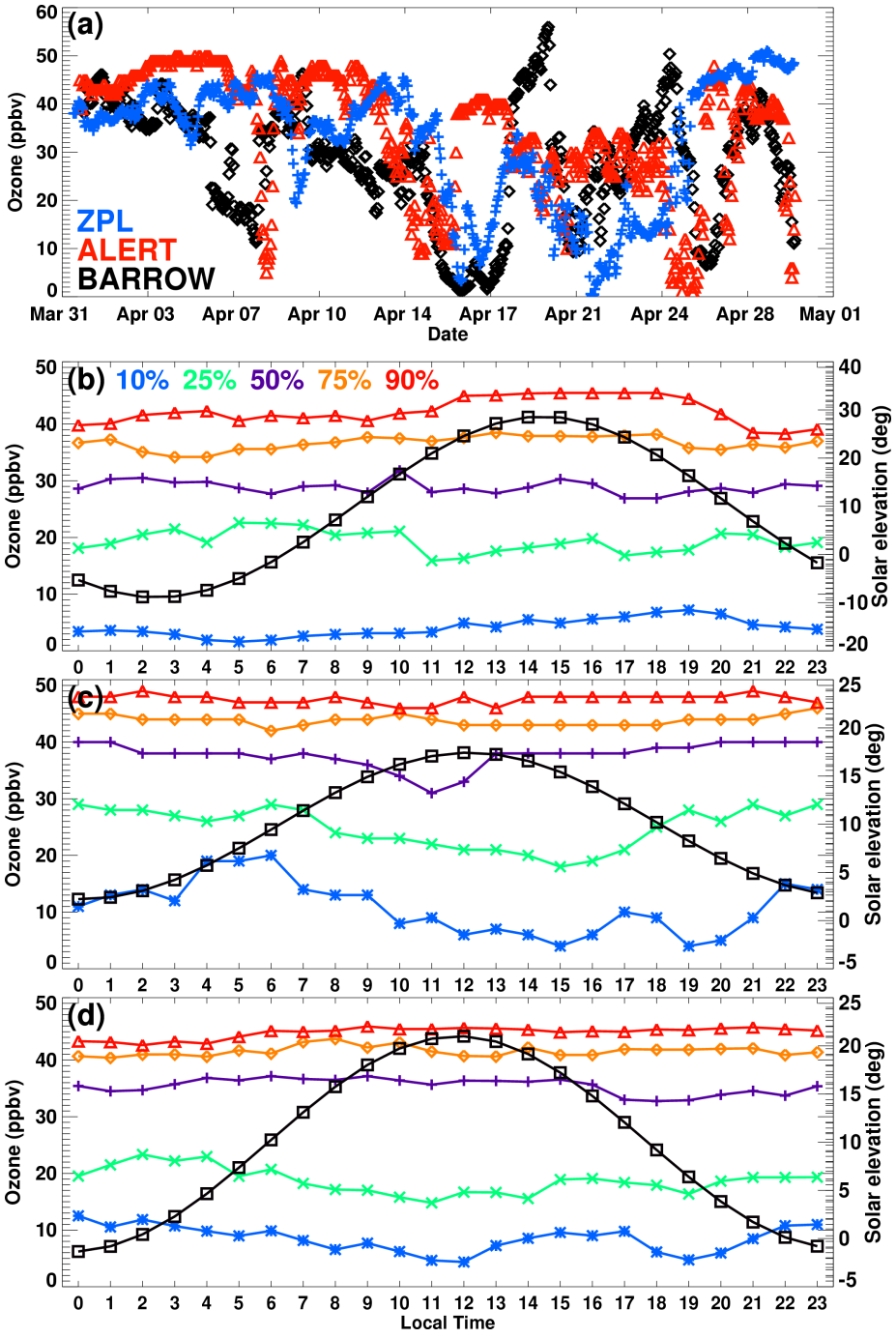

Figure 2.1 (a) Time series of surface ozone concentrations in April 2008 at Barrow (black), Alert (red), and ZPL (blue), and the diurnal variations of surface ozone in percentiles of 10, 25, 50, 75, and 90% at (b) Barrow, (c) Alert, and (d) ZPL. To compute the ozone value for a given percentile, we bin the observations in a given hour together (30 data points in the hourly bin in April). We then calculate the percentile values in the hourly data bins. The 10th percentile value means that 90% of the data points are higher than this value in a data bin. The black line in panels (b), (c), and (d) shows the monthly mean solar elevation.

We examine the relationships between ODEs and the air mass history of BrO exposure using 5-day back trajectories calculated from the polar MM5 simulations and tropospheric BrO vertical columns. We first computed tropospheric BrO vertical columns along the back trajectory using BrO measurements in the past 5 days. We then computed the correlations between hourly surface ozone concentrations and BrO vertical columns for the day of ozone observations (D-0) and the previous ith day (D-i), where i=1…5. [e.g., Parrish et al., 2010]. These coefficients are then averaged to obtain the daily mean values for D-i (i=0…5). In this type of time-delayed correlation analysis, the R value is calculated under similar conditions except for the time shift. Therefore, the change of R value as a function of time is the most important.

Figure 2.3 shows the time-lagged daily mean correlation coefficients between ozone and 6 tropospheric BrO vertical column products at the three surface sites. As we previously discussed in Section 2.2.2, the uncertainties in the estimates of tropospheric BrO columns introduce noise into the correlation analysis that can reduce the correlation between ozone and column BrO. This effect appears to be a function of the strength of the correlation as well. Since the correlation (R value) is a function of covariance between ozone and tropospheric column BrO, ODEs clearly drive the ozone variance at these sites, implying that the (anti)correlation is higher from the dataset with more variance. The number of hours and the duration of ODEs at Alert and ZPL are less than that at Barrow (Figure 2.1). The highest (anti)correlation is indeed found at Barrow. The six estimates of tropospheric BrO columns show consistent results at this site. At ZPL, five of the six column BrO estimates show consistent correlation changes as a function of time lag except for OMI-RAQMS, which has the lowest correlation with DC-8 BrO

measurements (see the Appendix A.10). At Alert, the agreement among six tropospheric BrO columns is poor, due in part to a smaller number of ODEs (Figure 2.1) and hence a lower (anti)correlation between ozone and column BrO and in part to the larger uncertainties in the tropospheric BrO column estimates at high latitude locations [Zeng et al., 2003; Choi et al., 2012].

At ZPL, the (anti)correlations are usually the largest in D-0 or D-1, indicating a strong local influence. The results for Alert are ambiguous, although the general pattern of stronger D-0 and D-1 (anti)correlations is consistent with the diurnal change of 10th and 25th percentile ozone discussed in the previous section. At Barrow, however, the (anti)correlations for D-1, D-2, and D-3 are stronger than D-0, suggesting a more significant transport effect than at the other two sites.

To demonstrate the change of transport patterns associated with ODEs, we show the patterns of two-day back trajectories for ODE (ozone mixing ratio < 20 ppbv) and non-ODE cases separately (Figure 2.4). The largest transport difference is found at Barrow, suggesting a significant transport effect. During ODE periods, the air mass usually comes from the Chukchi Sea (the northwest of Barrow) where tropospheric BrO columns are high (Figure 2.2). During non-ODE periods, however, air mass comes from the Beaufort Sea where we did not find the enhancement of tropospheric BrO. The patterns of back trajectories for ODEs and non-ODEs are similar at Alert, consistent with the dominating effect of local chemistry (Figures 2.1 and 2.3). At ZPL, the patterns of back trajectories for ODEs and non-ODEs are different but the difference is not as large as at Barrow. The ODE cases at this site are associated with transport from the northwest, but the non-ODE cases do not have a clear transport direction.

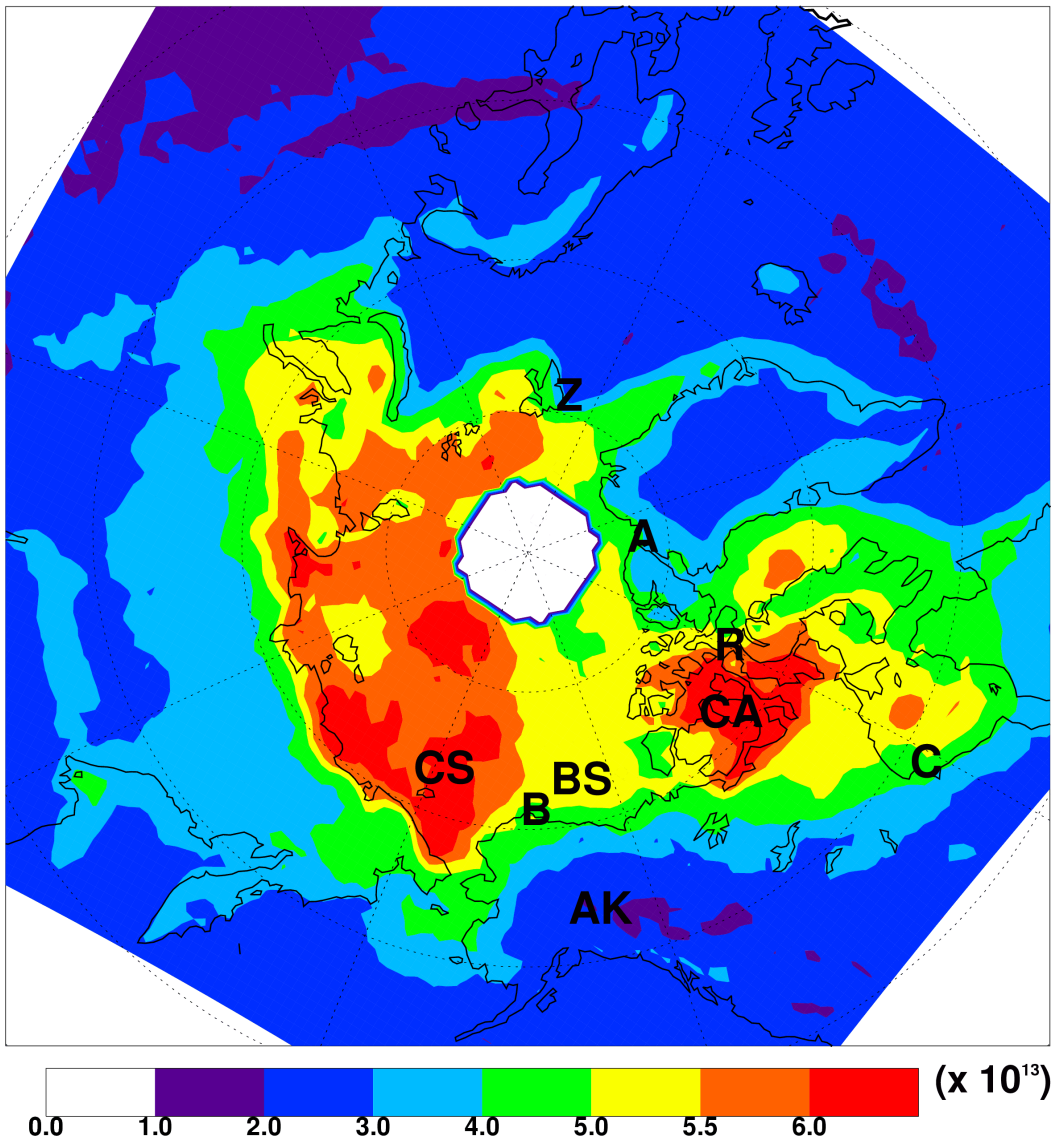

Figure 2.2 Monthly mean tropospheric BrO vertical column density (VCD, molecules/cm2). "A" denotes the location of Alert, "B" for Barrow, "C" for Churchill, "R" for Resolute, and "Z" for Zeppelinfjellet (ZPL), "CA" for Canadian Archipelago, "CS" for Chukchi Sea, "BS" for Beaufort Sea, and AK for Alaska. The GOME-2-SCIA2ND result is shown representatively. Results for OMI-SCIA2ND, GOME-2-20th, OMI-20th, GOME-2-RAQMS, and OMI-RAQMS BrO VCDs show similar distribution patterns (See Appendix A.5).

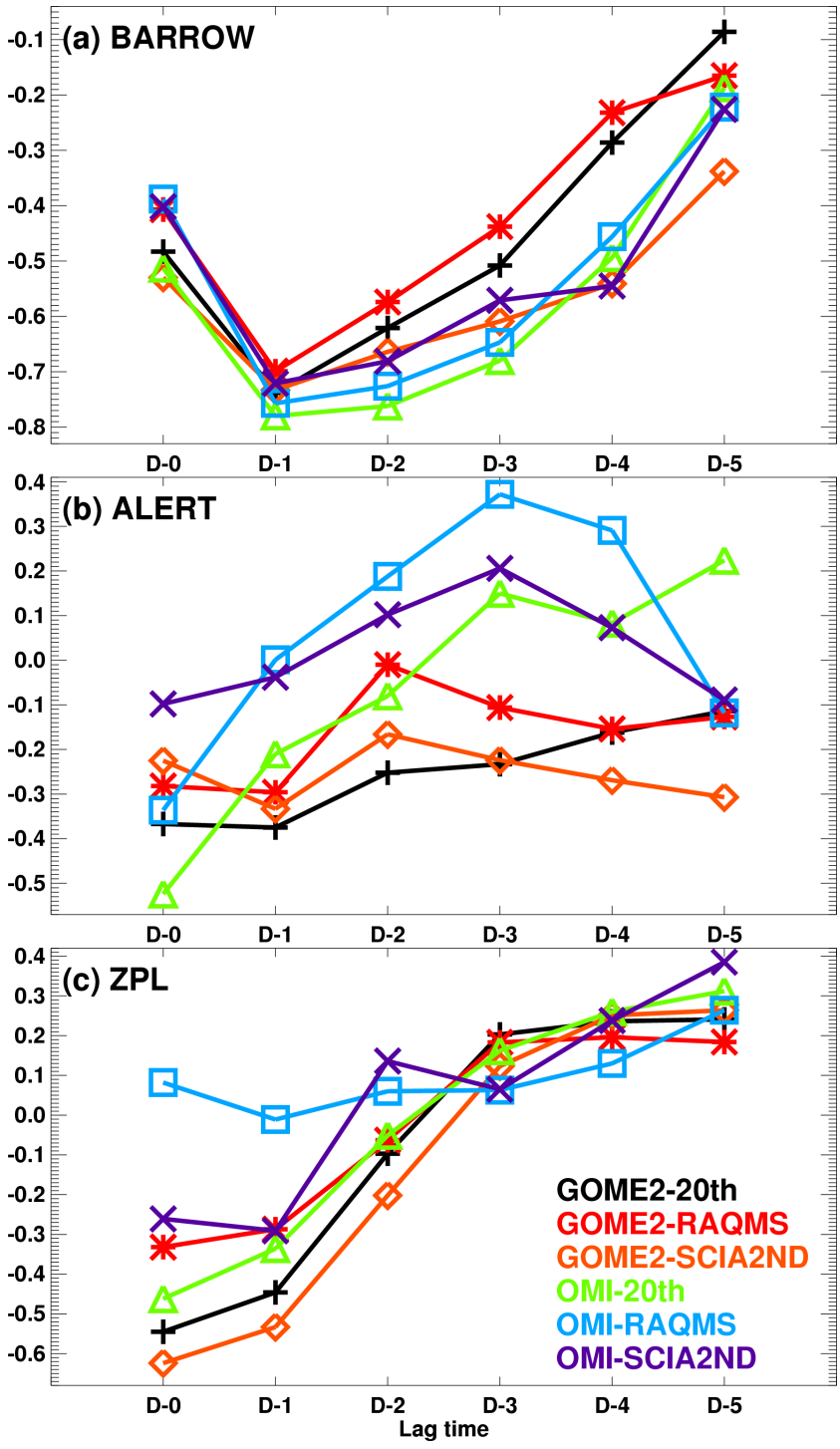

Figure 2.3 Time-lagged daily mean correlation coefficients (R values) between surface ozone and tropospheric BrO VCD at (a) Barrow, (b) Alert, and (c) ZPL. D-i denotes ozone correlation with BrO VCD taken along the back trajectories on the previous ith day (see text for details). We used six tropospheric BrO VCD estimates, GOME-2-20th (black), GOME-2-RAQMS (red), GOME-2-SCIA2ND (orange), OMI-20th (green), OMI-RAQMS (blue), and OMI-SCIA2ND (violet).

We obtained additional information by analyzing aircraft (NASA DC-8 and NOAA WP-3D) observations, which provide better regional coverage than surface sites. We found 34 ODE cases (9 from in situ measurements on DC-8, 12 cases from in situ measurements on WP-3D, and 13 cases from DC-8 UV-DIAL measurements), including 17 strong ODEs and 17 partial ODEs. Since the aircraft measurements cannot provide a time series of ozone at a given location, the correlation analysis of Figure 2.3 cannot be performed with aircraft data. Instead, we calculated daily averaged BrO tropospheric columns along the two-day back trajectories (Figure 2.5). Strong ODEs usually take place near the Chukchi Sea, a region with high tropospheric BrO columns. Note that the mean BrO column during the period of ARCTAS and ARCPAC experiments is shown in Figure 2.5. However, partial ODEs are found over not only the Chukchi Sea, but also the Beaufort Sea. Partial ODEs over the Beaufort Sea are usually affected by transport from the Canadian Archipelago, another region of enhanced tropospheric BrO columns. On average, strong ODEs encountered higher tropospheric BrO columns than partial ODEs. The back trajectory results also show that the average BrO column encountered by ODEs and partial ODEs is highest at the day of measurement and decreases rapidly along the back trajectory in the previous 1-2 days, implying that transport is not as large a contributor as in situ chemical loss to the observed ODEs.

The northern region of Alaska appears to be affected mostly by ozone-poor air masses originating from the Chukchi Sea. Transport from the Canadian Archipelago that also had high BrO loading does not contribute to ODEs significantly in this region. Previously, Zhao et al. (2008) and Begoin et al. (2010) also showed that the Chukchi Sea is the dominant source of ozone-poor air mass with high tropospheric BrO and transport

from this region may affect surface monitoring sites at northern high latitudes. In general, both aircraft and surface measurements (at Barrow) suggest that the duration of transport effects is within 2 days.

These findings do not rule out the existence of the large scale and long-range transport of ozone-poor air mass in the Arctic spring found by Bottenheim et al. (2009) and Jacobi et al. (2010). One possible explanation for the lack of evidence of long-range

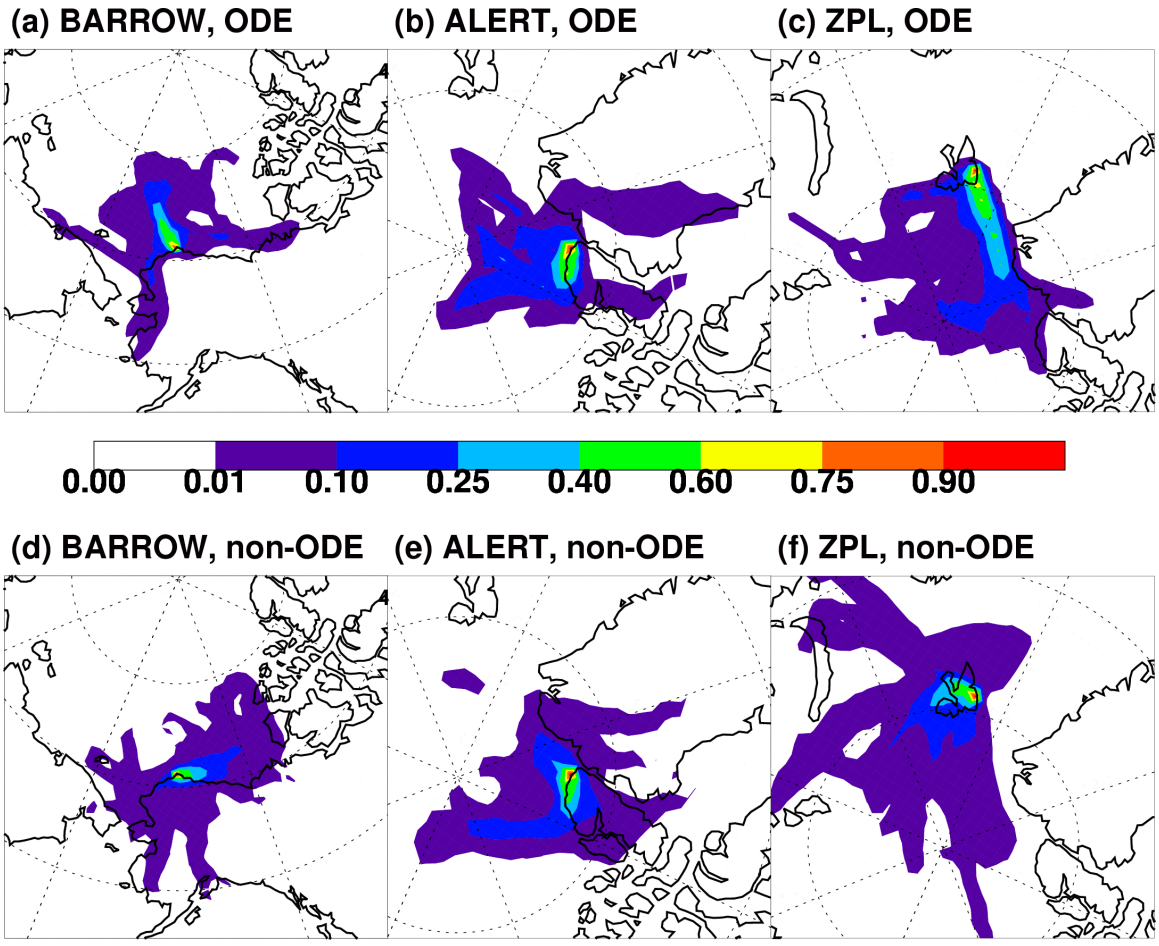

Figure 2.4 Transport patterns using two-day back trajectories at (a) Barrow for ODEs, (b) Alert for ODEs, (c) ZPL for ODEs, (d) Barrow for non-ODEs, (e) Alert for non-ODEs, and (f) ZPL for non-ODEs. Color shows the probability of back trajectories passing through the grid box.

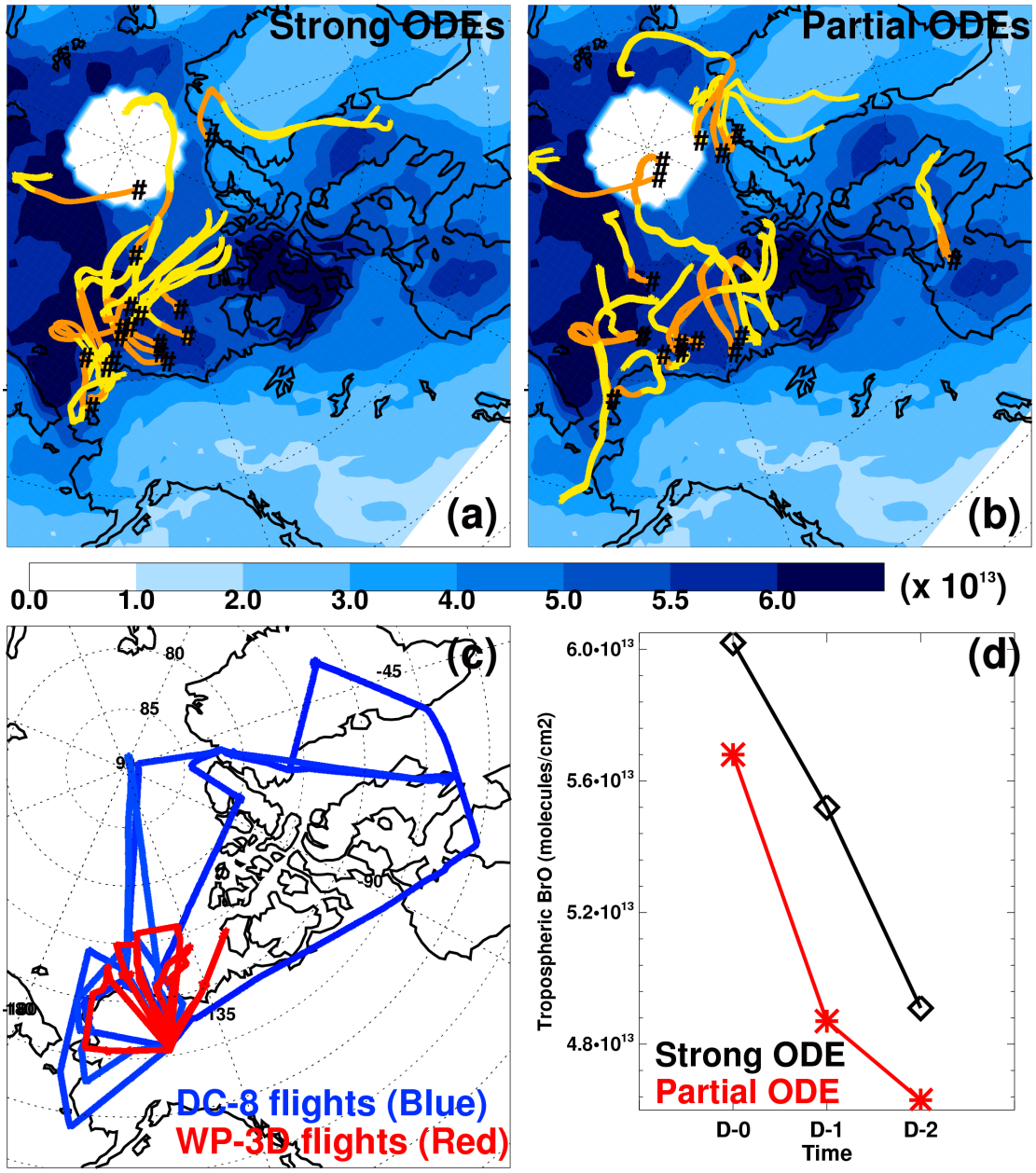

Figure 2.5 Two-day back trajectories for (a) strong ODEs and (b) partial ODEs in aircraft measurements, (c) aircraft flight tracks, and (d) averaged tropospheric BrO columns along the back trajectories during strong and partial ODE periods. In panels (a) and (b), orange lines denote back trajectories up to 1 day, and yellow lines for 1-2 days prior to the time of ozone measurements. The average BrO columns during the period of aircraft measurements (from April 1 to 21) are also shown in panels (a) and (b) with blue color shading. In panel (d), we averaged tropospheric BrO VCDs along the back trajectories with 0-, 1-, or 2-day time delays. The GOME-2-SCIA2ND BrO VCDs are used here. Results using OMI-SCIA2ND, GOME-2-20th, OMI-20th, GOME-2-RAQMS, and OMI-RAQMS BrO VCDs show similar patterns (See the Appendix A.6-10).

transport in this study is that we did not observe ODEs lasting as long as what was found in these two previous studies (Figure 2.1). The large scale and long-range transport of low-ozone air mass would result in local ODEs lasting a few days. Since these two previous studies did not have a quantitative proxy for BrO concentrations, the method we developed in this study could be used to quantify the time lag between the occurrence and the time of observation of an ODE.

2.3.3 The influence of temperature on ODEs

There are indications that ozone depletion is stronger in cold conditions [e.g., Zeng et al., 2003; Pöhler et al., 2010; Nghiem et al., 2012]. Recently, Seabrook et al. (2011) reported DIAL observations of ODEs at 60-700 m from 9 March to 2 April 2008 in the Amundsen Gulf (71°N, 121–124°W). They found a general correlation of ODEs with low temperature and that all ODEs occur below -25°C. For the purpose of comparison, we show in the supplement (see the Appendix A.11) the relationship between ozone and temperature at Barrow, which is located at the same latitude as the Amundsen Gulf. While most of the ODEs in February occurred at temperature lower than -25°C, a significant portion of ODEs in March occurred at temperature warmer than -25°C. ODEs in April and May are associated with even warmer temperatures (<-8°C in April and <-3°C in May, not shown).

The warming trend in spring could potentially mask the relationship between ODE and temperature. In our investigation of this relationship, we first removed the linear trends in temperature and ozone, and then computed linear correlations between de-trended daily surface ozone and temperature at Barrow, Alert, and ZPL (Figure 2.6).

We also show the correlations between aircraft measured ozone and potential temperature (0-1 km). Potential temperature is used for aircraft measurements to account for temperature variations with altitude. Since the effect of temperature on ozone will likely take time to develop, we used daily average for the surface data and the average of each ODE encounter for aircraft data. Significant correlations (R=0.63-0.80) are obtained for the three surface sites. Despite the large spatial coverage of aircraft data, where surface and transport conditions vary, a moderate correlation (R=0.51) is still obtained between ozone and potential temperature.

Mechanisms responsible for the observed positive correlations between ozone and temperature have been proposed in the literature. The formation of a stable boundary layer could be a necessary condition to reduce the exchange of ozone-depleted air mass with ozone-rich air mass above the inversion layer [Tarasick and Bottenheim, 2002; Lehrer et al., 2004], and to enhance the efficiency of ozone depletion by bromine [Jacobi et al., 2010]. Pöhler et al. (2010) proposed, on the other hand, that open ocean surface is warmer than the ambient atmosphere in the Arctic spring. When cold air mass moves over the open leads, the increased temperature gradient enhances the atmospheric exchange allowing a greater release of bromine from the ocean to the atmosphere, which leads to more frequent ODEs.

Another question yet to be answered is if there exists a threshold of temperature below which ODEs tend to occur. ODEs often occur at temperatures < -20 °C [Tarasick and Bottenheim, 2002]. We discussed previously the more recent DIAL observations of a threshold temperature value of -25 °C by Seabrook et al. (2011). Examining surface and aircraft measurements in this analysis or the observations at Barrow since 1979, we did

not find a clear threshold value of temperature for the occurrence of ODEs. This result is consistent with other recent studies [Bottenheim et al., 2009; Jacobi et al., 2010; Neuman et al., 2010]. Our analysis indicates that a potentially important parameter is temperature variation, i.e., ODEs tend to occur during periods of decreasing temperature [Zeng et al., 2003]. The temperature variation could be a reflection of the pressure change related to the change of synoptic conditions [Jacobi et al., 2010]. However, the proposed mechanism of a large-scale pool of ozone-poor air mass coupled with a stable boundary layer and long-range transport does not seem to apply to the observations presented in this study because the durations of ODEs in this study are much shorter than those analyzed by Jacobi et al. (2010) and the ODEs are either in situ or enhanced by short-range (1-2 days) transport.

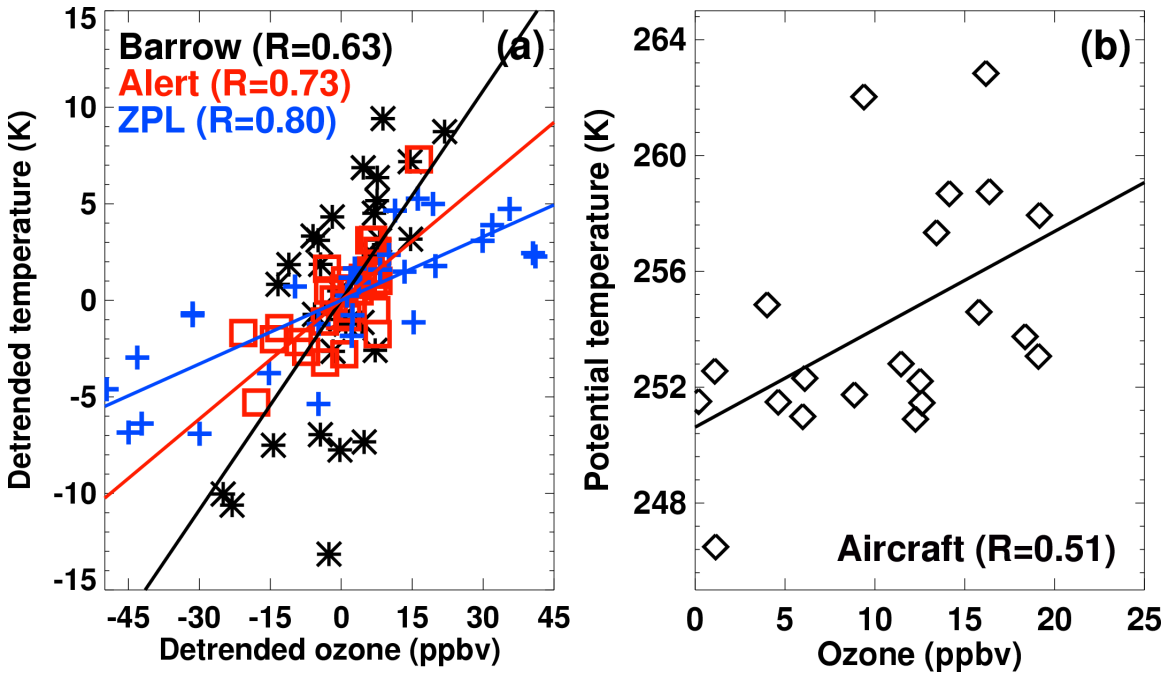

Figure 2.6 (a) Correlations between the de-trended daily average ozone and temperature at Barrow (black), Alert (red), and ZPL (blue), and (b) correlations between average ozone and potential temperature for ODEs in aircraft measurements.

2.3.4 Vertical structure of the ODEs

Previous studies reported that Arctic ODEs could occur above the boundary layer [Tarasick and Bottenheim, 2002; Zeng et al., 2006] up to 1500 m [Strong et al., 2002]. The large vertical extent of an ODE can be driven either by an equally deep BrO layer or by mixing with ozone-depleted air masses from the boundary layer. We make use of the extensive ozonesonde measurements at three sites, Barrow, Resolute, and Churchill during the ARCIONS campaign to examine the vertical structure of the ODEs.

We first compare the vertical profiles of the ozone and temperature for ODE and non-ODE cases (Figure 2.7). The vertical extent of ODEs varied greatly by site. At Barrow, ozone increases rapidly above 200 m. Similarly the average depth of ODEs at Resolute is about 300 m, although the increase of ozone with altitude is not as drastic as in Barrow at 200 m. In contrast, weak ODEs at Churchill extend almost uniformly to about 800 m similar to previous ODEs observed up to 2km altitude in this region [Ridley et al., 2003]. More striking is the difference of ozone profiles between ODE and non-ODE cases. At Churchill, the difference extends to 2 km. At Resolute, large differences are seen up to 800 m and small difference also extended to 2 km. Only at Barrow, the difference disappeared above 1 km.

In contrast to the ozone profiles, ODE cases have lower temperature than non-ODE cases at all three sites up to 2 km. The largest temperature difference is at Churchill. We also show the temperature lapse rate (dT/dz) in Figure 2.7 to examine the vertical stability of the boundary layer. At Barrow and Resolute, a clear temperature inversion (positive lapse rate) layer of 400 m forms not near the surface but above 200 m during ODEs. The temperature inversion layer at Resolute is 100-300 m higher than at Barrow,

leading to a deeper ODE layer at the site than in Barrow. During non-ODE periods, the inversion is weaker at both sites. Analysis in the previous sections suggests the influence of transport of ozone-poor air mass to Barrow, and the strong inversion layer during ODEs is essential to suppress mixing from above and to maintain low ozone below the temperature inversion layer.

The latitude of Churchill (58.7°N) is lower than the other surface and ozonesonde sites, and the regions sampled by aircraft. We find a very different vertical temperature structure at this site from Barrow and Resolute. The surface temperature gradient is about -10 K/km, implying strong vertical mixing. From surface to 2 km, there is no temperature inversion layer during ODEs, although an isothermal layer existed at around 1.2 km. In general, the thermal stability is weaker during ODE than non-ODE cases up to 700 m, which is opposite to Barrow and Resolute. The effect of vertical mixing is reflected in the consistent ozone difference between ODE and non-ODE cases up to 2 km.

We showed in Figure 2.6 positive correlations between ozone and temperature during ODEs in surface and aircraft observations. Here we calculated the linear correlations between ozone and potential temperature from the ozonesonde measurements. Figure 2.8 shows the vertical profiles of linear correlations at Barrow, Resolute, and Churchill. At Barrow, below the thermal inversion layer, a large positive correlation is found ($R > 0.6$). Above the inversion layer, R values decrease rapidly. At Resolute and Churchill, however, the positive correlation ($R > 0.6$) extends to > 2 km and ~ 1.5 km, respectively. It is interesting to note that at all three sites the correlation increases with altitude from the surface in the lower 300 m, reflecting in part the increasing thermal stability away from the surface (Figure 2.7).

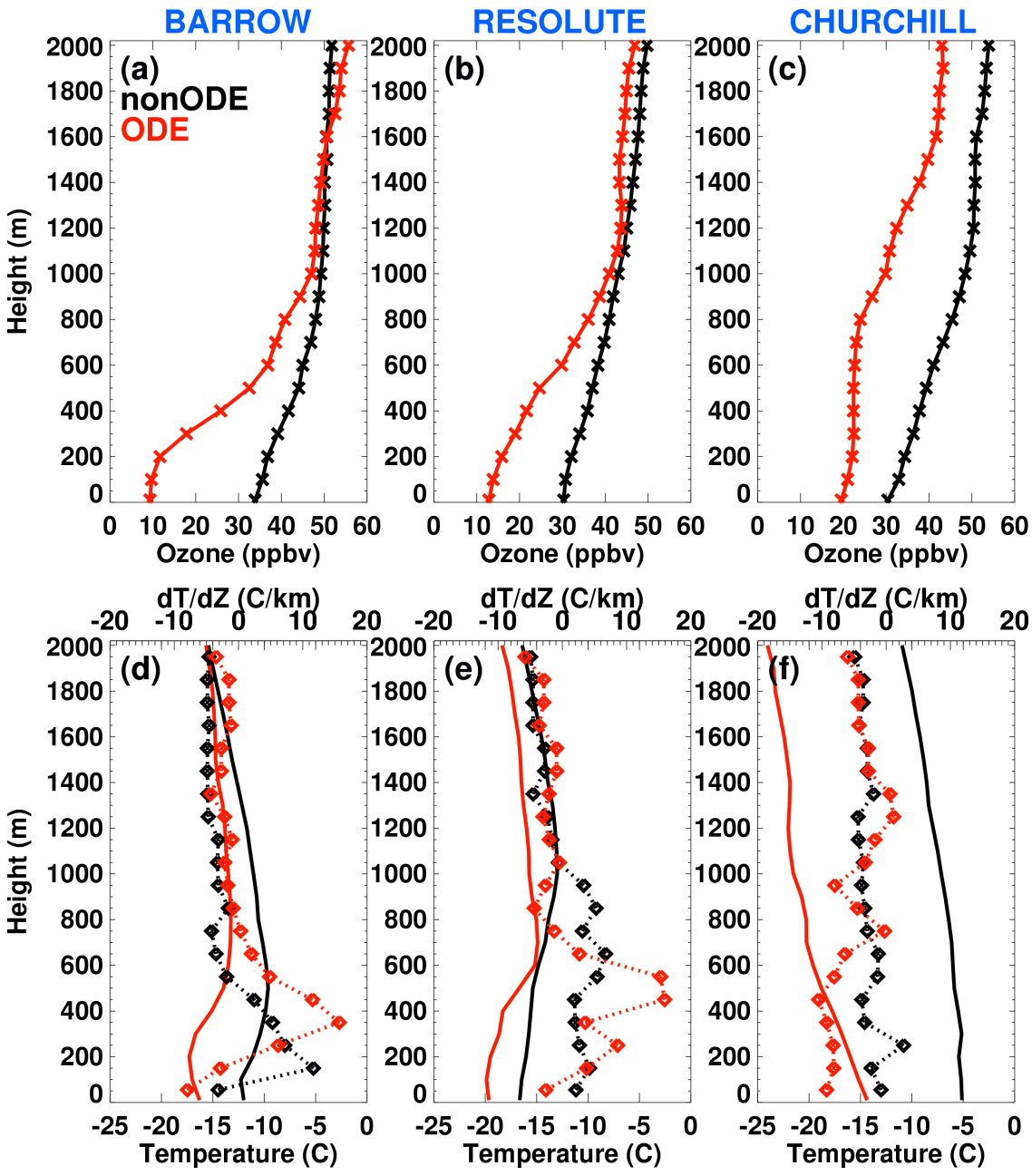

Figure 2.7 Mean vertical profiles of ozone in the top row, and temperature (solid lines) and its lapse rate (dashed lines) in the bottom row for ODE (red) and non-ODE (black) periods in the ARCIONS campaign at Barrow, Resolute, and Churchill (Section 2.1.1). ODEs were observed for 6 days at Barrow and Resolute, and 2 days at Churchill.

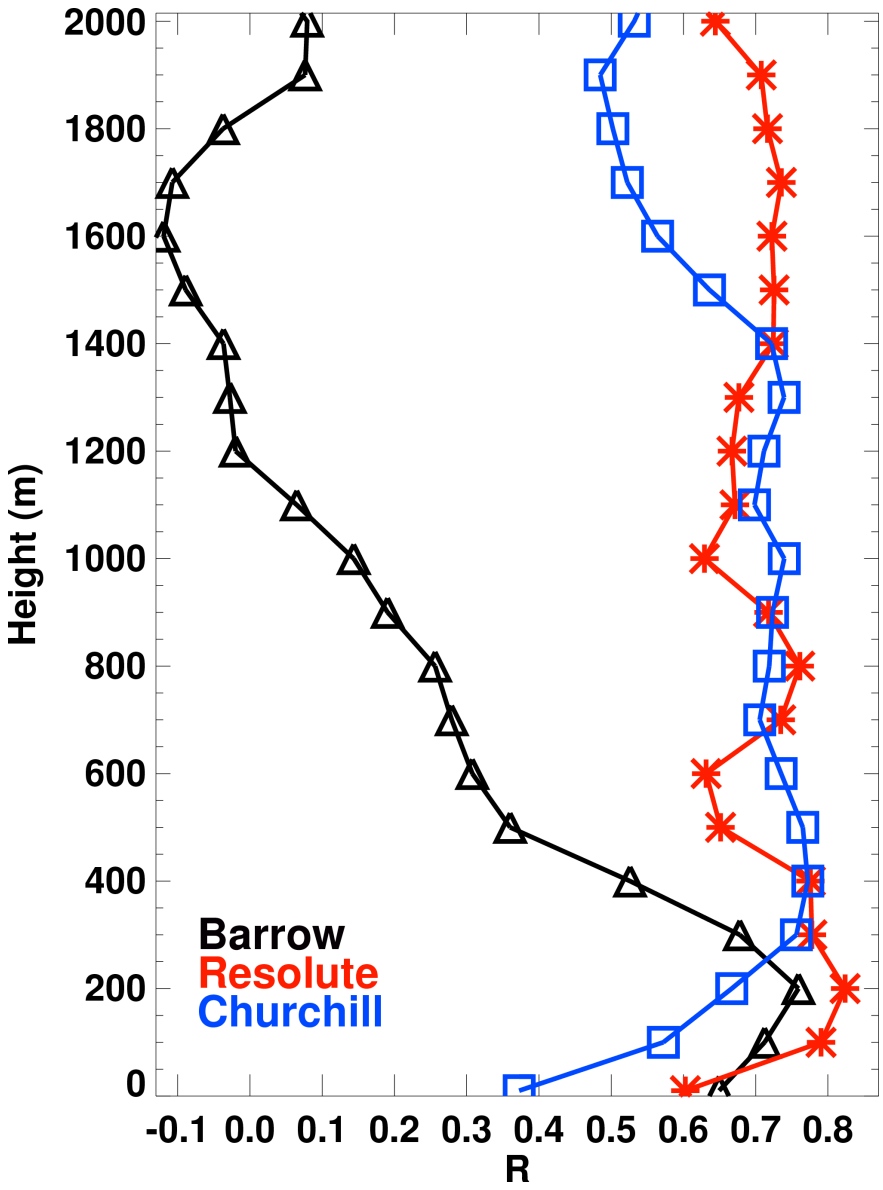

Figure 2.8 Vertical profiles of linear correlation coefficients (R values) between potential temperatures and the ozone data measured by ozonesonde in the ARCIONS campaign at Barrow (black), Resolute (red), and Churchill (blue).

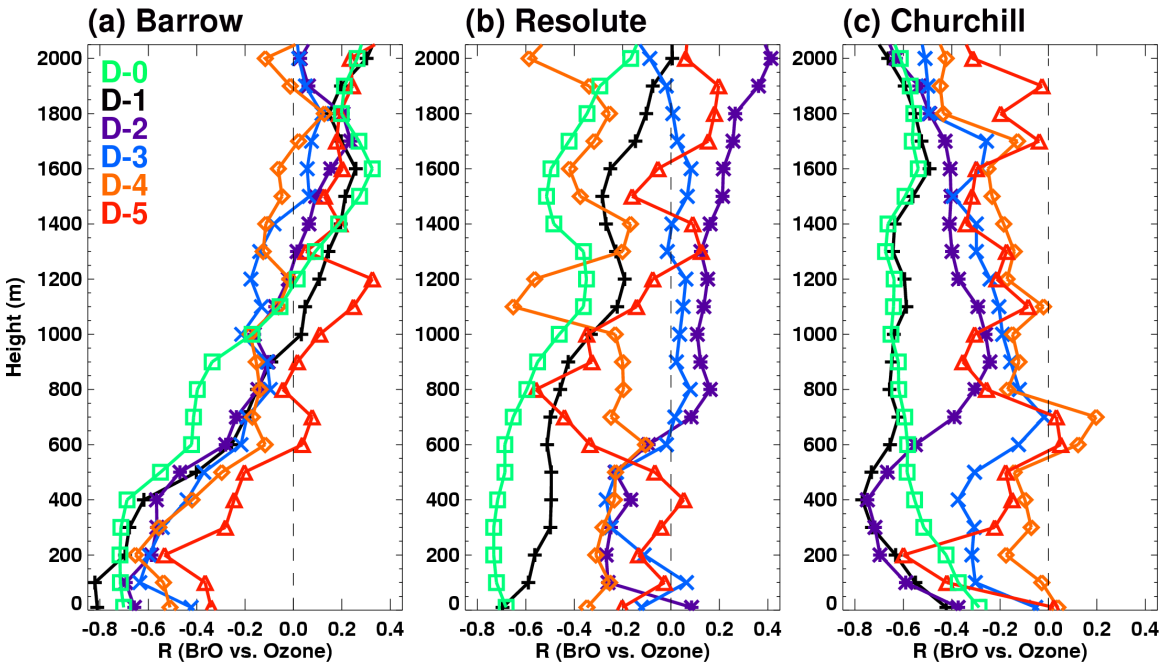

Figure 2.9 Vertical profile of linear correlation coefficients (R values) between time-lagging tropospheric BrO VCDs (D-0, D-1, D-2, D-3, D-4, and D-5) and ozone data measured by ozonesonde at (a) Barrow, (b) Resolute, and (c) Churchill. The GOME-2-SCIA2ND BrO VCDs are used here. Results using OMI-SCIA2ND, GOME-2-20th, OMI-20th, GOME-2-RAQMS, and OMI-RAQMS BrO VCDs show similar patterns (see the Appendix A.12-16).

Ozonesonde measurements provided additional information not available from surface and aircraft data. We investigate now if and how tropospheric BrO columns relate to the vertical structure of ODEs. Similar to the analysis in Section 2.3.1, the temporal correlations between time lagged (D-0 to D-5) BrO columns and ozonesonde measurements in the ARCIONS campaign were calculated at a given altitude from the surface to 2 km. Figure 2.9 shows vertical profiles of correlation coefficients at Barrow, Resolute, and Churchill. At Barrow, a strong negative correlation near the surface is consistent with the analysis using surface ozone measurements (Figure 2.3). The 1-day delayed BrO column has the largest negative correlation with ozone, implying the effect of short-range transport. The magnitude of negative R values decreases rapidly above 400

m, consistent with the ozone and thermal stability structure (Figures 2.7 and 2.8), suggesting that BrO driven ozone loss is limited to the shallow boundary layer [Tackett et al., 2007].

At Resolute and Churchill, the layer of significant negative correlation ($|r| > 0.5$) between ozone and BrO columns extends to ~ 1 km and 2 km respectively. In the altitude range of ODEs (Figure 2.7), the largest correlations are between concurrent ozone and BrO (D-0) data, suggesting that transport is not a significant factor for ODEs at Resolute. However, the correlation at Churchill is the largest with 1-day (D-1) or 2-day (D-2) delayed BrO below 600 m, indicating the effect of transport. Back trajectory analysis shows that the transport was from the Canadian Archipelago, a region with enhanced tropospheric BrO (Figure 2.2), which is consistent with findings during the TOPSE experiment [Ridley et al., 2003; Zeng et al., 2003]. Over the Hudson Bay, located near Churchill, substantial amount of iodine monoxide (IO) was observed [Mahajan et al., 2010], which may also contribute to the ODEs in this region.

The correlation analysis of ozone with potential temperature (Figure 2.8) and tropospheric BrO columns (Figure 2.9) suggests that the vertical extent of BrO-driven ozone loss is larger than that of ODEs (Figure 2.7). In particular, we find significant negative correlations between ozone and tropospheric BrO column in the free troposphere at Churchill. The strong negative correlation of ozone with current (D-0) or 1-day delayed (D-1) BrO extends from 600 m to 2 km altitude (Figures 2.7 and 2.9). In contrast, the negative correlation between ozone and tropospheric BrO column is weaker near the surface and has a longer time delay (1-2 days) in the unstable boundary layer. Convective transport of boundary layer BrO into the free troposphere is possible at this

site. McElroy et al. (1999) first reported the evidence of free-tropospheric BrO based on aircraft measurements, and hypothesized that the free-tropospheric BrO is lofted from the surface by the strong convection. Begoin et al. (2010) showed strong upward lifting up to 3 km over the high-BrO region in the Arctic.

2.4 Discussion of tropospheric column BrO retrieval validation

Retrievals of tropospheric BrO columns from satellite observations have large uncertainties. In order to deal with these uncertainties, we used 3 different methods to estimate the stratospheric BrO columns (including stratospheric BrO observations from SCIAMACHY) with two satellite products (GOME-2 and OMI) to produce 6 estimates of tropospheric BrO columns. Despite the difference of correlations with in situ measurements of bromine compounds (BrO, Br_2+HOBr, and soluble bromide), the satellite products showed generally consistent correlation characteristics with ozone measurements, i.e., the correlation change (not necessarily the correlation values) with time or altitude is consistent. One exception is in the correlation analysis of Alert surface ozone, indicating that applications of satellite column BrO to the high latitudes (> 80° N) require more careful scrutiny. The consistency in the diverse datasets of surface, ozonesonde, and aircraft ozone measurements implies that the estimated tropospheric BrO column can be effectively used to understand ODE characteristics in the Arctic spring.

An important question that we have not yet directly addressed is the feasibility of validating tropospheric column BrO estimates with in situ observations. We discuss here the constraints of in situ measurements on tropospheric column BrO estimates and the

implications for validating satellite BrO measurements. First, we point out that the analysis approach we used in this study is somewhat different from the work by Choi et al. (2012), who carried out detailed case studies. While providing rich information on selected cases, the selection of cases is subjective and can inadvertently lead to qualitative arguments difficult to ascertain quantitatively with available measurements. The analysis approach in this study is based on the correlation statistics using all the measurement data. It does not provide the rich context of a case study, but it provides a more robust quantitative measure for data validation. We chose to use the method of linear regression, for example, between satellite column and in situ measurements of BrO. One caveat in this type of data validation analysis is that there is only one degree of freedom left (a constant to adjust) when the correlation between the two datasets is good. In other words, it is usually not difficult to match the magnitudes of the two datasets when the correlation is good. When the correlation is not good, there is little reason to compare the magnitudes between the two datasets. The quality of correlation is therefore fundamentally more important for initial data validation than the magnitude comparison.

During the ARCTAS experiment, BrO measurements were available in only two flights on April 16 and 17. Previous studies [Choi et al., 2012; Liao et al., 2012b] showed good correlations between satellite retrieved BrO columns and in situ observations. Although we did not use the same satellite BrO product in this study, we found high correlations in several column BrO estimates (Figure A.1). In contrast, neither Choi et al. (2012) (Table 4 of their paper) nor this study found significant correlation between satellite retrieved tropospheric column BrO and in situ BrO observations from 5 ARCPAC flights (April 12, 15, 18, 19, and 21). The reason is unclear. We note that there

are 4 different estimates of stratospheric column BrO and two satellite total column measurements by combining Choi et al. (2012) with this study, which captures a reasonable range of variations for stratospheric column BrO estimates. The ARCTAS measurements were obtained further north, where there were a higher fraction of BrO measurements above the detection limit compared to the ARCPAC measurements. Without additional BrO measurements, a true validation study based on in situ BrO measurements is therefore infeasible.

One approach is to conduct correlation analysis between tropospheric BrO column and other related in situ observations. The measurements of Br_2+HOBr were reported for 7 ARCTAS fights and 5 ARCPAC flights [Neuman et al., 2010; Liao et al., 2012b] and soluble bromide measurements were also available in the ARCTAS flights [Liao et al., 2012b]. These measurements were more abundant and had more data points above the detection limits than BrO measurements. Figures A.2-4 in the Supplement show that the products having higher correlations with ARCTAS BrO also tend to have higher correlations with Br_2+HOBr and soluble bromide measurements from the ARCTAS and ARCPAC experiments since a large portion of correlations is driven by the absence and presence of bromine species along the flight tracks (not the absolute values of bromine species).

Comparison with the in situ bromine measurements showed that the six tropospheric BrO estimates are different. The reasons could be arising from the difference in the process to obtain the tropospheric BrO columns such as the retrieval algorithm and the estimates of the stratospheric BrO columns, and also from the difference of total BrO column between OMI and GOME-2 due to the instrument

sensitivity and cloud interference. Currently there are no adequate measurements to resolve the quantitative contribution from these factors to the differences of all OMI and GOME-2 tropospheric BrO columns. In spite of the different correlations with in situ bromine measurements, the six tropospheric BrO estimates showed generally consistent correlation results with ozone, demonstrating a clear relationship between ozone and BrO when ODEs occurred.

Considering the observations available from the ARCTAS and ARCPAC experiments, the current quantitative constraints on the magnitudes of tropospheric (or stratospheric) BrO column are poor. However, judicious use of correlation analysis provides useful scientific insights into the processes of bromine-related ODEs as we have shown in this study. Our analysis results also help address two issues raised by previous studies [e.g., Choi et al., 2012 and references therein]. The first is the concern that BrO-ozone anti-correlation will be suppressed during severe ODEs. This problem is partially dealt with in this study by analyzing time-lagged BrO-ozone correlations and we only find evidence of short-range transport of ODEs (< 3 days). The second issue is the potentially large contribution of stratospheric BrO column particularly over the Hudson Bay region, masking the tropospheric (low BrO) signal. New observations that measure BrO through the entire tropospheric column are necessary to test this hypothesis. However, the correlation analysis of ozonesonde observations with satellite tropospheric BrO column at Churchill [Figures 2.7, 2.8, and 2.9), an ozonesonde site near Hudson Bay, suggests an alternative hypothesis that the tropospheric BrO and ODE layers were much deeper (up to 2 km) than at a site like Barrow (several hundred meters). In situ BrO and ozone observations might not measure drastic changes of ozone over such a region

with enhanced tropospheric BrO column since the distribution of the BrO column enhancement into a deep layer reduced average BrO concentrations and ozone loss is also mitigated by the vertical mixing of a large volume of air due to an unstable boundary layer.

2.5 Conclusions

Based on surface, aircraft and ozonesonde measurements, satellite-derived tropospheric BrO vertical columns, and back trajectory calculations, we investigated characteristics of the Arctic ODEs in spring 2008. The difficulties of using in situ observations from these experiments to validate tropospheric BrO columns derived from satellite measurements and judicious use of satellite observations to understand characteristics of ODEs are discussed in the previous section. During the ARCTAS and ARCPAC experiments, the BrO enhancement over the Chukchi Sea revealed by satellite measurements appears to be a major contributor to the ODEs observed by aircraft.

Time-lagged correlation analysis between ozone and tropospheric BrO columns allowed us to examine the relative importance of in situ ozone loss and transport. We did not find evidence for significant long-range (> 3 days) transport. ODEs appeared to occur within 1-2 day transport from the BrO source regions. The effect of in situ halogen-driven loss is also evident in the diurnal variation of surface ozone concentrations at Alert, Canada. Analysis of tropospheric BrO columns along back trajectories of flight tracks showed low-ozone air mass transported from adjacent high-BrO regions. There was a significant correlation between ozone and temperature in surface, ozonesonde, and

aircraft data, but we did not find evidence for a threshold temperature value, which implies that temperature variation is a stronger factor for ODE formation.

Both Barrow and Resolute are capped in the inversion layer at 400 and 600 m above, respectively, below which ODEs occur at these sites. In contrast, the boundary layer at Churchill is unstable from the surface to 500 m. At this site, we find a much deeper layer of ozone loss in ODE days than non-ODE days up to 2 km. The depth of the ozone loss layer is corroborated in the correlation analysis of ozone with tropospheric BrO column and potential temperature. The unstable boundary layer during ODEs could potentially provide a source of free-tropospheric BrO through convective transport and explain the significant negative correlation between free-tropospheric ozone and tropospheric BrO column at this site. In situ observations of bromine species will be needed to confirm and understand the sources and recycling of BrO in the free troposphere.

CHAPTER 3

INFLUENCE OF CLIMATE VARIABILITY ON NEAR-SURFACE OZONE DEPLETION EVENTS IN THE ARCTIC SPRING

3.1 Introduction

In the Arctic spring, ozone depletion events (ODEs) are often observed near the surface [Barrie et al., 1988; Simpson et al., 2007a]. Recent studies based on satellite and in situ observations suggest that ODEs appear widespread [Zeng et al, 2003, 2006; Bottenheim et al., 2009; Jacobi et al., 2010]. During ODEs, reactive bromine radicals (Br and BrO), produced and recycled by heterogeneous reactions on snow [Jones et al., 2010; Yang et al., 2010], sea ice [Simpson et al., 2007b; Gilman et al, 2010], and aerosol surfaces [Yang et al., 2008; Frieβ et al., 2011], not only deplete ozone but also have broad impacts on the Arctic environment. For example, when gas-phase elemental mercury (GEM) is oxidized by bromine radicals to reactive gaseous mercury (RGM) and deposited to the Arctic Ocean [Xie et al., 2008], it contributes to atmospheric mercury deposition events (AMDE) [Schroeder et al., 1998; Steffen et al., 2008]. Bromine radicals also oxidize volatile organic compounds (VOCs) [Keil and Shepson, 2006] or dimethylsulfide (DMS) [von Glasow and Crutzen, 2004].

The frequency of Arctic ODEs varies greatly from year to year (to be shown in Figure 1). We explore if some of the ODE inter-annual variability is attributable to climate variation in the Arctic, a region sensitive to climate change [Solomon et al.,

2007]. The occurrence and duration of ODEs are a function of bromine activation and recycling [Simpson et al., 2007a; Liao et al., 2012b] and air mass transport [Bottenheim and Chan, 2006; Koo et al., 2012]. Our current understanding of bromine activation and recycling is too limited to examine how they are affected by climate variability. For example, bromine activation may be enhanced by high wind speed and blowing snow [Jones et al., 2010; Frieβ et al., 2011]. However, we do not find a relationship between the inter-annual variation of ODE frequency and that of wind speed in April. First-year sea ice may also enhance bromine activation and recycling [Simpson et al., 2007b], but the large increasing trend of first-year sea ice area [Nghiem et al., 2007; Howell et al., 2009] does not explain the variation of observed ODE frequencies, which show large inter-annual variations rather than a clear trend as in the sea ice.

Air-mass transport and mixing, on the other hand, are obviously affected by climate factors. Storms over the north Pacific are known to transport ozone-rich air from mid-latitudes to the Arctic and are associated with weak ODE occurrence [Jacobi et al., 2010]. We diagnose the variability of regional climate through teleconnection patterns, such as Western Pacific (WP) pattern [Linkin and Nigam, 2008], Pacific North America (PNA) pattern [Leathers and Palecki, 1992], North Atlantic Oscillation (NAO) [Hurrell 1995], Arctic Oscillation (AO) [Thompson and Wallace, 1998], and Pacific Decadal Oscillation (PDO) [Mantua et al., 1997]. Previously, NAO and PNA patterns have been considered as a proxy to diagnose transport of pollutants such as CO [Eckhardt et al., 2003], CO_2 [Murayama et al., 2004], and aerosols [Di Pierro et al., 2011] into the Arctic. The Polar/Eurasia teleconnection patterns appear to influence the trend of AMDEs in the Arctic [Cole and Steffen, 2010]. Similarly in this work, we examine how the variability

of Arctic spring ODEs relates to regional climate variability. For this purpose, we use long-term ozone measurements made over the past 30 years at three Arctic surface sites.

3.2 Data and Methods

In this study, we used long-term (at least > 15 years) in situ ozone measurements at three surface sites in the Arctic region, Barrow (71.3°N, 156.8°W, 1980-2009) by the NOAA Earth System Research Laboratory [Oltmans and levy, 1994], Alert (82.5°N, 62.3°W, 1993-2008) in the Canadian Air and Precipitation Monitoring Network [Anlauf et al., 1994], and ZPL (78.9°N, 11.9°E, 1990-2008) by the Norwegian Institute for Air Research [Solberg et al., 1996]. Surface ozone concentrations at these sites have been monitored using continuously operating UV absorption systems with an accuracy of 0.5-2 ppbv [Helmig et al., 2007]. Ozonesonde data are not used because they are too limited in providing useful information on the inter-annual variation of ODE frequency in April.

To investigate the influence of regional climate variability on the Arctic ODEs, we used five monthly teleconnection indices including WP, PNA, NAO, AO and PDO. Rotated Principal Component Analysis (RPCA) [Wallace and Gutzler, 1981] was used to calculate monthly indices of WP, PNA, and NAO, and Empirical Orthogonal Functions (EOF) applied to the monthly mean 1000-hpa height anomaly poleward of 20°N in the northern hemisphere were used to compute a monthly AO index [Thompson and Wallace, 1998]. The PDO index was obtained from the leading principal component of monthly sea surface temperature variability in the North Pacific poleward of 20°N [Mantua et al., 1997]. All climate variability indices used in this study except PDO were obtained from the NOAA Climate Prediction Center (CPC). The PDO index was

obtained from the Joint Institute for the Study of the Atmosphere and Ocean (JISAO) at the University of Washington.

In addition to the regional climate indices, we also examined large-scale dynamics using the National Centers for Environmental Prediction/National Center for Atmospheric Research (NCEP/NCAR) reanalysis data [Kalnay et al., 1996], which are obtained from the NOAA web site (http://www.esrl.noaa.gov/psd/data/gridded/reanalysis/). The jet stream across the Pacific was diagnosed using 300-hPa winds. The Pacific storm track was diagnosed by tracking the low-pressure centers at sea level every six hours based on an algorithm developed by Hoskins and Hodges [2002]. The tracking results were re-gridded onto regular grids (2.5° by 2.5°) by considering both the intensity and distance of the tracked cyclones around a given grid point [Cressman 1959]. By removing the climatology mean of the storm track intensity, we obtained the anomaly of storm track intensity. The procedure adopted here to obtain the intensity of the storm track is widely used for the analysis of regional cyclonic activity [Myoung et al., 2009]. Based on the NCEP/NCAR reanalysis data, the anomaly of SLP was also estimated using the 30-year climatology (1981-2010).

3.3 Results and discussions

Here we use the normalized ODE frequency in April, which is defined as the ratio of the hours of ozone mixing ratio < 10 ppbv to total observation hours in a month [Oltmans et al., 2012]. The normalized ODE frequency is a good indicator to show the range of monthly mean ozone concentration (Figure 3.2a). The time series and histograms of ODE frequencies in April at Barrow, Alaska (71.3°N, 156.8°W), Alert,

Canada (82.5°N, 62.3°W), and Zeppelinfjellet (ZPL), Norway (78.9°N, 11.9°E) are compared (Figures 3.1 and 3.2b). The ODE frequency is usually highest at Barrow and lowest at ZPL. The most striking feature at all the sites is the large inter-annual variability. A high ODE year is sometimes followed by a low ODE year.

To explore the relationship between inter-annual variation of ODEs and large-scale climatic patterns, we compute nonparametric Spearman's rank correlation coefficients (ρ) of ODE frequencies at three sites with five indices of climate variability; WP, PNA, AO, NAO, and PDO (Figure 3.3). Bootstrap (20000 times) is used to estimate the uncertainties. Very similar results are obtained using Pearson's correlation coefficient. The three most significant correlations are between the WP index and ODE frequencies at Barrow and Alert, respectively, and between the NAO index and ODE frequency at ZPL. We will show later that a smaller correlation with the WP index at ZPL is due to a decadal change in the effect of WP on ZPL ODEs (to be shown in Figure 3.9). In the decade of 2000s, all three sites show consistent negative correlations between ODE frequency and the WP index. We do not find another climate index that has such consistency across the three sites.

Similar results are obtained by examining the average index values for strong ODE years in comparison to weak ODE years (Figure 3.4). We selected five years with the most frequent ODEs and five with the least frequent ODEs, respectively, at each site in this analysis. Strong ODE years have a negative average WP index and weak ODE years have a positive average WP index at Barrow and Alert. The index phase changes for the other teleconnection patterns between strong and weak ODE years are not as drastic at these two sites. We also compare the anomalies of sea level pressure (SLP) for

strong and weak ODE years at Barrow and Alert (Figure 3.5) with those for positive and negative WP index years (Figure 3.6), The SLP anomalies in weak ODE years clearly differ from strong ODE years. The distribution pattern of the former (latter) is much closer to the SLP anomaly distribution in positive (negative) WP index years.

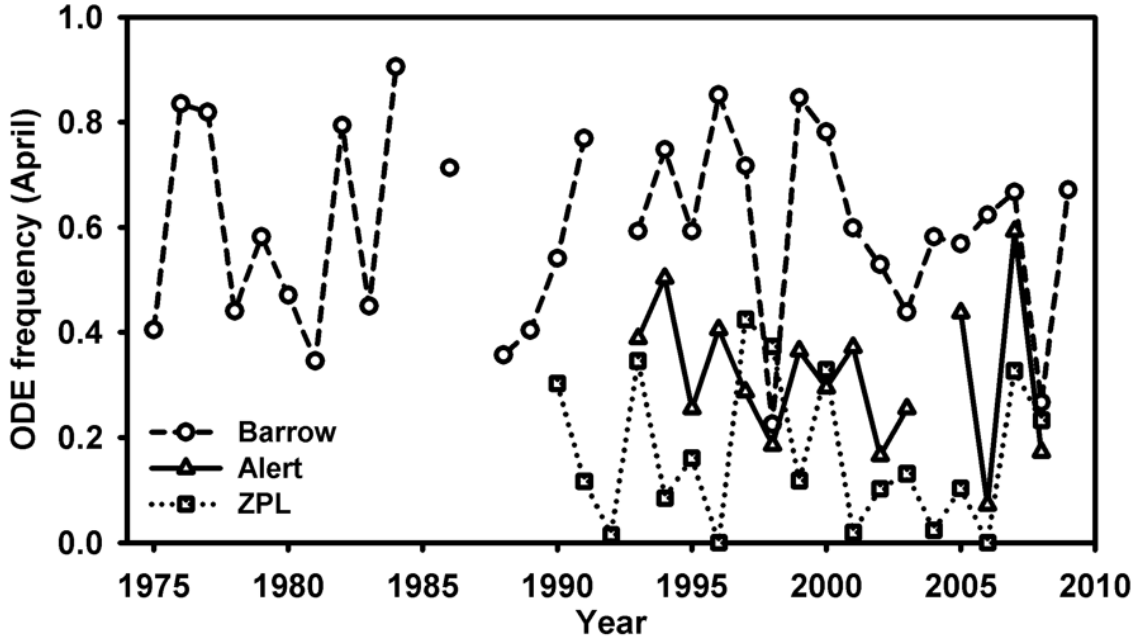

Figure 3.1 Observed ODE frequencies in April at Barrow, Alert, ZPL.

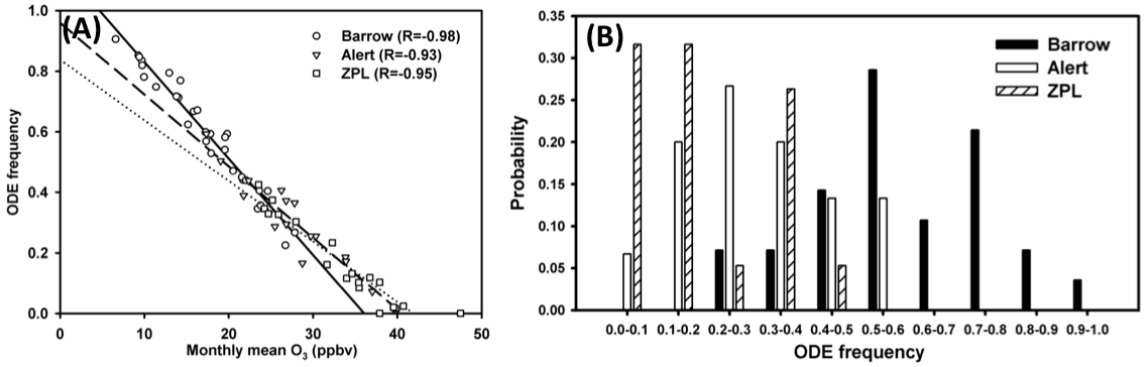

Figure 3.2 (a) Correlation of monthly mean surface ozone mixing ratio with ODE frequency in April at the three monitoring sites, Barrow (1980-2009), Alert (1993-

2008), and Zeppelinfjellet (ZPL) (1990-2009). (b) The probability distribution of ODE frequency in April at Barrow, Alert, and ZPL.

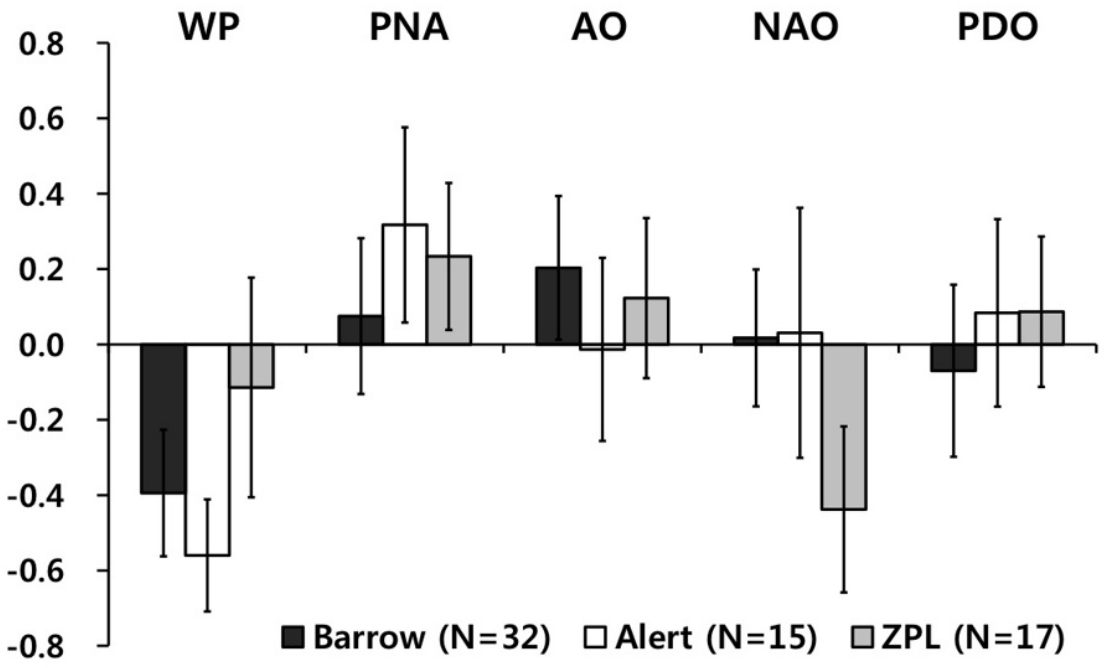

Figure 3.3 Spearman's Rank correlation coefficients (ρ) of ODE frequencies at the three monitoring sites with five teleconnection indices in the Northern Hemisphere, including Western Pacific (WP) pattern, Pacific-North America (PNA) pattern, Arctic Oscillation (AO), North Atlantic Oscillation (NAO), and Pacific Decadal Oscillation (PDO). Vertical bars show 1-σ uncertainties estimated with 20000 bootstraps. The number of years of available ozone measurements at each site is shown in the parentheses.

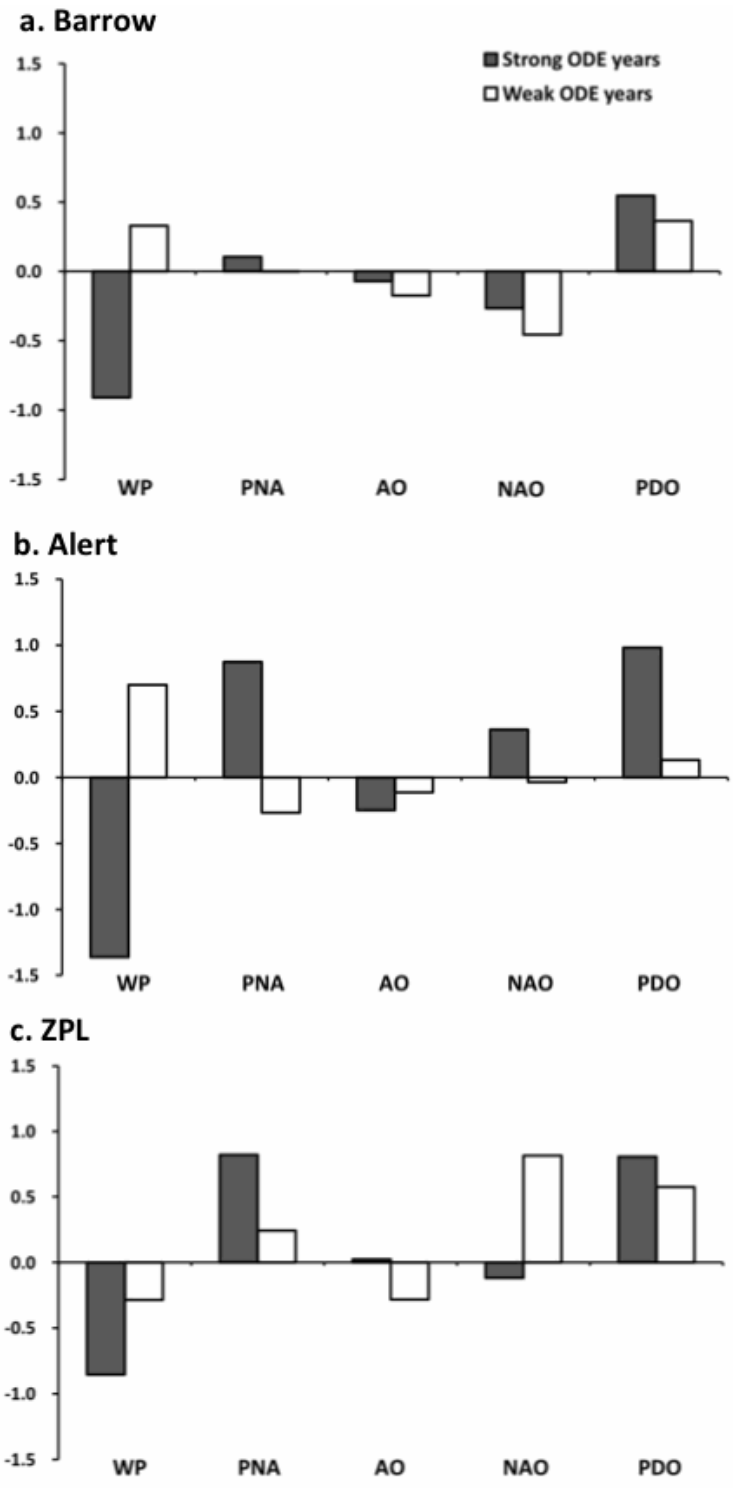

Figure 3.4 Averaged regional climate variability indices in April for the 5 strongest and weakest ODE years, respectively, at (a) Barrow, (b) Alert, and (c) ZPL.

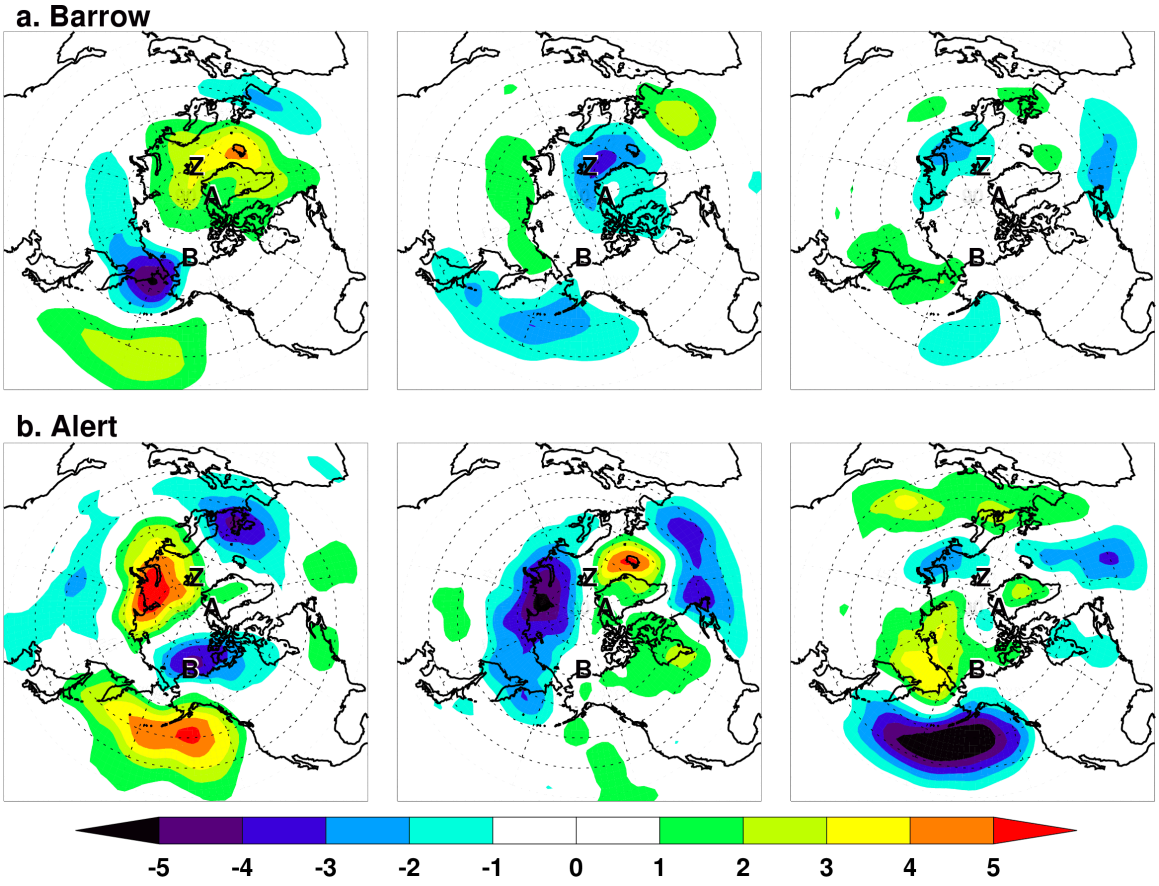

Figure 3.5 Sea level pressure (SLP) anomalies in April during weak (left), moderate (middle), and strong ODE years at (a) Barrow and (b) Alert. Five years of strongest, closest to the mean, and weakest ODE years are shown.

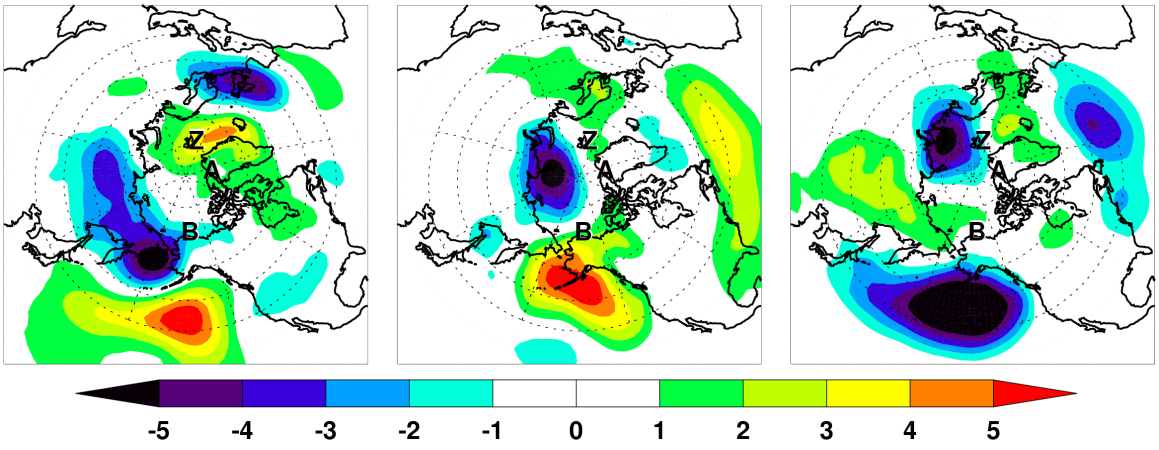

Figure 3.6 Same as Figure 3.5 but for SLP anomalies during positive (left), moderate (middle), and negative (right) phase years of WP patterns.

As discussed previously, atmospheric transport can strongly affect ODEs in the Arctic. In the northern hemisphere, the WP pattern is associated with the variability of jet stream and storm track in the Pacific [Lau 1988; Linkin and Nigam 2008]. The cross-Pacific jet stream is zonally extended much further towards North America in the negative than positive phase of the WP pattern [Rivière 2010]. The changing jet stream pattern further affects the intensity of the northern Pacific storm track [Lee et al., 2010]. These dynamic modulations associated with the WP pattern appear to be related to Rossby wave breaking [Rivière 2010] and meridional temperature gradient change over the western Pacific [Lee et al., 2010].

Since the chemical production of ozone is very slow in spring [Wang et al., 2003], ODEs are mainly terminated by mixing with ozone-rich air. Previously, migration of low-pressure systems from mid-latitudes to the Arctic was found to cause termination of Arctic ODEs [Jacobi et al., 2010] due in part to transport of ozone-rich air masses by storms. Atmospheric mixing is also important in ODE formation because the Arctic ODEs are usually observed in a thermally stable atmosphere, which reduces mixing with ozone-rich free tropospheric air [Zeng et al., 2006; Koo et al., 2012]. The vertical mixing caused by storms mixes low-ozone with high-ozone air and terminates ODEs.

The hypothesis that we test here is if the negative WP phase is associated with jet stream and storm track conditions that favor ODEs in the Arctic. At Barrow and Alert, the Pacific jet stream extends much closer to North America in strong ODE years than weak ODE years (Figure 3.7). A strong jet stream acts as a barrier of meridional mixing between mid-latitudes and the Arctic. More evidence is found in the change of the Pacific storm track that extends from East Asia through the Bering Sea towards Barrow. It is

weaker in strong ODE years than weak ODE years (Figure 3.8). A weak storm track leads reduced air-mass transport to the Arctic and vertical mixing between boundary layer and free tropospheric ozone. Both a strong jet and a weak storm track over the Pacific are inductive to ODE occurrence in the Arctic, resulting in the negative correlation between ODE frequency and WP index (Figures 3.3 and 3.4). In contrast, the intensity of the Atlantic storm track does not show a large difference between strong and weak ODE years at Barrow and Alert (Figure 3.8), implying that these sites are not affected significantly by Atlantic storms.

ZPL is situated much further away from the Pacific compared to Barrow and Alert. It is, therefore, not surprising that we found a weaker correlation between WP index and ODE occurrence at this site. Figure 3.10 shows that neither the zonal extension of the Pacific jet stream nor storm track intensities show as clear a difference between strong and weak ODE years of ZPL as at Barrow or Alert (Figures 3.7 and 3.8).

However, further analysis reveals an interesting shift of WP influence on ZPL from 1990s to 2000s. Comparing the ozone measurements among the three sites shows a clear decadal-scale change in the correlations of ZPL ODE frequency with the other two sites. Figure 3.9a shows that ODE frequencies are positively correlated between Barrow and Alert in the 1990s (1990-1999) and 2000s (2000-2009). In contrast, the ZPL ODE frequency has negative correlations with the other two sites in the 1990s but switches to a neutral or positive correlation in the 2000s. Figure 3.9b shows negative correlations between the WP index and ODE frequency at Barrow or Alert in the 1990s and 2000s, although the correlation at Barrow is weak in 1990s. While the ODE frequency at ZPL has a small and insignificant positive correlation with the WP index in the 1990s, the

correlation turns largely negative in the 2000s. In fact, the three sites have consistently negative correlations between the WP index and ODE frequency in the 2000s.

We then examine the storm track distributions in strong and weak ZPL ODE years separately in the 1990s and 2000s (Figure 3.11a). In the 1990s, the storm track originating in the Pacific did not reach ZPL. In the 2000s, the Pacific storm track activities were more intense near ZPL in weak ODE years than strong ODE years. This is consistent with the finding in Figure 3.8 that a strong Pacific storm track enhances atmospheric mixing and the transport of ozone-rich air masses from lower latitudes, leading to a lower ODE frequency.

More insight into the atmospheric condition is found in the anomaly of SLP in the 1990s and 2000s (Figure 3.11b). The SLP anomalies appear to be similar in strong ZPL ODE years in the 1990s and 2000s, characterized by a low-pressure anomaly over the Kara-Barent Sea where satellite observations indicated high BrO columns [Zeng et al., 2003, 2006; Koo et al., 2012]. During the weak ODE years when we expected more mixing with lower latitude ozone-rich air masses, the SLP anomaly in the 1990s is different from the 2000s. The average SLP anomaly of the 1990s is similar to the negative phase of the AO. The average SLP anomaly of the 2000s in weak ZPL ODE years, on the other hand, is similar to the positive phase of WP pattern, reflecting the effect of WP pattern on ODEs at ZPL (Figure 3.9).

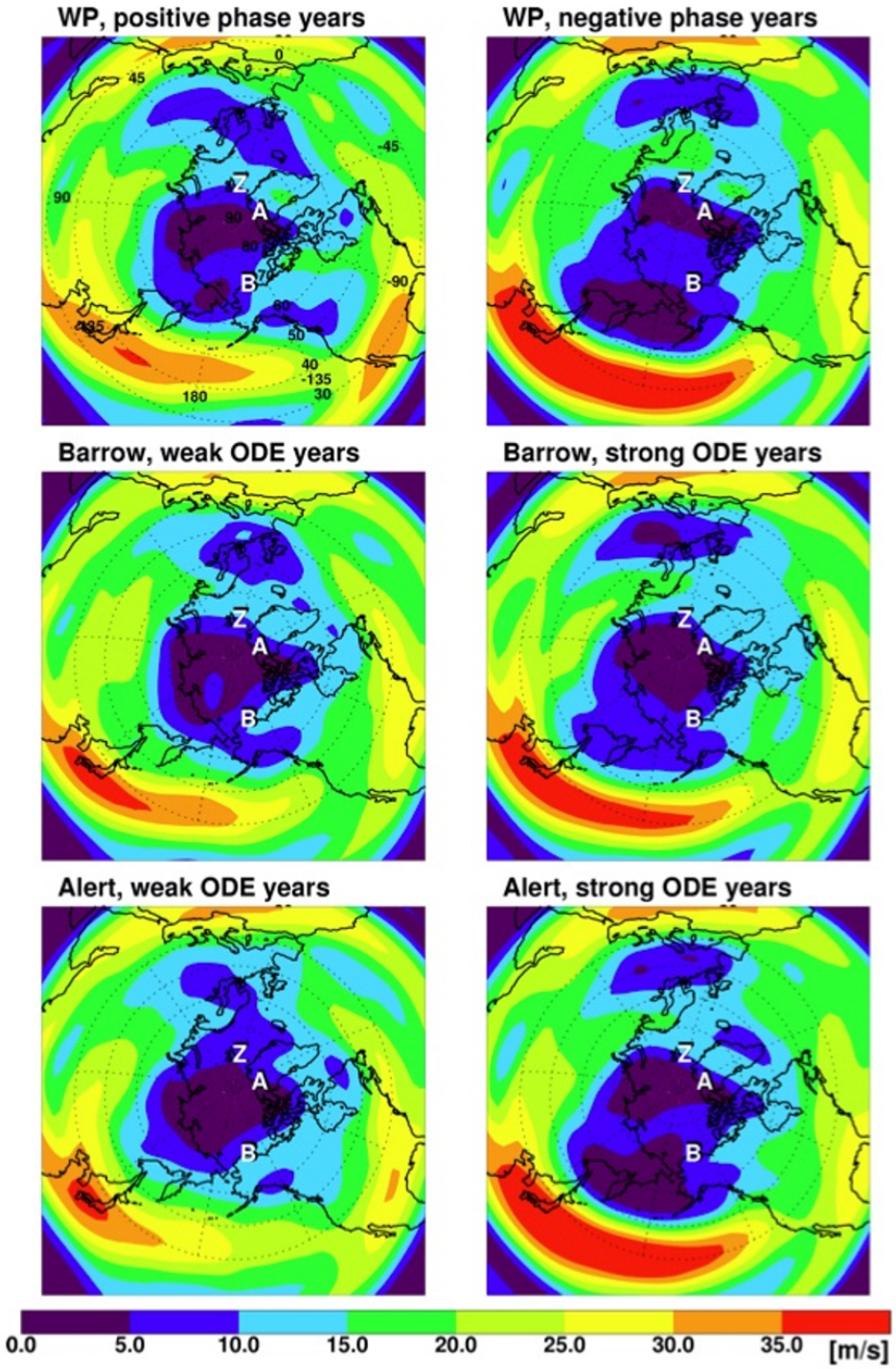

Figure 3.7 Composite images of 300-hpa wind speed in the Northern Hemisphere during the positive and negative phase years of WP pattern (top), and weak and strong ODE years at Barrow (middle) and Alert (bottom). For each case, 5 most extreme years are selected and averaged. The locations of Barrow, Alert, and ZPL are marked B, A, Z, respectively. The unit of color bar is m/s.

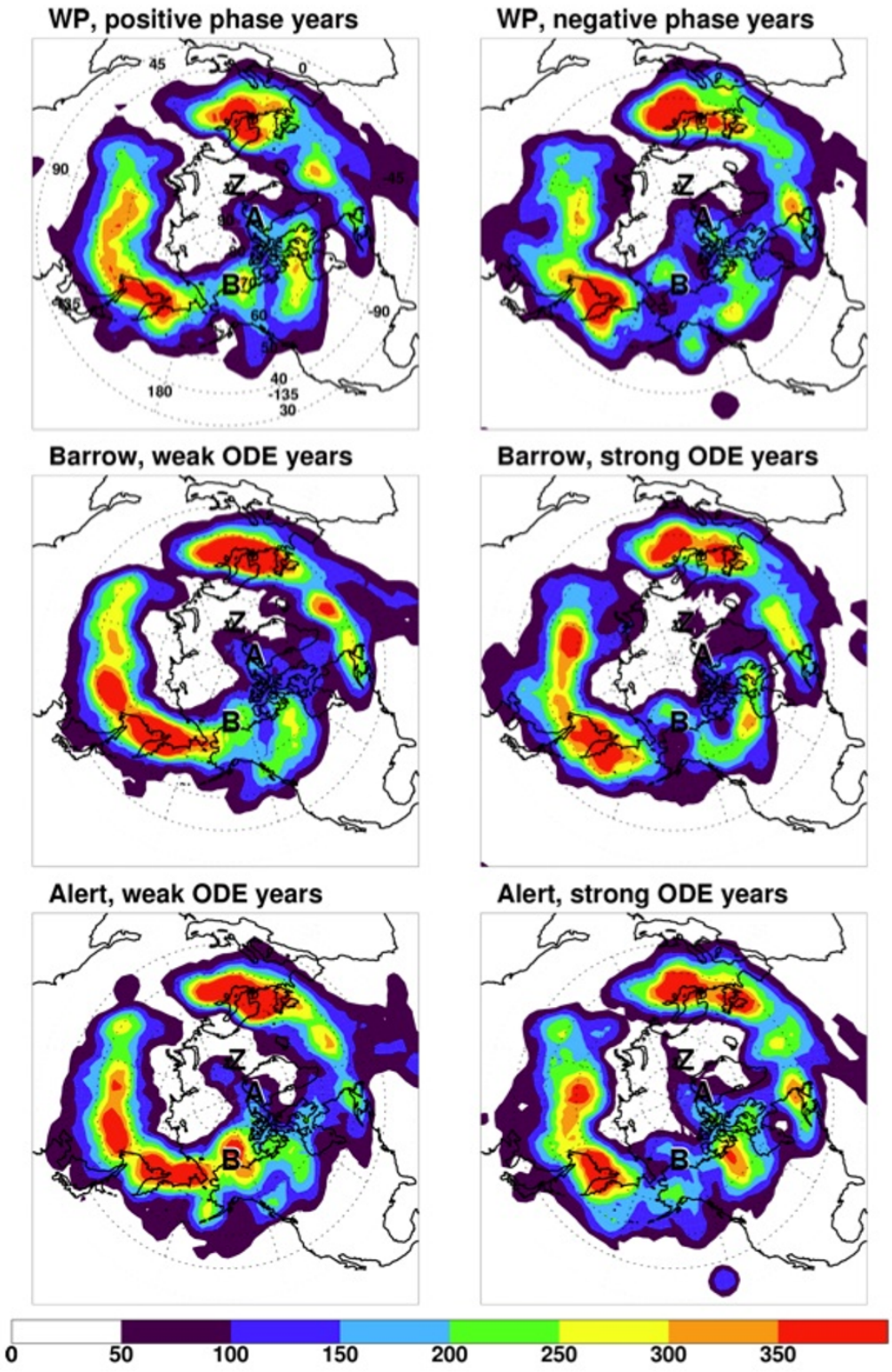

Figure 3.8 Same as Figure 3.7 but for composite images of storm track intensity in the Northern Hemisphere. The unit of color bar is Pa.

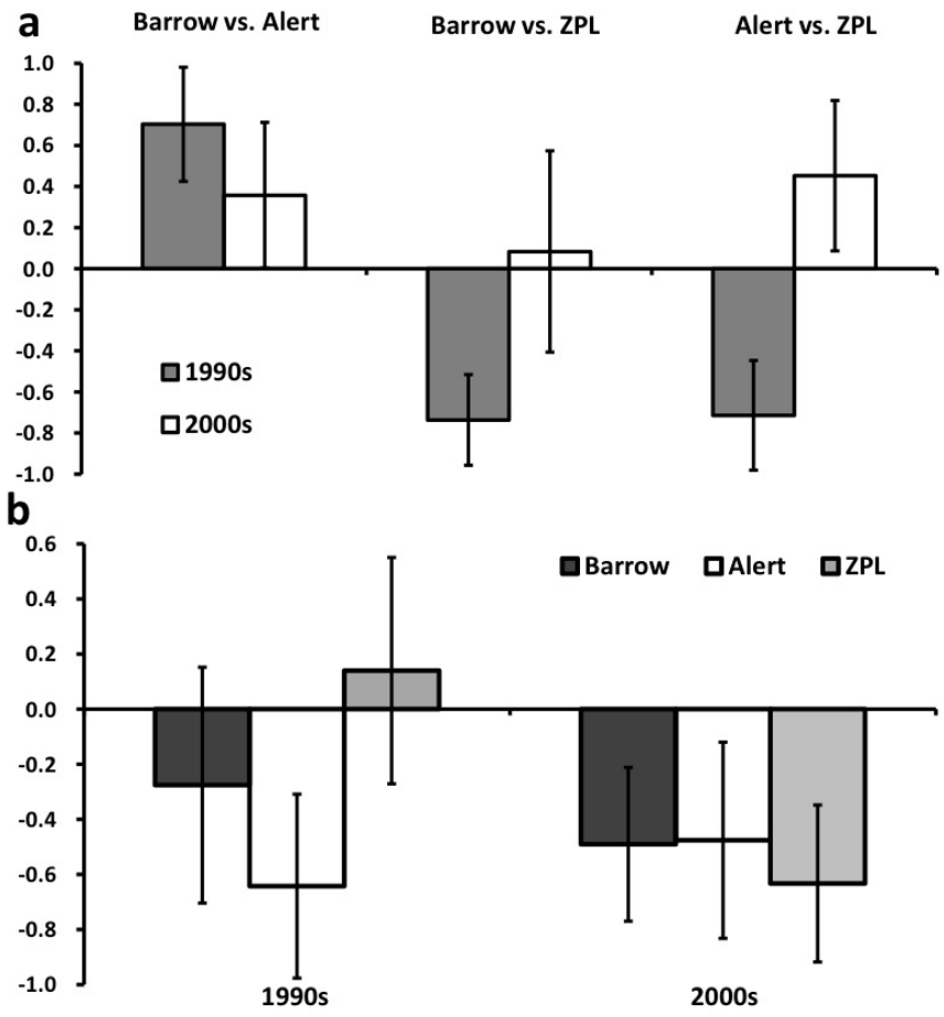

Figure 3.9 (a) Rank correlation coefficients (ρ) of ODE frequency among Barrow, Alert, and ZPL in 1990s (gray) and 2000s (white). (b) Rank correlation coefficients of the WP index with ODE frequency at the three sites in 1990s and 2000s. Vertical bars show 1-σ uncertainties estimated with 20000 bootstraps.

3.4 Conclusions

We study in this work the impacts of regional climate variability on near-surface ODE frequencies at Barrow, Alert and ZPL in the past three decades. Barrow and Alert tend to have higher ODE frequencies in the negative than in the positive phase of the WP pattern (Figures 3.3, 3.4, and 3.12) when a stronger Pacific jet stream and less intense storm track activities lead to less lateral and vertical mixing with ozone-rich air. The influence of the WP pattern at ZPL is stronger in the 2000s than the 1990s. The high Arctic appears to be influenced more strongly by the WP pattern in the 2000s than 1990s. The reason is unclear. One possibility is the high sensitivity of Arctic climate to aerosol loadings over East Asia, which has been increasing rapidly in 2000s [Levy et al., 2008; Streets et al., 2013]. Another possibility is the global climate change in the recent decade [Solomon et al., 2007]. Tropical climate variability, such as ENSO, can also affect the WP pattern [Yeh and Kirtman, 2004], through which ODEs in the Arctic spring can be influenced. Further studies are needed to evaluate these mechanisms. We find that the chemical environment of the Arctic, including ODEs and consequently atmospheric mercury deposition, is sensitive to regional climate variability. The results presented here suggest that the long-term change of WP pattern is a key factor in understanding and projecting potential impacts of future global climate changes on the Arctic chemical environment in spring.

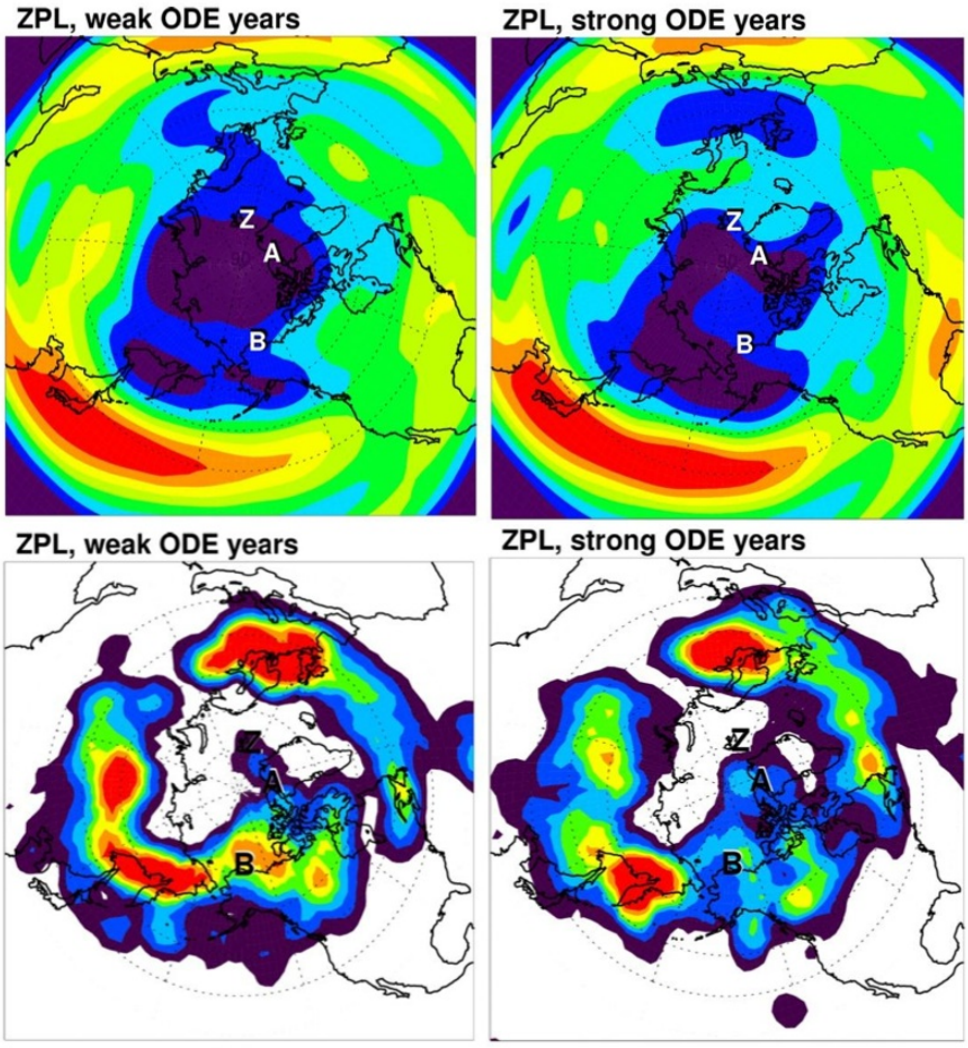

Figure 3.10 Same as Figures 3.7 and 3.8 but for ZPL.

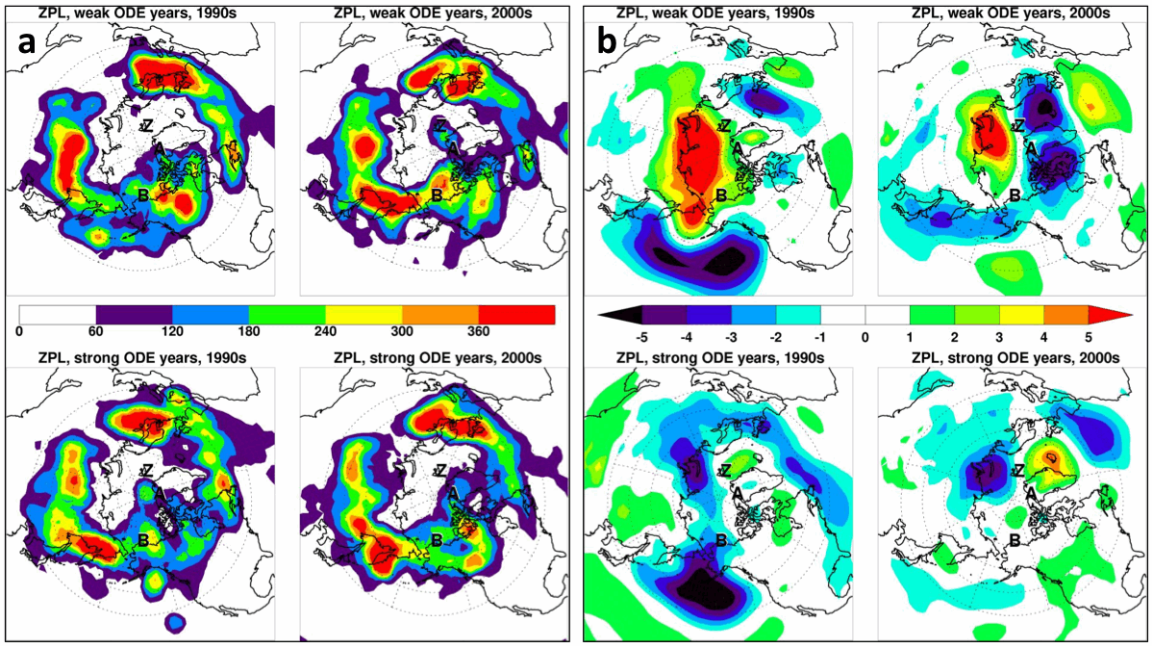

Figure 3.11 Composite images of (a) storm track intensity and (b) surface SLP anomaly in April of the northern hemisphere during weak and strong ODE years at ZPL (marked as Z) in the 1990s and 2000s. The locations of Barrow, Alert, and ZPL are marked B, A, and Z, respectively. The three strongest and weakest ODE years are shown for each decade.

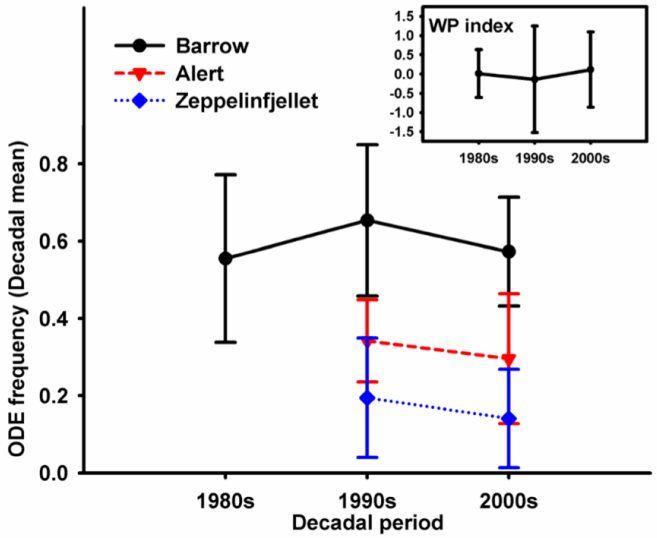

Figure 3.12 Decadal mean of WP index (right top) and ODE frequencies at Barrow (black), Alert (red), and ZPL (blue).

CHAPTER 4

SIGNIFICANT FACTORS INFLUENCING THE SPATIOTEMPORAL VARIATION OF SURFACE OZONE DEPLETION: THE ONSET, PROGRESSION, AND TERMINATION

4.1 Background and Motivation

In the Arctic spring, ozone near the surface rapidly decreases. Locally this ozone depletion event (ODE) typically results from the catalytic photochemistry of bromine in the heterogeneous (gas and particle) phase [Barrie and Platt, 1997; Simpson et al., 2007a]. Box and 1-dimensional model simulations for ODEs [Fan and Jacob, 1992; Sander and Crutzen, 1996; Michalowski et al., 2000; Evans et al., 2003; Piot and Glasow, 2009; Liao et al., 2012a] basically capture the effect of bromine chemistry to deplete the polar surface ozone but most of model studies were executed assuming the ideal [e.g., Piot and Glasow, 2009] or simplified ambient conditions [e.g., Evans et al., 2003]. In particular, the solar radiation and the particle phase are largely uncertain in the model. It has been known that the reaction between BrO and HO_2, one of strong reactions influencing the bromine explosion [Wennberg, 1999; Simpson et al., 2007a] is quite dependent on the diurnal pattern of photochemistry [Liao et al., 2012a] and bromine chemistry in the heterogeneous phase prefers to the snow particle [Jones et al., 2010; Frieß et al., 2011]. Thus, the large uncertainties of ambient conditions in the model are the reason for limitations not to capture the variation of real measurements of bromine species.

In addition, the occurrence of many ODE cases appears due to the transport of ozone-depleted air mass [Bottenheim and Chan, 2006; Bottenheim et al., 2009; Koo et al., 2012]. Since the Arctic Ocean generally plays a role as a source of ozone-poor air masses [Halfacre et al., 2013; Van Dam et al., 2013], the pattern of wind blowing and transport in the synoptic scale is another significant factor influencing to the extent of local ODEs. Also, the extent and structure of ODEs are affected by the ambient meteorological conditions such as temperature [e.g. Zeng et al., 2003], pressure system [e.g. Jacobi et al., 2006; Begoin et al., 2010], and vertical stability [e.g., Lehler et al., 2004; Koo et al., 2012]. Again, these conditions should be considered to better understand the spatiotemporal characteristics of ODEs.

As mentioned, much of the research has focused on the chemical and physical processes of bromine-driven ODEs [Simpson et al., 2007a]. We use a different approach in this study by analyzing long-term observations at two surface sites, Barrow, Alaska and Alert, Canada. Instead of focusing on the selected cases of ODEs [e.g. Zeng et al., 2006], we analyze the onset, progression, and termination of ozone depletion seasons (ODS), composed of all effective ODEs in springtime. Basically bromine chemistry and consequent ozone loss are photochemically activated. Therefore we expect a time difference between Barrow and Alert due to a latitudinal difference. Both photochemistry and transport also affect the temporal variation of observed ODEs, reflecting the time progression of ODE occurrences at the surface sites. The condition for the termination of ODEs reveals the crucial situation to maintain the recycling of bromine in the heterogeneous phase. Very little research has analyzed the termination of the ozone depletion season all these are now still questionable. In this study, the observation-based

data analysis is executed to improve our understanding for the uncertain parts of ODEs. This analysis will provide the necessary constraints for testing if known chemistry theories for bromine activation and recycling can be applied in chemical transport models to simulate the observed ODE characteristics.

.

4.2 Data description

We analyzed in situ measurements of surface ozone measurements at Barrow, Alaska (71.3°N, 156.8°W, 1979-2008) and Alert, Canada (82.5°N, 62.3°W, 1993-2008). Surface ozone has been monitored by the National Oceanic and Atmospheric Administration (NOAA) Earth System Research Laboratory (ESRL) at Barrow [Oltmans and levy, 1994], and the Canadian Air and Precipitation Monitoring Network at Alert [Anlauf et al., 1994] based on UV absorption systems with an accuracy of 0.5-2 ppbv [Helmig et al., 2007].

There have been many kinds of ODE definition [Halfacre et al., 2013], but here we use 10 ppbv of ozone mixing ratio as a criteria [Tarasick and Bottenheim, 2002; Koo et al., 2012] to consider the strong ODE only. Also to have enough ozone-depleted conditions, we exclude the case of ozone depletion showing shorter than 6 hours. Based on this standard, in every year the first and last dates of ODE were selected as an onset and termination date of ozone depletion season (ODS). For every month from February to June, we also estimated the monthly ODE frequency, which is defined as the ratio between the hours of ODEs and total hours in a month [Oltmans et al., 2012].

We compared ozone data with some dataset of local meteorology (e.g., temperature) obtained from data archive of NOAA National Climate Data Center

(NCDC). Also we use ambient meteorological features such as wind speed, wind direction, and the anomaly of surface pressure obtained from the National Centers for Environmental Prediction and the National Center for Atmospheric Research (NCEP/NCAR) reanalysis data [Kalnay et al., 1996].

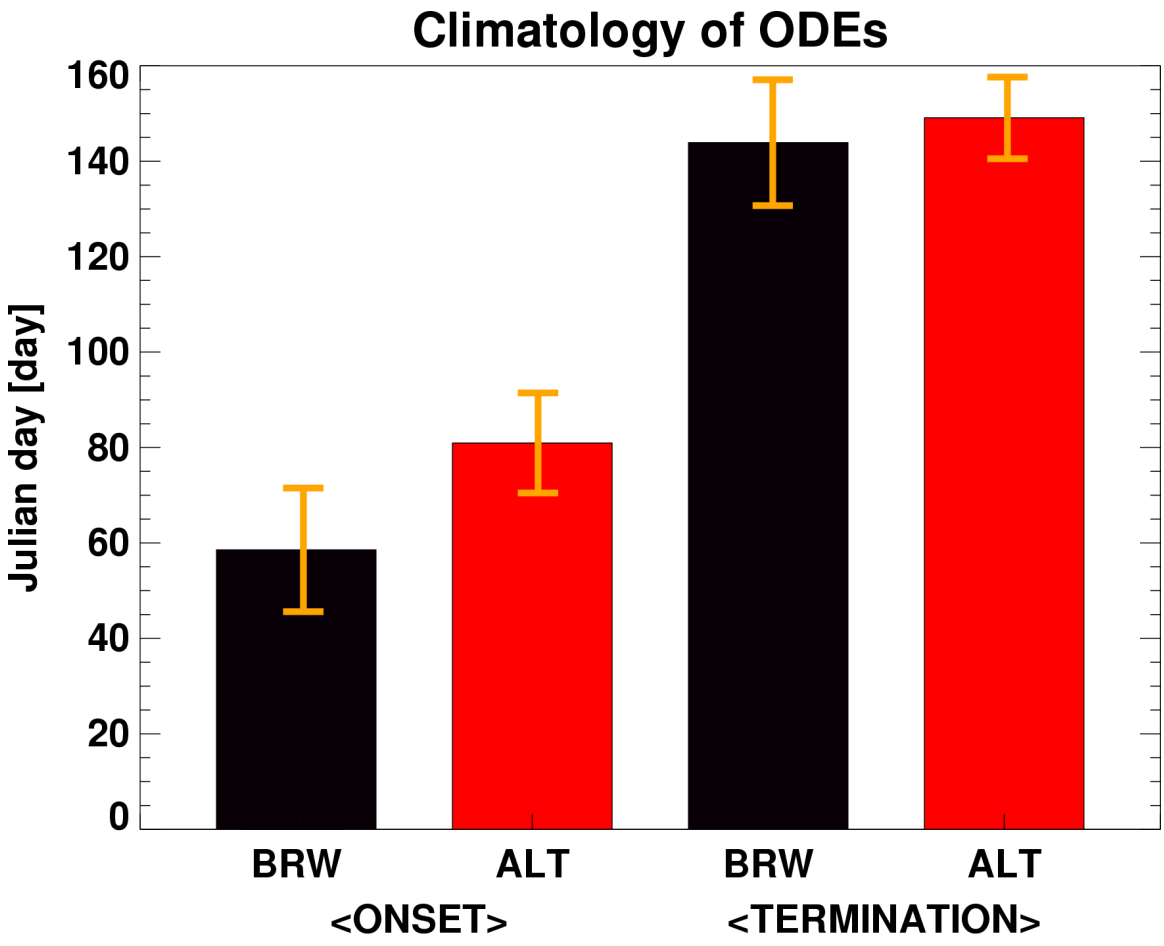

Figure 4.1 The average of onset, termination, and duration of ODEs at Barrow (black bar) and Alert (red bar). Ozone measurements used in this study is from the year 1979 to 2008 for Barrow, and from the year 1993 to 2008 for Alert. Unit is a Julian day. Orange lines indicate the range of 1 - σ standard deviation.

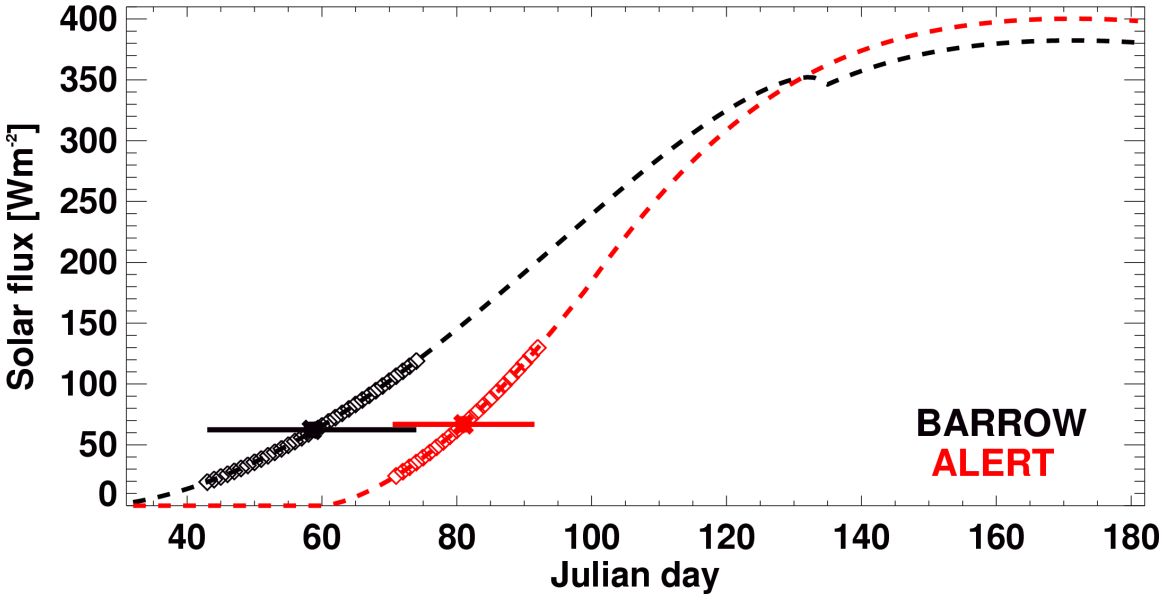

Figure 4.2 Daily total solar flux (Wm^{-2}) at Barrow (black dash) and Alert (Red dash). The loading of aerosol and cloud is not assumed. Two large dots indicate the daily total solar flux for the mean onset day of ODEs at Barrow and Alert. The range of 1-σ standard deviation (horizontal bar) and corresponding daily solar flux (square dots) is also presented.

4.3 Results and discussions

The temporal characteristics of ODS at Barrow and Alert are different in the Arctic spring. Figure 4.1 compared the mean day of year (DOY) for onset and termination of ODS at Barrow and Alert. The average onset dates of ODS are DOY 58 at Barrow but DOY 81 at Alert, showing about three week difference. The average termination date of ODS is DOY 144 at Barrow and DOY 149 at Alert, which are almost close. In other words, surface ozone depletion at Barrow climatologically initiates about three weeks earlier than Alert, but terminates in a similar period. Thus, ODS at Barrow seems a little longer than that of Alert.

4.3.1 Influential factors for the onset of ODS

We need to explain the reason of different onset day of ODS (the first day of ODEs, showing ozone < 10 ppbv longer than 6 hours as mentioned in Section 4.2) between Barrow and Alert. Since the ODE is the photochemical process, we first examine the information about solar insolation. Most of days in the high latitude has no daytime in the winter, and therefore ozone photochemistry is inactive. Due to the difference of latitude, the beginning of daytime at Barrow is earlier than Alert. The daytime begins around DOY 28 at Barrow and DOY 61 at Alert, which are however different from the average onset dates of ODS. This implies that the existence of solar radiation itself may not the only essential condition to initiate ODEs.

The length of daytime also looks associated with the onset date of ODS, but daytime on the average onset day of ODEs at Barrow (~ 9 hours) is not same with that at Alert (~ 13 hours). Finally, we calculated the daily total solar intensity, Q [W/m^2] based on Liou (2002) as shown in the Equation 1.

$$Q \cong \frac{S}{\pi}\left(\frac{a}{r}\right)^2 (\sin\varphi \sin\delta H + \cos\varphi \cos\delta \sin H) \qquad \text{(Eq. 1)}$$

S is the solar constant [W/m^2], and a and r is the mean and instantaneous distance between the sun and the earth [km], respectively. H is a half-day, the time period from solar noon to sunrise or sunset, φ is the latitude, and δ is the solar inclination angle (all angle unit is radian). How to calculate Q in detail is referred to Liou et al. [2002].

The Q values on the average onset dates of ODS are quite close between two sites, such as ~ 62 W/m^2 at Barrow and ~ 67 W/m^2 at Alert (Figure 4.2). With considering Q values of all onset dates during whole periods, the range of Q values are almost same between two sites, indicating that high enough depletion of local surface

ozone may require a minimum amount of solar radiation energy. Since the diurnal variation of solar radiation differs from each site mainly according to the latitudinal difference, different onset dates of local ODS seems inevitable to have the consistent condition of solar intensity.

This finding seems meaningful to better understand the initiating process of ODEs. The surface ozone depletion in the Arctic spring is the catalytic process though the recycling of atmospheric bromine though the heterogeneous phase, called bromine explosion [Fan and Jacob, 1992; Vogt et al., 1996; Michalowski et al., 2000]. If bromine radicals acted as a catalyst (e.g., BrO) releases by even weak sunlight [Spicer et al., 2002], theoretically the ODE should be maintained until the ozone reaches to zero. Owing to the difference from the real situations, however, ambient conditions to make the bromine explosion really exploding have been uncertain [Simpson et al., 2007]. As shown, our results show a certain amount of solar flux is required to facilitate the beginning of ODEs, and it seems about 60 to 70 W/m^2 in terms of daily total solar intensity (Figure 4.2).

We expected the consistent onset dates of ODEs because the location of the Sun does not change much annually. But the onset dates of ODS are not same in every year, then we need to consider some other factors related to and the variation of onset dates. We first presume that the possibility of light attenuation or blockage by high turbid conditions. In spite of relatively less frequency, about 50 to 90 % of days in winter and spring are cloudy [Intrieri et al., 2002; Dong et al., 2010], and it is plausible to diminish the solar intensity in the periods having short daytime. The other possibility is the weak extent of bromine release. Arctic atmospheric bromine is originated from the sea salt in

the ocean and it is believed that the bromine release mostly occurs over open leads and polynyas in the sea ice [Pöhler et al., 2010]. During the cold wintertime, the occurrence of open leads and polynyas is slender and the amount of atmospheric bromine may not be abundant to have strong ozone depletion. Climate variability also may influence the background level of polar surface ozone. In particular, Western Pacific (WP) teleconnection pattern seems related to the extent of ODEs in the Arctic spring by affecting the strength of meridional mixing [Koo et al., 2013].

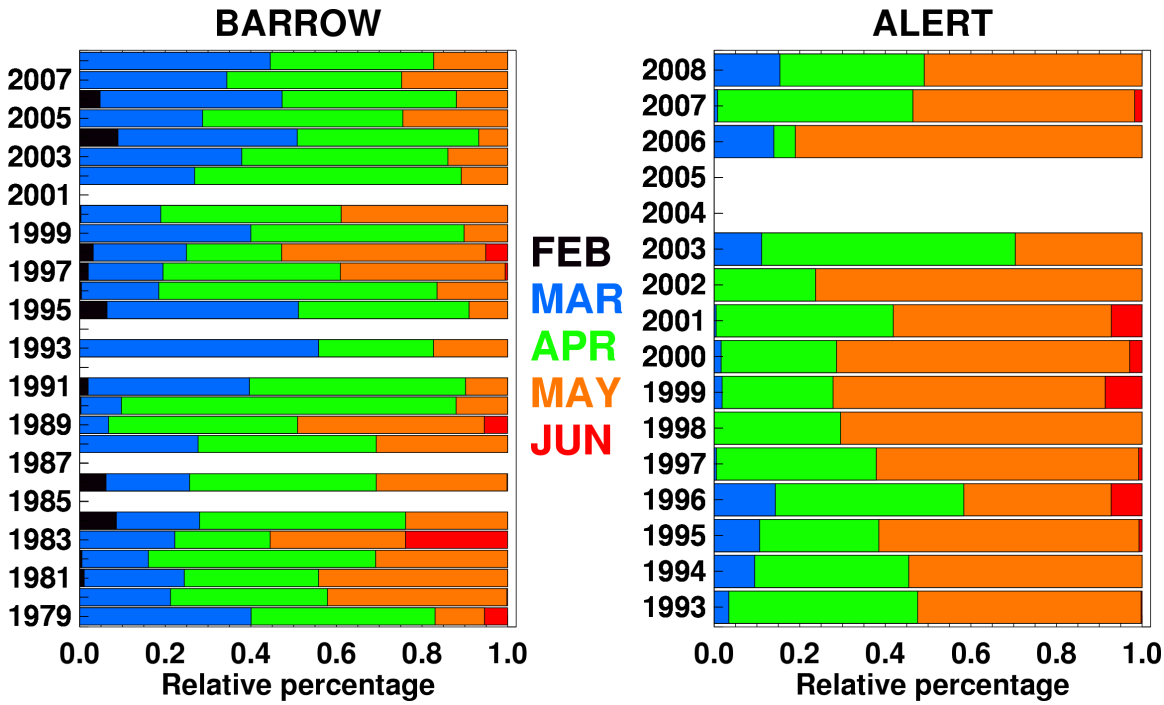

Figure 4.3 Relative percentage of monthly ODEs at Barrow (left) and Alert (right) for February (black), March (blue), April (green), May (orange), and June (red). To disregard the annual variation, the number of ODEs in each spring is normalized.

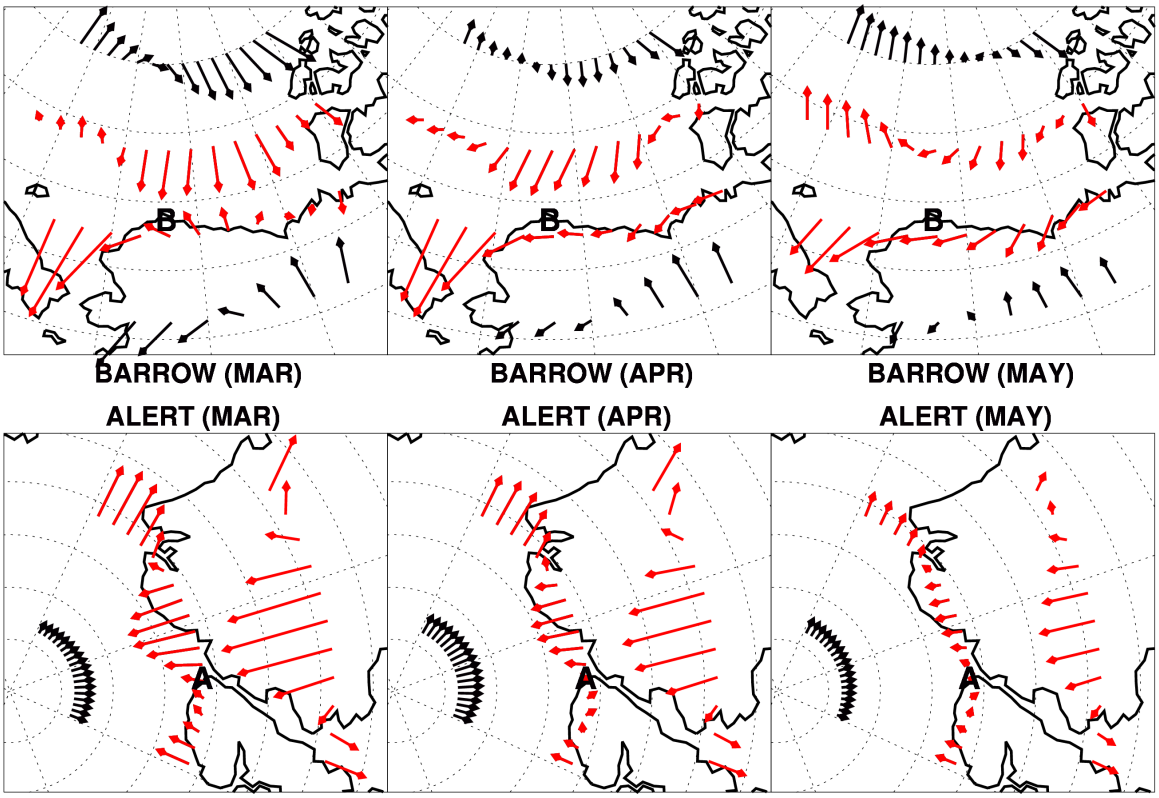

Figure 4.4 Monthly mean wind fields in March (left), April (middle), and May (right) near Barrow (top) and Alert (bottom). Each arrow implies the mean wind speed and direction during 30 years from the year 1979 to 2008 near Barrow, and during 16 years from the year 1993 to 2008 near Alert.

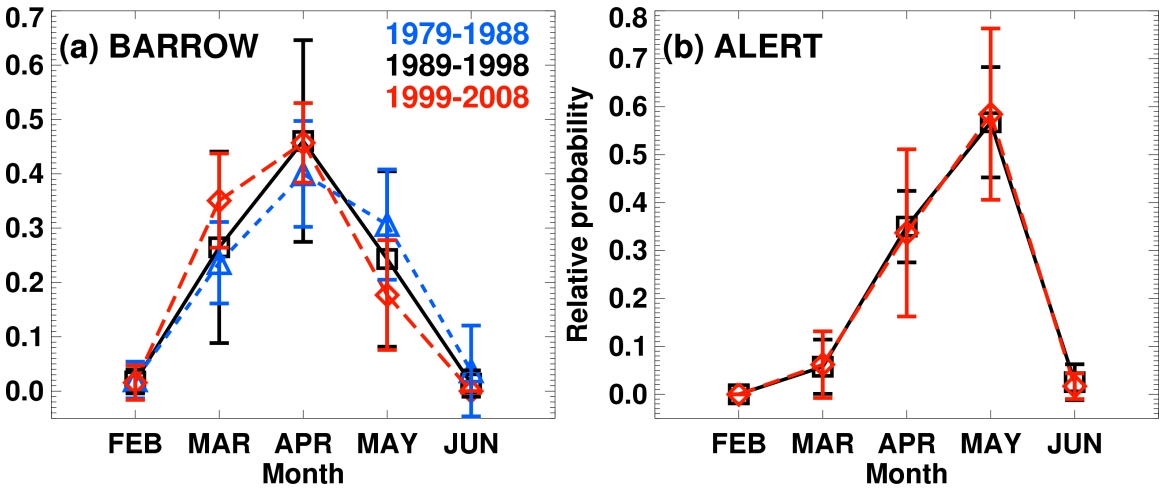

Figure 4.5 The decadal pattern of relative percentage of monthly ODEs at Barrow (left) and Alert (right). Mean values are calculated for three decadal periods, which are from the year 1979 to 1988 (blue), from 1989 to 1998 (black), and from 1999 to 2008 (red). Vertical lines indicate the range of 1 - σ standard deviation.

4.3.2 Influential factors for the progression of ODS

Although ODEs in the Arctic occurs frequently in the spring, the main period of ODEs between two sites is different and also varies in a long period. Figure 4.3 shows the Monthly probability of ODEs at Barrow and Alert. For the year-to-year comparison despite the annual difference of ODE occurrence, the number of ODEs was first normalized and monthly proportion of ODEs was estimated for each month in spring (February to June). A month showing the most frequent ODEs is April at Barrow but May at Alert. Since April and May already has long enough daytime, photochemical environment does not change in general. Namely, solar intensity looks no more significant factor to explain this monthly disparity.

Since the transport of ozone-poor air mass affects the extent of local ODEs [Bottenheim and Chan, 2006; Koo et al., 2012; Oltmans et al., 2012], we examine the monthly wind patterns near two sites in March, April and May (Figure 4.4). Corresponding to the period of surface ozone measurements, monthly wind patterns are averaged from 1979 to 2008 near Barrow, and from 1993 to 2008 near Alert. Wind inflow into Barrow generally appears from the Arctic Ocean located in the north of Alaska during whole spring due to the Beaufort High [Serreze and Barrett, 2011] connected with the Beaufort Gyre in the Arctic Ocean [Proshutinsky et al., 2009], but the pattern of wind blowing to the Barrow site looks different. In March, wind near the coastal area blows from the land to the ocean, which compensates the impact of general wind blown from the Arctic Ocean. The wind from the inland becomes weak in May, but also the wind from the Arctic Ocean becomes weak in May. Consequently, the contribution of wind from the Arctic Ocean to Barrow is the largest in April. Considering

the Arctic Ocean covered with sea ice is general source of ozone-depleted airmass [Oltmans et al., 2012; Halfacre et al., 2013; Seabrook et al., 2013], the effect of wind from ocean can explain the largest frequency of ODEs at Barrow in April.

The most frequent ODEs at Alert in May can be also explained based on the effect of the wind from the Arctic Ocean. As shown in Figure 4.4, the wind flows dominantly from inland of Greenland to ocean. This wind pattern is due to the strong katabatic flow from the inland of the Greenland whose altitude is higher than the coastal area [Morin et al., 2005]. Katabatic flow is resulted from sinking of cold air from the high altitude. As temperature increases, this katabatic flow is gradually getting weak and the wind from ocean reversely becomes strong. As a result, ODEs at Alert is more affected by the transport of ozone-depleted airmass from the ocean, which is the reason of the most frequent ODEs in May.

Monthly frequency of ODEs also shows the trend in a decadal time scale. Figure 4.5 shows the monthly proportion of ODE frequencies in the spring for three decadal periods such as 1979 to 1988, 1989 to 1998, and 1999 to 2008. At Barrow, we found that proportion of ODEs increases in March, but decreases in May. To explain this trend, we compare the monthly average pattern of wind field between two decadal periods, 1979 to 1988 and 1999 to 2008 (Figure 4.6). In March, we find the wind from inland becomes weak in 1999 to 2008, and the wind from ocean more influence the airmass at Barrow resulting in the increase of ODE frequency in March. Large proportion of ODEs in March may also attribute to the increase of first year sea ice to produce more ozone-depleted airmass [Oltmans et al., 2012].

In May, wind from ocean becomes weak in 1999 to 2008, also resulting in the decrease of ODE frequency in May. The decadal change of wind pattern seems associated with the pattern of sea level pressure (SLP). During the decade with stronger wind from ocean, largely enhanced of SLP anomaly over the Beaufort Sea and North Pole (Figure 4.7), where Beaufort High generally appears. Probably the strong Beaufort High makes the strong wind blowing from the Arctic Ocean to the Alaska.

Opposite to the pattern at Barrow, monthly ODE frequency at Alert does not show decadal variation. Different from the variation of Beaufort High, affected by the large-scale atmospheric variability [Serreze and Barrett, 2011], katabatic flow does not change much in the long period. Since the frequency of ODEs at Alert is annually consistent, other environmental situations influenced by ODEs (e.g., atmospheric mercury deposition) may be relatively more stable and consistent at Alert than those at Barrow.

4.3.3 Influential factors for the termination of ODS

At last, we investigate the termination of ODEs at both Barrow and Alert. Average termination dates of ODS appear similarly at the end of May for both Barrow and Alert. In average, the termination dates of ODS are DOY 144 at Barrow and DOY 149 at Alert, namely the ODS at Barrow ends only 5 days earlier than those at Alert. Different from the onset dates of ODS, the end of ODS at both sites appears in a similar time period. No longer ODEs imply the inactive bromine chemistry with ozone. To maintain the catalytic process of bromine chemistry, the supply of particle phase is the most essential. Recently most of studies indicate that the snow is the effective media for the bromine recycling [Jones et al., 2010; Frieß et al., 2011; Abbott et al. 2012]. The

snow coverage in the Arctic rapidly decreases from the late May and disappears around June, meaning the ineffective environment of ozone depletion with bromine chemistry.

Time series of daily mean temperature (Figure 4.8) illustrate the gradual decrease of the temperature gap between Barrow and Alert, and finally the similar range of temperature around the termination of ODEs at both regions. At both sites, the temperature of termination dates ODS is around -5 °C, close to the zero. This basically indirectly shows that the end of ODS relevant to the snow melting, which decreases the particle phase of bromine explosion. Additionally, the extent of bromine release from the open leads and polynyas to the polar atmosphere is proportional to the vertical thermal contrast between relatively colder ocean surface and warmer air [Pöhler et al., 2010]. Thus, bromine release becomes weaker as surface air temperature increases, resulting in the weak ODEs.

Our finding for the role of surface air temperature to the termination of ODS will be more considered to understand the relationship between the temperature and the level of ozone in the Arctic, which is one of debating issues. Tarasick and Bottenheim (2002) showed the ozone depletion occurs when the ambient air temperature is smaller than -25 °C, but Newman et al. (2010) found ODEs even near -10. At least our finding identifies the criteria of temperature that enables the ODEs. Further, it suggests that we need to consider more condition of ambient particle and vertical temperature profile in order to understand the role of temperature on the process of ODEs. Besides, previous studies the termination of ODEs can be happened by the vertical intrusion of ozone-rich air by the wind shear above boundary layer [Strong et al., 2002] or the low pressure system [Jacobi et al., 2010], and the horizontal inflow of ozone-rich air by the low-pressure system

[Jacobi et al., 2010]. It also seems necessary to evaluate these effects comparing the termination of local ODEs.

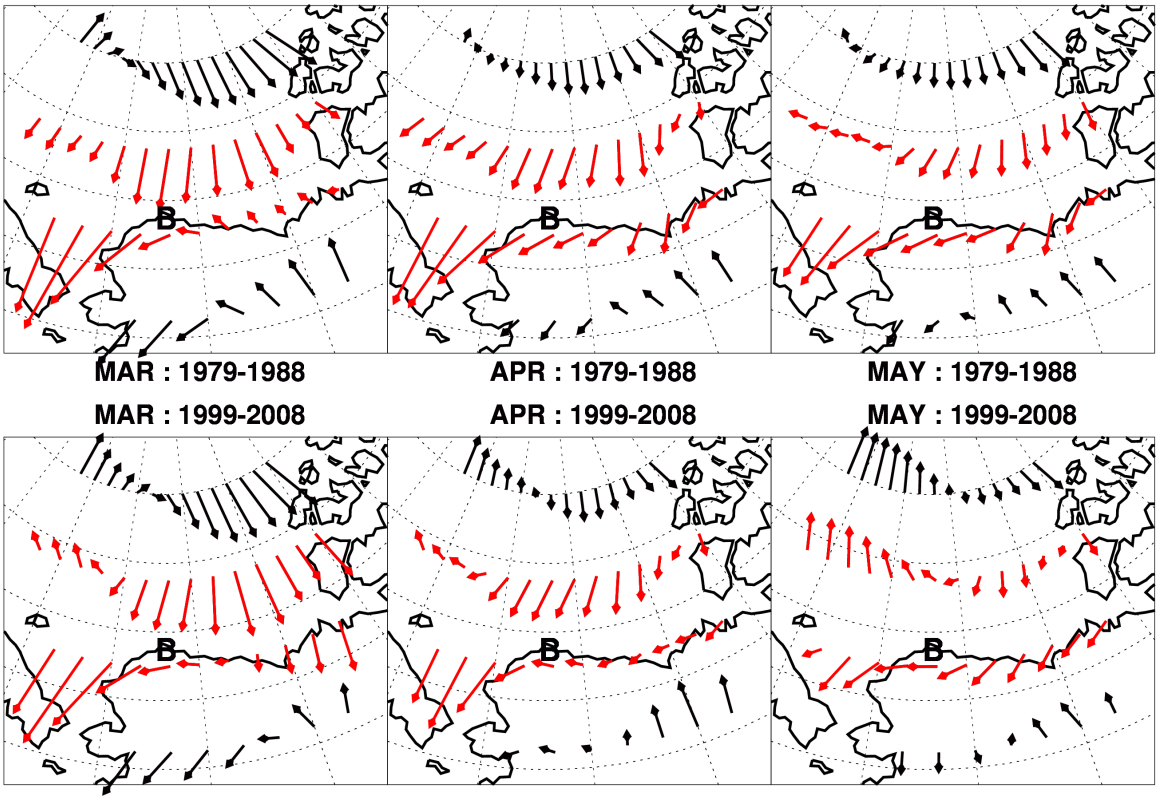

Figure 4.6 Decadal mean of monthly wind fields for March (left), April (middle), and May (right) near Barrow. Each arrow implies the mean wind speed and direction during the decade from the year 1979 to 1988 (top), and from the year 1999 to 2008 (bottom).

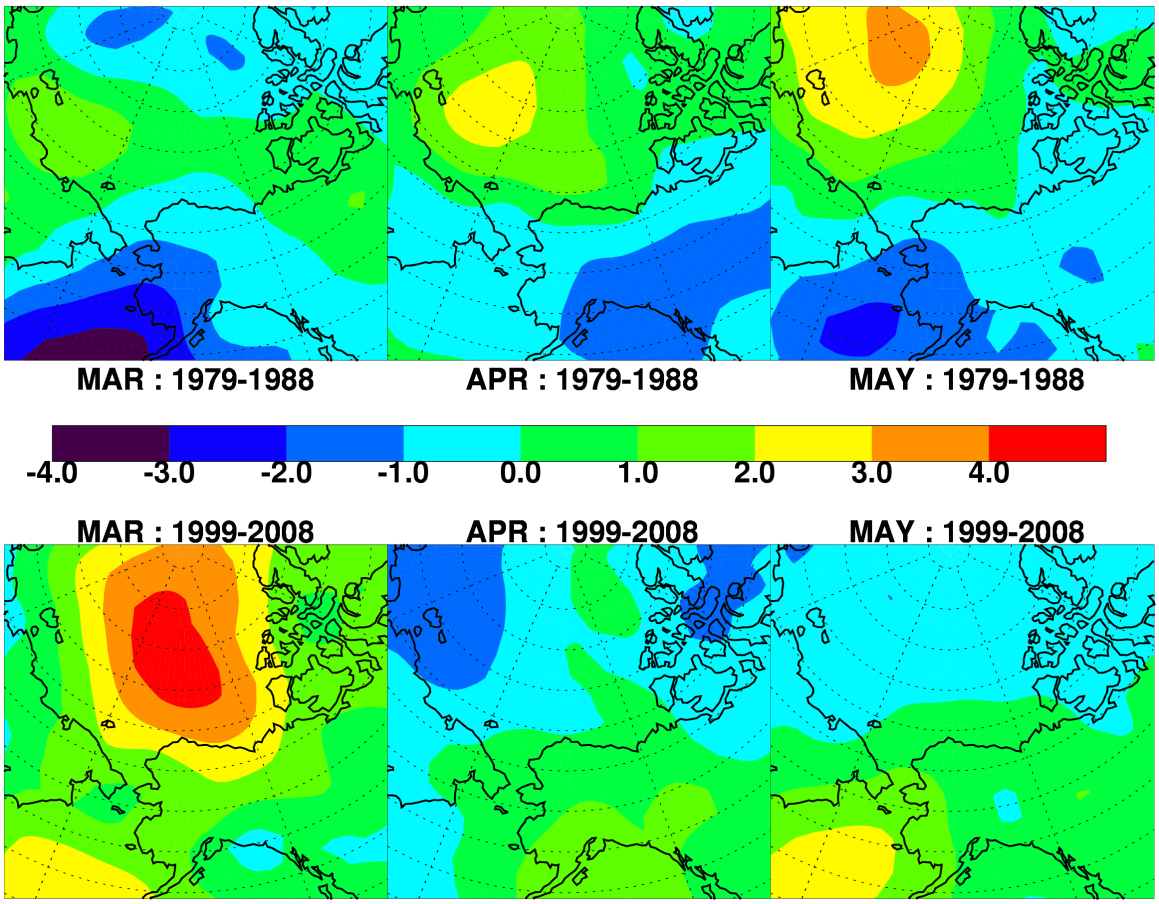

Figure 4.7 Decadal mean of sea level pressure anomalies for March (left), April (middle), and May (right) near Barrow. Two decades, 1979-1988 (top), and 1999-2008 (bottom) are compared.

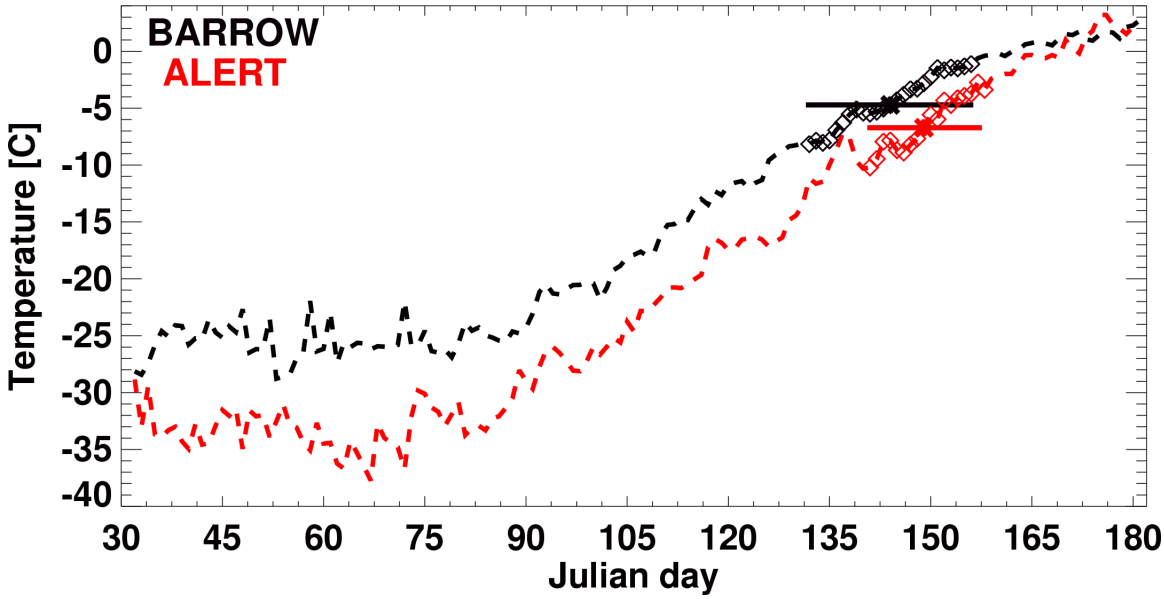

Figure 4.8 Daily mean surface temperature (°C) at Barrow (black dash) and Alert (Red dash). Two large dots indicate the daily mean temperature for the mean termination day of ODEs at Barrow and Alert. The range of 1-σ standard deviation (horizontal bar) and corresponding daily mean temperature (square dots) is also presented.

4.4 Conclusions

Comparing the onset, progression, and termination patterns of ODS between Barrow and Alert, we examined the spatiotemporal features of surface ozone depletion and the influence of ambient environmental conditions. In spite of catalytic chemical processes of the recycling of atmospheric bromine, we found that the certain amount of solar intensity is required to have enough depletion of surface ozone. And the same amount of daily total solar intensity in the onset dates can explain the difference of initiation of ODS between two sites. Once the solar radiative condition is guaranteed, the wind inflow from the Arctic Ocean that is the typical source area of ozone-poor air masses or bromine-included particle seems the most important factors to control the extent of local ODEs. Particularly the frequency of ODEs at Barrow shows the decadal-

shift due to the large-scale atmospheric variation affecting to the synoptic wind patterns. Warm air temperature is associated with the termination of ODS, revealing the important role of snow surface as a effective heterogeneous phase of bromine chemistry with ozone depletion.

The spatiotemporal difference of ODS, reflecting the role of ambient conditions, means that the variation of Arctic environment is sensitive to the climate change. In the future, we need to investigate the variation of ODS patterns more for the purpose of understanding other chemical issues in the Arctic such as mercury deposition or oxidation potential related to the Arctic haze. Thus, the experiments of in-situ measurements or model simulations will be required to collect more accurate information of solar flux, spatial distribution of wind pattern, and surface temperature with airborne condition of particle in accordance to the amount of depleted ozone.

CHAPTER 5

THE YEAR-ROUND PATTERN OF SURFACE OZONE AT SOUTH POLE: A REVERSAL TREND IN RECENT THREE DECADES

5.1 Background and motivation

South Pole is the only site in the Antarctica to have been monitored surface ozone continuously longer than three decades. This station is located in high altitude (2810 m) and air conditions here are generally affected by the katabatic flow from the east Antarctic plateau [Crawford et al., 2001; Davis et al., 2008; Wang et al., 2008]. In spite of pristine area, surface ozone at South Pole is affected by high NO_x related to snow photochemistry [Grannas et al., 2007], known active over the east Antarctic plateau [Crawford et al., 2001; Davis et al., 2008; Wang et al., 2008]. The air-mass transport from the mid-latitude seems a dominant source of nitrogen [Crawford et al., 2001]. The rate of surface ozone photolysis also looks associated with the amount of UV flux from the space controlled by the thickness of stratospheric ozone layer [Schnell et al., 1991]. Mercury generally related to the surface ozone depletion was also detected substantially at South Pole but does not affect the surface ozone level due to no existence of surface halogen8. These are mostly episodic photochemistry, therefore much influence the surface ozone pattern in austral summer.

The surface ozone level at South Pole could be modulated by regional and large-scale atmospheric patterns since the east Antarctic plateau is the region sensitive to the variation of stratospheric ozone [Thompson and Solomon, 2002; Thompson et al., 2011].

The ozone hole in austral summer affects the pattern of atmospheric circulation in the Southern Hemisphere [Thompson and Solomon, 2002; Son et al., 2010; Thompson et al., 2011], resulting in the perturbation of stratosphere-troposphere exchange (STE) [Thompson et al., 2005]. This large-scale feedback relates to the representative climate variability in the Southern Hemisphere, called Southern Annular Mode (SAM). Surface temperature over the east Antarctica tends to be cool during the positive polarity of SAM [Thompson and Solomon, 2002; Gillert and Thompson, 2003; Turner et al., 2005]. Global model simulations somewhat captured the similar temperature pattern of east Antarctica with considering the forcing by ozone depletion substances in the stratosphere [Son et al., 2009l McLandress et al., 2011]. Thus the SAM and STE are the strongest in the austral spring and summer, when the stratospheric ozone depletion appears4.

However, the patterns of stratospheric ozone and SAM do not fully explain the surface environment in the Antarctica, particularly the recent warming trend [Shindell et al., 2004; Screen and Simmonds, 2012] and the expansion of sea ice [Zhang 2007; Bintanja et al, 2013]. Recent increase of the Antarctic surface temperature seems decoupled from the temporal pattern of SAM [Shindell et al., 2004] and more caused by the ocean warming [Ding et al., 2011] or the regional emission increase enhancing the greenhouse gas concentration in the global scale [Gillert et al., 2008]. Sea ice extent in the Southern Hemisphere, which is related to the surface temperature, shows an increasing trend. While still the stratospheric ozone depletion and SAM are still considered as driving forces [Turner et al., 2009], recently natural climate variability is also believed as another important factors to explain the sea ice pattern [Screen and Simmonds, 2012].

These large-scale situations, however, have not been much investigated with the in-situ observed ozone pattern at the Antarctic surface. As mentioned, long-term variation of surface ozone in Antarctica was rarely investigated due to the lack of long-term observations. Only at South Pole, an interesting reversal trend of surface ozone for recent three decades was reported [Oltmans et al., 2006, 2013], showing decrease from the early 1980s but turning to increase after the middle of 1990s. While previously the strength of ultraviolet radiation from the space [Schnell et al., 1991] or summertime ozone increase6 were in part examined to explain the surface ozone trend in austral summer, but why the surface ozone shows year-round reversal trend in decadal scales is rarely understood now. Here we focus on the seasonal pattern of surface ozone trend at South Pole, and examine the relationship to the known atmospheric situations around the Antarctica. This work will let us know how much the chemical background in Antarctic continent is affected by the large-scale atmospheric variability or even global climate change.

5.2 Data and methods We used the surface ozone measurements at South Pole during 30 years (1981-2010). The South Pole station (89.98° S, 24.80° W) is located in the edge of Antarctic eastern plateau and the altitude from the sea level is 2810 m (see Appendix B.1). Surface ozone measurements has been operated by the NOAA Earth System Research Laboratory (ESRL) using the UV absorption techniques and contributed to the WMO World Data Centre for Greenhouse gases (WDCGG, http://ds.data.jma.go.jp/gmd/wdcgg/). All ozone data for this study were retrieved with 1-hour time resolution from the WDCGG data archive and the data accuracy in the range of 0.5-2 ppbv [Helmig et al., 2007] is adequate for this study. For Figure. 5.1, we compared

the trend of 90, 50, and 10th percentiles of surface ozone. Percentile values of ozone were selected in hourly ozone levels for each season. Thus, 90th percentile value means only 10 % of ozone levels are larger than this value in each season.

Ozonesonde also has been launched occasionally at South Pole. Due to the deficiency of data, we only used ozonesonde measurements from 1991 to 2010 and the months with single ozonesonde launching were not considered in the study. Using these data, we calculated the climatologically mean vertical profile of ozone and surface delta ozone at each season for Figure 5.2. Delta ozone is here defined as the difference of surface ozone between the real observation and background level [Crawford et al., 2001], showing the activity of surface ozone chemistry. We presume that background level of ozone is originated from the upper level. Hence, we extrapolated background ozone levels at the surface using the third-order regression from the vertical mean profile of 0.5 to 4.0 km height above from surface (see Appendix B.2). Positive delta ozone implies the measured ozone level is higher than background estimation, revealing indirectly the surface ozone production.

We examined potential temperature information using NCEP-DOE reanalysis 2 data (NDR2) [Kanamitsu et al., 2002]. NDR2 shows strong consistence with in-situ measurements in the Antarctica3 and have been used for the analysis of climate pattern in this region [Thompson and Solomon, 2002; Turner et al., 2005; Thompson et al., 2011]. To examine the atmospheric variability with surface ozone at South Pole, we estimated the potential temperature over the east Antarctic plateau, which is the averaged potential temperature over the area higher than 3000 m altitude in the Antarctica.

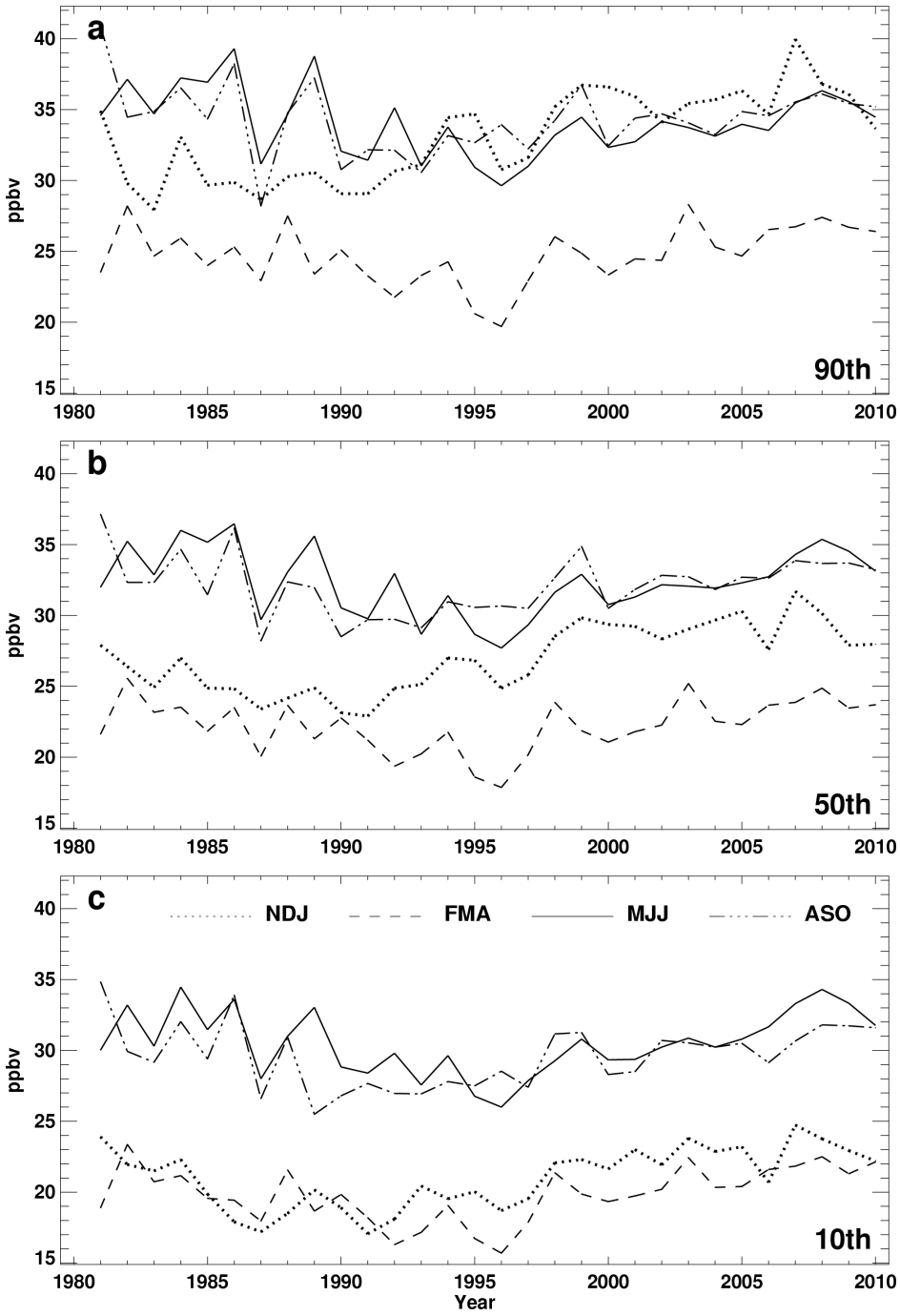

Figure 5.1 Reversal trends of surface ozone during 30 years at the South Pole. Results shows the 30-year (1981 to 2010) trends of surface ozone in percentiles of (a) 90 %, (b) 50 %, and (c) 10 % for four seasons – spring (August to October, ASO), summer (November to January, NDJ), autumn (February to April, FMA), and winter (May to July, MJJ).

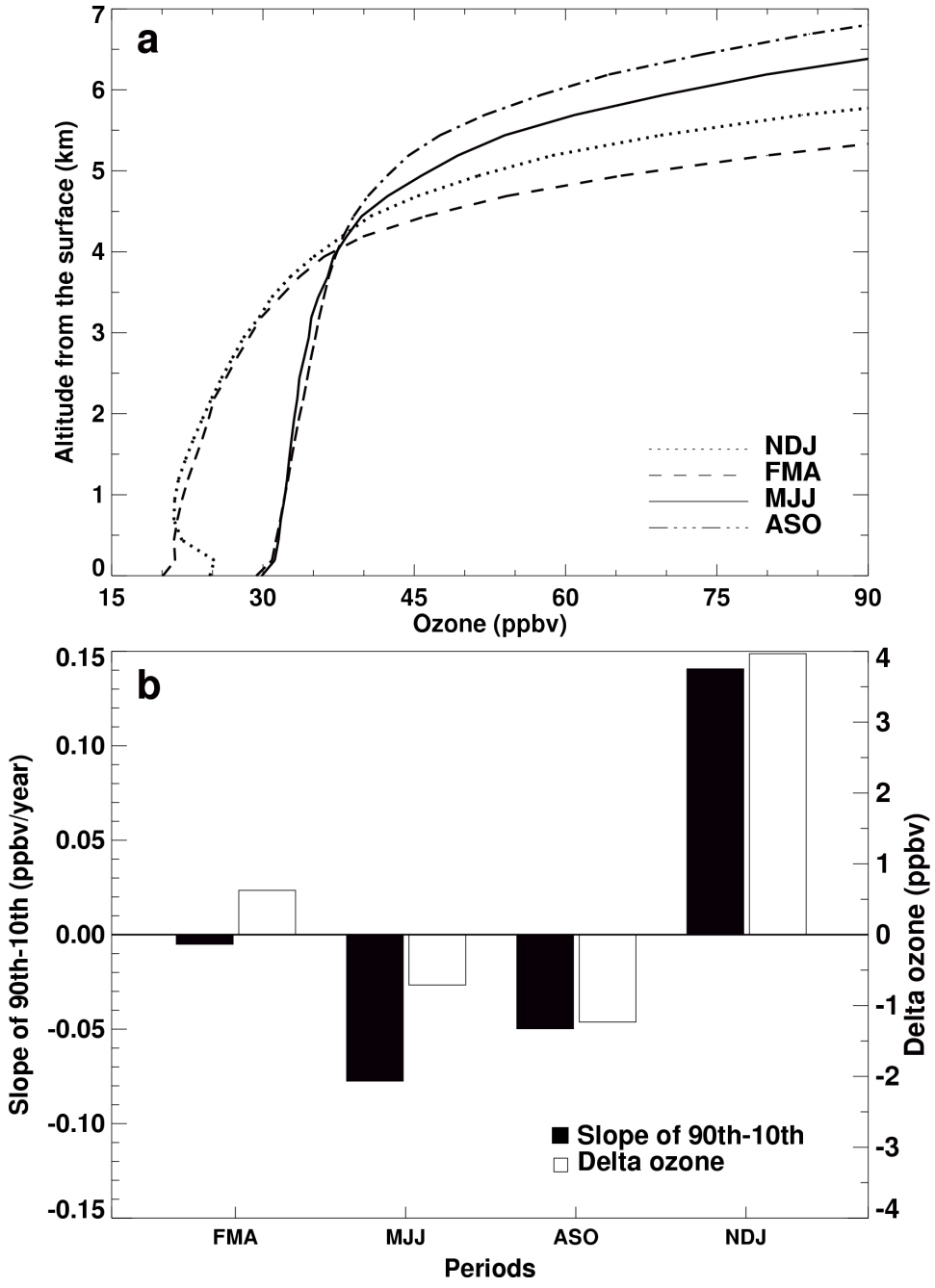

Figure 5.2 Ozone productions in the winter at the South Pole. a, Vertical profiles of seasonal mean ozone at the South Pole during 20 years from 1991 to 2010. The line colors and shapes for each season are same in Figure 1. b, The linear trends of the difference between 90th and 10th percentile of ozone are presented (black bar) and compared with the delta ozone at the surface for four seasons (white bar).

For the comparison to the trend of surface ozone at South Pole, we examined the annual mean (Figure 5.2), seasonal mean (Figure 5.4) and 5-year running mean (Figure 5.5) of potential temperature at the 500-hpa level where the correlation with ozone is maximum.

5.3 Results and discussions

We first look into the three decadal (from 1981 to 2010) trend of observed surface ozone at South Pole for each season (Figure 5.1). We examine the trend for the 90th, 50th, and 10th percentiles of surface ozone separately to see the variability at the different ozone level. In spite of the inter-annual variability, generally three percentiles of surface ozone decrease during the first half of 30 years but increase during the latter half. This reversal trend pattern appears consistently for all seasons, implying the annual mean trend of ozone at the South Pole [Oltmans et al., 2006, 2013] is not driven by specific seasonal properties. The austral summer (from November to January) only shows the difference between among percentiles; 10th percentiles show a reversal trend similar to other seasons, whereas 90th percentiles show an increasing trend during 30 years. It means that ozone production (shown in high percentiles) at South Pole becomes getting larger in austral summer while background ozone (shown in low percentiles) follows the general reversal trend.

Comparison of seasonal mean vertical profile of observed ozone at South Pole (Figure 5.2a) also indicates the discrepancy in austral summer. Generally the level of ozone is higher as the altitude increases due to the subsidence of ozone aloft [Crawford et al., 2001], however the surface ozone during the summer exceeds the ozone in the lower troposphere, revealing the enhancement of ozone production at the surface. We calculate

how much the surface ozone is produced for each season using delta ozone, an estimated value showing the ozone production (see Methods). Generally delta ozone is largely positive (i.e., high ozone production) in austral summer season (Figure 5.2b). We also compare the delta ozone with the trend of difference between 90th and 10th percentile of ozone at each season. Similarly, only summer is the period showing positive trend, meaning that the surface ozone production becomes more active and contributes to the increase of the high percentile of ozone.

Released NO_x through the snow photochemistry seems the driving force of surface ozone production in austral summer. Despite rare local anthropogenic sources, substantial atmospheric NO_x in summer has been reported in the east Antarctic plateau area [Crawford et al., 2001; Davis et al., 2008]. The origin of nitrogen in the Antarctic plateau is supposed to be the transported air mass from the lower latitude where anthropogenic pollution and biomass burning occurs, and NO_x can be produced in summer by the photolysis in the snow-air heterogeneous phase [McLandress et al., 2011]. In fact, the snow NO_x flux estimated based on a parameterization method using the measured dataset in the Antarctic Tropospheric Chemical Investigation (ANTCI) campaign [Wang et al., 2008] also shows a small increasing trend in summer (Figure 5.6).

This ozone production does not appear in other seasons due to the weak solar radiation, therefore it affects the summer trend much. However, ozone enhanced enough in summer can also change the background of surface ozone during whole year. Namely the recent increasing trend of surface ozone might be partly induced by the high ozone level in summer. Nevertheless, there might be another factor to better explain the year-

round trend of surface ozone at the South Pole. And based on the little seasonal discrepancy of ozone trend, the low-frequent variability of large-scale atmosphere seems highly associated with.

As mentioned, ozone at South Pole is affected by air-mass transport from the east Antarctic plateau. Thus we investigate the atmospheric pattern over east Antarctic plateau using National Centers for the Environmental Prediction – Department of Energy (NCEP-DOE) Reanalysis 2 dataset (NDR2) [Kanamitsu et al., 2002]. Since correlations between ozone and temperature can be used to speculate the dynamical effect besides chemical processes [Solomon et al., 2005], the decadal trend of potential temperature from NDR2 is compared with that of observed surface ozone. As a result, we find that lower-tropospheric potential temperatures over the east Antarctic plateau show reversal trends same as the surface ozone at South Pole (R=0.73) (Figure 5.3a). As what surface ozone shows (Figure 5.1), the trend of potential temperature is also consistent for all seasons (Figure 5.4). Comparing 5-year running average (Figure 5.5), surface ozone and potential temperature shows a much higher correlation (R=0.92), clarifying the steady and low-frequent feature of both reversal trends. These high correlations between surface ozone and potential temperature at different vertical heights are strong enough below 400-hpa level (A maximum correlation at 500-hpa level), but disappear in the upper layers (Figure 5.3b).

In-situ temperature measurements generally have reported the near-surface cooling in the east Antarctic region until the late 1990s [Thompson and Solomon, 2002; Turner et al., 2005] but warming in the recent 2000s [Steig et al., 2009; Screen and Simmonds, 2012]. The temperature cooling in the 1990s has been interpreted by the

influence of positive phase of SAM [Thompson and Solomon, 2002; Thompson et al., 2011]. But in the 2000s, the SAM cannot explain the warming trend any more [Shindell et al., 2004; Screen and Simmonds, 2012]. Previous global model study indicated the role of SAM to the temperature trend of extratropical region is much less in early 21th century than the late 20th century trend, and supposed the Antarctic continental temperature will be more affected by the global warming than SAM [Shindell et al., 2004]. This means that SAM, despite the possible impact to the Antarctic surface until the 1990s [e.g., Schneider et al., 2004], is not a dominant factor to influence the surface ozone during whole recent three decades. In other words, STE processes according to the variation of stratospheric ozone do not seem to influence the reversal trend of surface ozone. This hypothesis is consistent with a weak correlation between surface ozone and potential temperature above the upper troposphere (Figure 5.3b). We also compared the surface ozone produced from the Community Atmospheric Model (CAM) 5.0 with or without considering the variation of stratospheric ozone in recent three decades. Both simulations, however, do not show much discrepancy each other (Figure 5.7). Besides surface ozone, global model did not capture the trend of Antarctic sea ice extent [Sigmonds and Fyfe, 2010; Bitz and Polvani, 2012]. All these findings again show the weaker effect of the stratospheric ozone hole to the Antarctic surface.

The reversal trend of surface ozone at the South Pole then seems more affected by the patterns of lower tropospheric atmosphere. A positive correlation between surface ozone and potential temperature reveals that stronger horizontal mixing during warm periods possibly enhances ozone inflow from the mid-latitude region. Particularly in the recent decade, the Antarctic sea ice extent is getting expanded due to oceanic

thermohaline stratification around Antarctica by warm atmosphere and ocean [Zhang 2007; Bintanja et al., 2013], and the amount of global emission has been increases [Gillert et al,, 2008]. Therefore, larger thermal contrast between Antarctic sea ice and Southern Hemispheric Ocean also intensifies the stronger meridional mixing of atmosphere resulting in larger air-mass transport from mid-latitude, resulting in recent sharp increase of surface ozone at South Pole. Likewise, increasing ozone production in summer (Figure 5.2b) seems attributed to the larger transport of mid-latitudinal nitrogen. Further, this large meridional mixing better explain why surface ozone at South Pole shows year-round trends in contrast with the summertime impact of stratospheric ozone and SAM.

5.4 Implications

Since the continuous increases global emission will be anticipated [Solomon et al., 2007], the warming trend of Southern Hemispheric atmosphere and ocean seems highly feasible in the future, meaning the higher enhancement of background ozone at South Pole. Previously global chemistry models also expected a large increase of surface ozone in the Southern Hemisphere due to the stratospheric ozone recovery and climate change [Zeng et al., 2010; Zhang et al., 2013]. This enhanced ozone background will presumably affect the Antarctic climate through, for example, the change of tropospheric radiation budget or chemical environment. But still we cannot totally neglect the possible influence of natural climate variability [Polvani and Smith, 2013] to the surface ozone trend. More long-term observations and model experiments of the Antarctic surface ozone will be required to diagnose its effect.

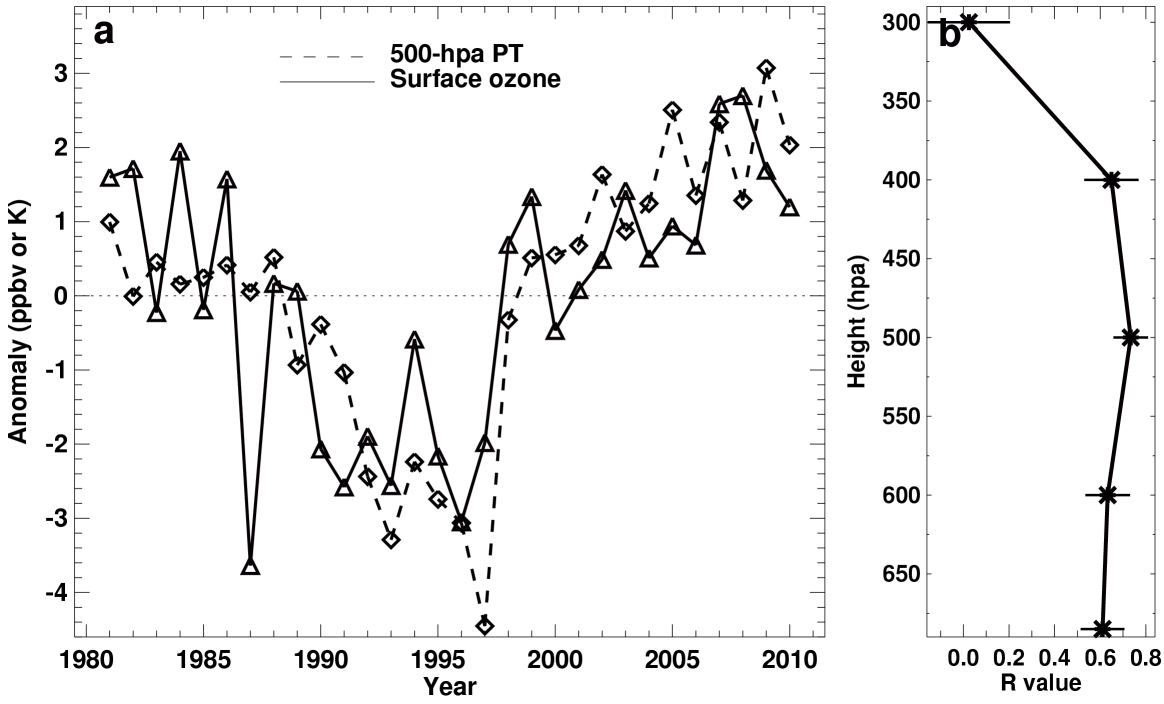

Figure 5.3 The relationship of surface ozone at the South Pole to the potential temperature over the East Antarctic plateau. a, The 30-year trend of anomaly of annual mean surface ozone (in-situ observation) at the South Pole (solid) and annual mean potential temperature (NCEP/NCAR reanalysis) in the 500-hpa level over the East Antarctic plateau (dash). b, Vertical profile of correlation coefficients of surface ozone with potential temperature at the surface, 600-, 500-, 400-, and 300-hpa height levels. Horizontal bar indicates of the 1-σ standard variation of correlations based on the 2000 bootstraps.

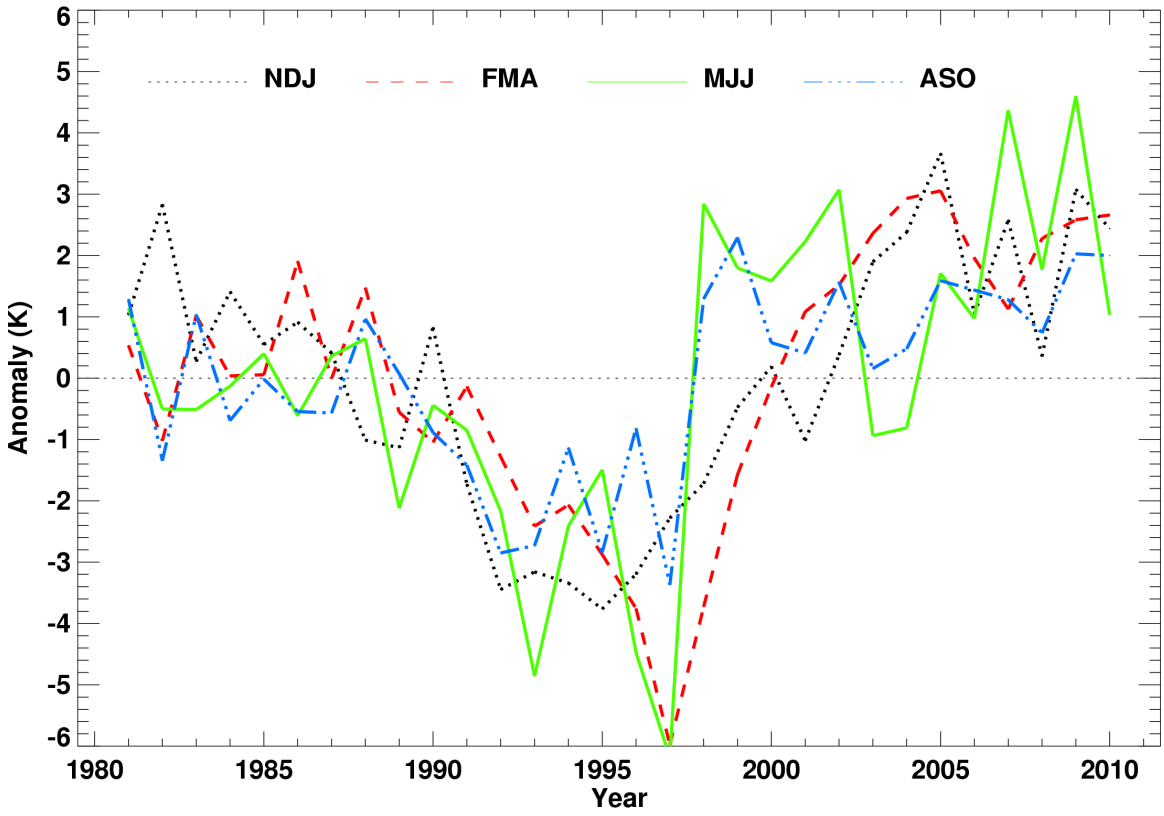

Figure 5.4 The seasonal mean trend of NDR2 500-hpa potential temperature anomalies over the east Antarctic plateau for four seasons, spring (August to October, ASO), summer (November to January, NDJ), autumn (February to April, FMA), and winter (May to July, MJJ).

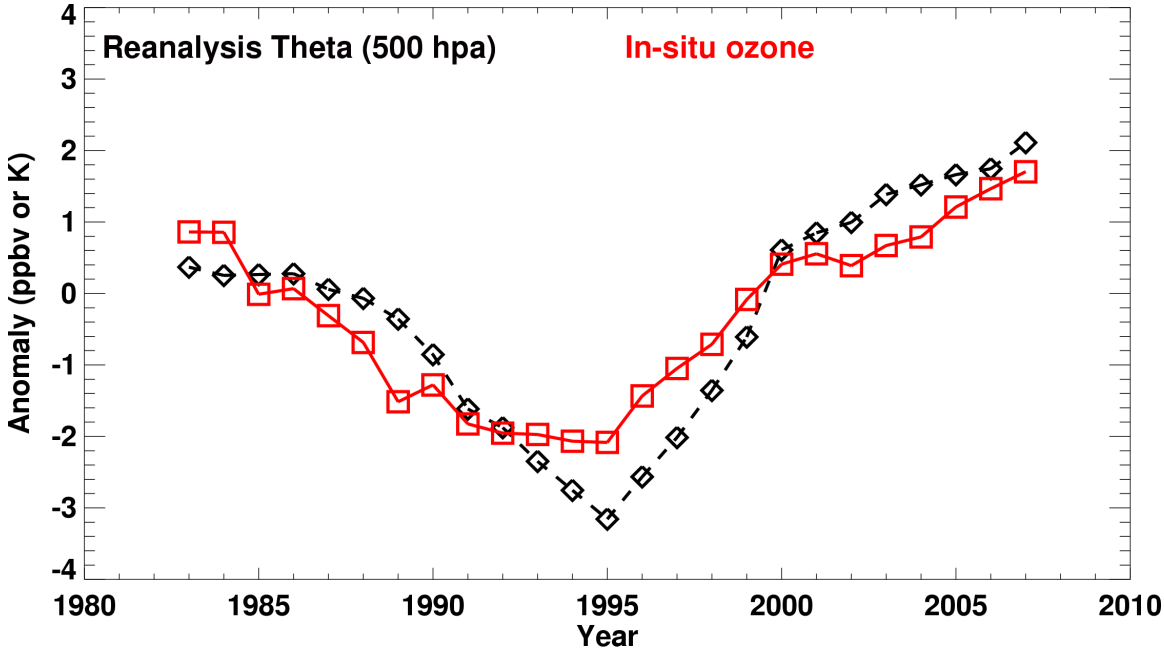

Figure 5.5 The trend of 5-year moving average of NDR2 500-hpa potential temperature anomalies over the east Antarctic plateau (black dash) and in-situ observed ozone anomalies at South Pole (Red line).

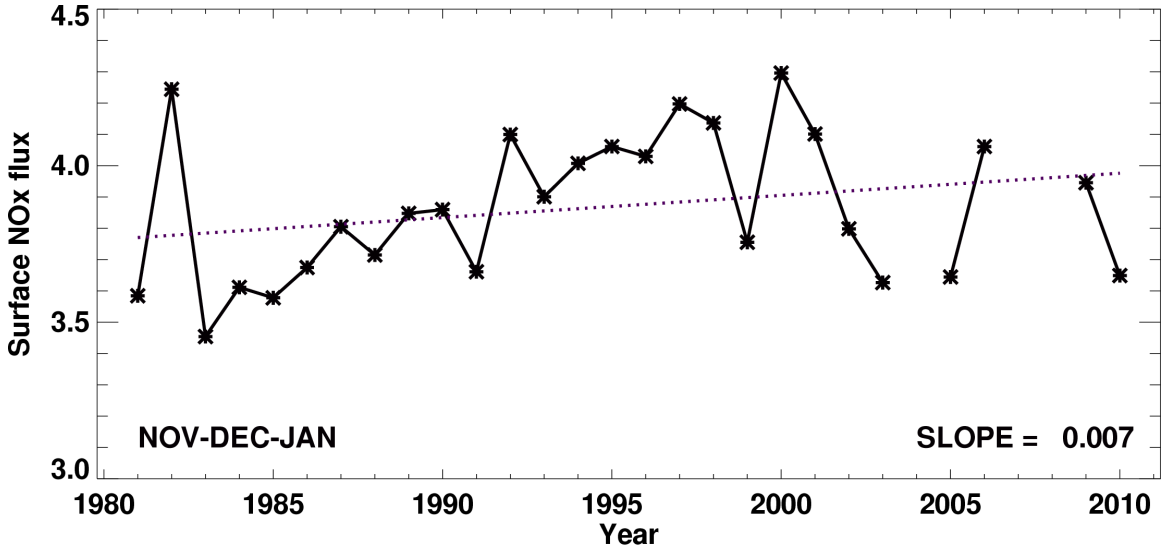

Figure 5.6 The trend of estimated surface NO_x flux during the austral summer (November, December, and January).

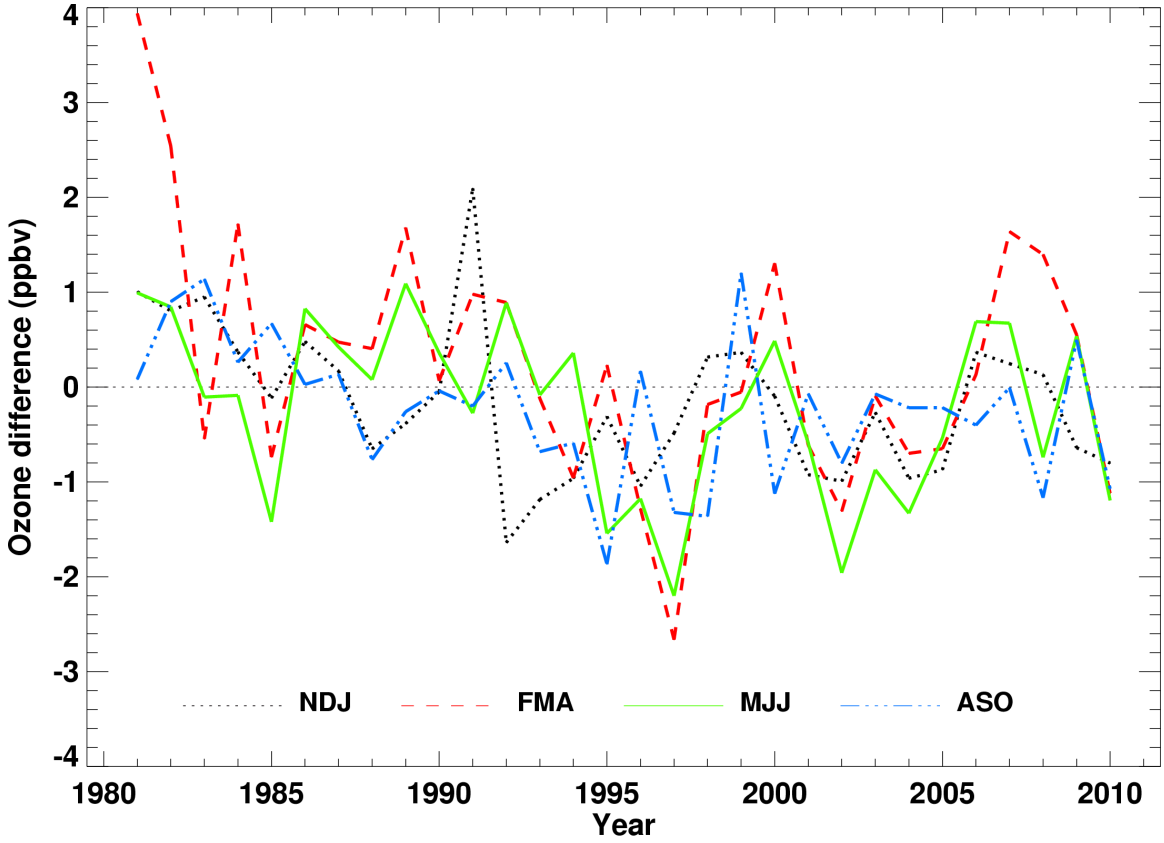

Figure 5.7 The inter-annual variation of surface ozone difference at South Pole between two CAM5 simulations: prescribing climatology stratospheric ozone (Sim_clim) and prescribing stratospheric ozone (Sim_sparc) from AC&C/SPARC dataset. Namely, ozone differences are obtained by subtracting ozone produced with Sim_clim from Sim_sparc. To see the pattern at South Pole, the ozone values in the grids of lowest latitude are averaged. Ozone differences are calculated for four seasons, spring (August to October, ASO), summer (November to January, NDJ), autumn (February to April, FMA), and winter (May to July, MJJ).

CHAPTER 6

CONCLUSIONS AND FUTURE WORK

6.1 Summary of findings

6.1.1 Regional difference of ODE structures in the Arctic spring

Previous analyses of measurements and related model experiments have, in general, focused on several intensive ODE events at specific locations. This study provides an understanding of regional variations of ODEs in the Arctic by analyzing several datasets for different locations in April 2008 (Chap 2). The study reveals the dependence of ODEs on source regions of ozone depleted and BrO enhanced air masses. The study uses an enhanced method to analyze back-trajectory patterns based on time lag data to clarify the influence of ozone depleted air mass transport on ODEs with an effective transport range of less than three days. Two satellite dataset, OMI and GOME-2, through analysis of BrO VCDs identify consistently high BrO regions in the Chukchi Sea and the Canadian Archipelago. Simple back-trajectory analysis based on local ozone level shows that regions of high BrO enhancement are also source regions for ozone-depleted air masses with the largest influence on ODEs.

Vertical scale analysis of ODE structure shows significant regional characteristics. ODEs at Barrow have the characteristics of a strong event in a shallow boundary layer where vertical stability promotes the near surface catalytic loss of ozone. The situation of this location is consistent with a long held view that vertical stability is a sufficient condition for ODEs. At Resolute and Churchill, however, ODEs are relatively

deep (even > 1 km) and are consistent with the hypotheses of other studies. ODEs at Churchill, in particular, are occurring in an unstable vertical column. These ODEs are consistent with the hypothesis that blowing snow is a favorable particle phase environment for a bromine explosion. Also, the ODE structure at Churchill supports the previous hypothesis that strong convection from the surface can contribute to the enhancement of free tropospheric BrO.

6.1.2 Influence of ambient conditions to polar surface ozone

It has been believed that cold air temperature contributes to the strong ODEs because (1) a stable boundary layer is a better condition for the catalytic loss of ozone with bromine chemistry and (2) large thermal contrast between warmer ocean surface and colder air surface can enhance the bromine release into the atmosphere. However, some previous studies did not find a meaningful relationship between ozone and temperature. In this study, a positive correlation was found between ozone and temperature for the three Arctic sites for the April 2008 data (Chapter 2) when both the ozone and temperature data were detrended (i.e., removing natural variability).

Comparison of long-term ozone measurements between Barrow and Alert also show a difference in temporal characteristics of ODEs (Chapter 4). The first ODE in a year is initiated after the minimum amount of solar intensity is guaranteed. This finding may indicate a threshold condition to activate the catalytic bromine photochemistry that results in a strong depletion of ozone. Once the bromine photochemistry is activated, however, wind strength from the ocean is a significant factor affecting the frequency of local ODEs; the stronger wind from the Arctic Ocean, the more frequent ODEs. Moreover at Barrow, the monthly pattern of ODE frequency also shows a decadal-shift

(the number of ODEs in March increases but those in May decreases) consistent with a decadal pattern change in wind from the Arctic Ocean. The termination of ODEs at Barrow and Alert are similar in that they occur when the temperature is close to 0 °C. This shows that the existence of snow is an important prerequisite to support the ODEs with bromine chemistry in heterogeneous phases (gas and particle phase). Snow condition also relates to the NO_x photochemistry in the polar region, which contributes to surface ozone production in austral summer over the east Antarctic plateau (Chapter 5).

6.1.3 Relation of polar surface ozone to large-scale atmospheric variability

It is understood that polar atmosphere is sensitive to large-scale atmospheric patterns and climate variability, inferring that the pattern of polar surface ozone is related. This study first investigated the relationship between surface ozone and large-scale atmospheric variability based on the long-term data analysis and several climate datasets.

Monthly ODE frequencies in the Arctic spring (April) show very large inter-annual variations at all monitoring sites of surface ozone (Chapter 3). Analysis of teleconnection indices and SLP anomalies shows a relationship between the WP pattern and ODE variations at Barrow and Alert. The pattern of the Pacific jet stream and storm track intensity, which are known to be partly associated with the phase change of WP pattern, also show a relationship to between the selected of strong and weak ODE periods; stronger jet stream and weaker storm track intensity for the years of strong ODEs and vice versa. Pacific jet and storm track look to control the strength of meridional mixing and airmass transport between the mid-latitude and the Arctic, which affect to the level of background ozone in the Arctic.

Similarly, surface ozone at South Pole, Antarctica also seems affected by the regional climate patterns. Observed surface ozone at South Pole shows a V-shape reversal trend during recent three decades; decreasing in the first half but increasing in the latter half (Chapter 5). Interestingly this ozone trend is year-round pattern, implying the potential influence of slow and steady forcing in the large scale. Lower tropospheric potential temperature from NCEP/NCAR reanalysis also shows the year-round reversal trend the same as the surface ozone, and their correlation is R=0.73 when comparing annual mean, and R=0.92 for comparing a 5-year running average. This finding also seems due to the effect of meridional mixing. Namely, the stronger meridional mixing generates larger inflow of warm and polluted air mass from the mid-latitude to Antarctica and induces the year-round reversal trend of ozone and temperature in the lower troposphere.

6.1.4 Implications for the polar and global climate environment

Near-surface ozone depletion with bromine chemistry (Chapter 2, 3, and 4) relates to the atmospheric mercury deposition events (AMDEs), which destroy the polar ecosystem. In the Arctic, sea ice melting becomes accelerated, resulting in the large increase of first year sea ice (FYI) and decrease of sea ice thickness. Since FYI has been considered as a strong source of atmospheric bromine, increases of FYI area will probably result in a large occurrence of ODEs in the Arctic spring, implying stronger AMDEs in the future. This is one reason why a better understanding of ODEs is important.

Since ozone has a large oxidation potential, strong ODEs may not play a role in diminishing Arctic pollution, such as Arctic haze. Based on the known features of climate

change at this time, the occurrence of ODEs will probably increase as mentioned, and the Arctic haze will appear more frequently due to larger global emission and increase of wild fire events adjacent to the Arctic. Therefore, it is anticipated that the Arctic pollution becomes longer and more serious. In the Antarctic, warmer and more polluted background air may contribute to the radiative forcing budget by surface and tropospheric ozone, which is also a greenhouse gas.

6.2 Recommendations for future work

6.2.1 Statistical approach to the effect of ambient conditions

This work shows that local ODE patterns are related to various atmospheric factors and that their effect is not negligible. However, these relationships are not well understood. A difficulty is that findings based on the specific time period or area may not be applied to interpret the features occurred in other area. Therefore there seems a need for more statistical analysis, which can identify the regional spatiotemporal characteristics such as underlying trends and features. For example, in this study a detrending process was applied to the analysis of the relationship between ozone and temperature (Chapter 2) and found good correlations between them consistent at the three surface sites in the study.

Ambient atmospheric conditions and meteorological information can now be examined using the various reanalysis datasets whose quality has been proved by many previous works in spite of some uncertainties. Also satellite measurements have provided qualified data for at least a decade. Year-to-year comparisons, trend analyses, and

extreme case studies for ozone and related air conditions will suggest better insights of polar surface ozone.

6.2.2 Projection of polar ozone trend in terms of climate change

Findings in Chapter 3 show that the influence of WP pattern to the Arctic ODEs has become larger in the recent decade. Although the effect of WP pattern will be investigated more, at least it can be used as a proxy to diagnose of local ODEs. If it is possible to anticipate the future WP pattern, projection of local ODEs and related environmental issues in the Arctic spring will be possible. The recent warming trend in the Arctic is another factor should be examined. The higher temperature accelerates the increasing trend of first year sea ice that has acted as one of large source regions for bromine release into the air, but decreases the snow coverage that provides the heterogeneous phase for the bromine chemistry of ozone depletion. Investigation of these two opposite effect will enable us to evaluate the climate effect to the polar atmospheric chemical environment. Increasing trends in ocean warming and global emission of greenhouse gases also will be able to affect the surface ozone in Antarctica (Chapter 5). Global climate change in the current direction may result in a higher polluted condition over the Antarctica.

6.2.3 Improving model simulations of near-surface chemistry

Model simulation is the most difficult part for the analysis of polar ozone depletion and bromine chemistry. Previous model studies usually used aerosol surface distribution to consider the particle phase in the model. But recent studies presented that (blowing) snow is the most efficient particle phase for bromine chemistry. Thus how to include the snow particle conditions is the key point to improve model performance.

Chlorine is another important species that the model should consider later. In spring 2009, high level of chlorine species was measured at Barrow [Liao et al., 2014c], which is totally different from previous knowledge. The reason to explain large amounts of chlorine will be a main goal of future model study. Besides, there are many unresolved issues of model study such as (1) vertical profile of ozone and bromine species, (2) the existence of free tropospheric BrO, (3) temporally reasonable trace to what real measurements show.

APPENDIX A

AUXILIARY MATERIALS FOR CHAPTER 2

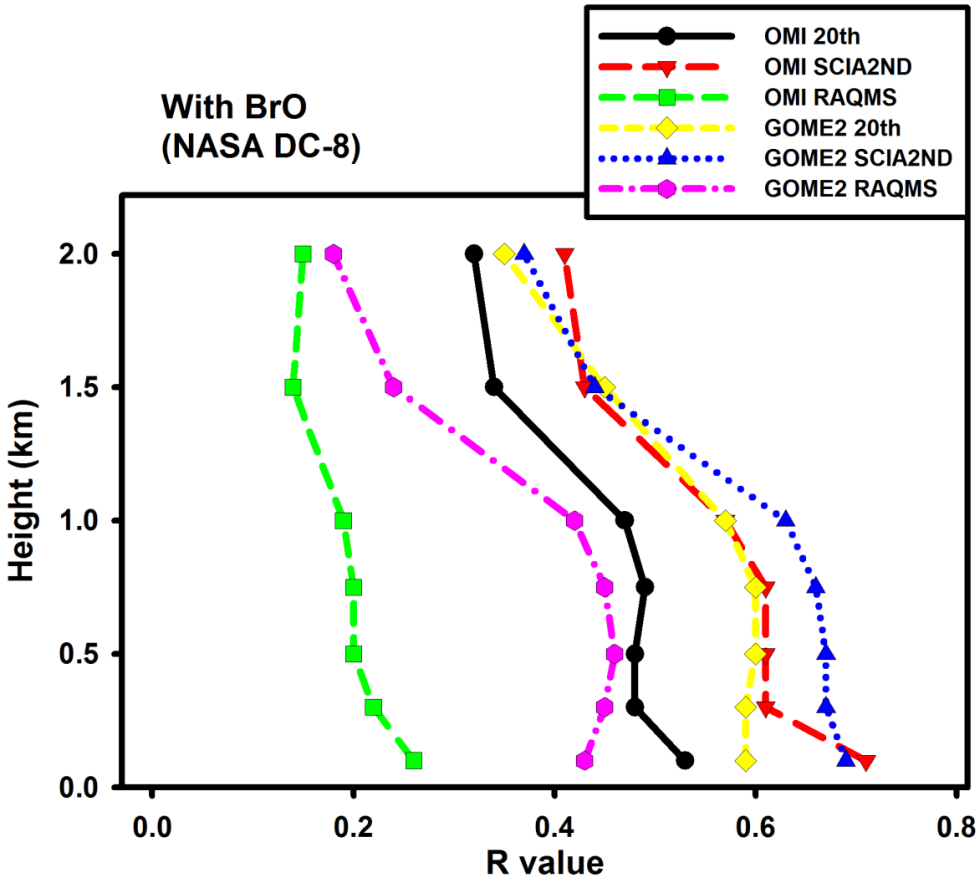

Figure A.1 Vertical profiles of correlation coefficients (R values) of retrieved tropospheric BrO columns with BrO measured from DC-8 Flights 9 and 10 (April 16 and 17). To correlate with tropospheric BrO columns with sufficient in situ data points, we integrate in situ aircraft observations of BrO, Br_2+HOBr, and soluble bromide from the surface to 7 altitude levels (100, 300, 500, 750, 1000, 1500, and 2000 m). Tropospheric column BrO measurements corresponding to the in situ data points were sampled along the flight tracks. WP-3D data were not used because no significant correlation was found with column BrO; the reason is unclear. We used six tropospheric BrO VCD products, which are OMI-20th (black), OMI-SCIA2ND (red), OMI-RAQMS (green), GOME2-20th (yellow), GOME2-SCIA2ND (blue), and GOME2-RAQMS (purple).

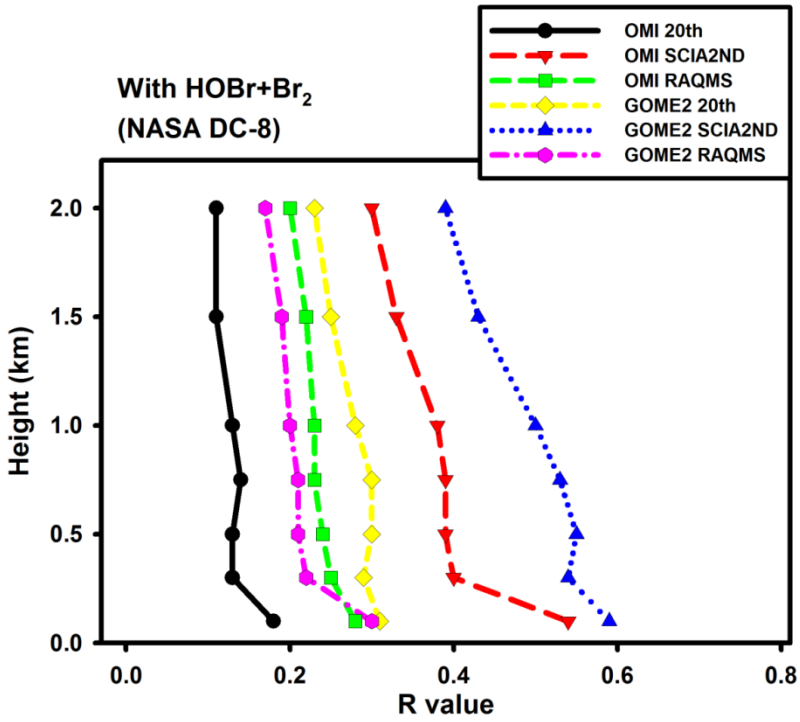

Figure A.2 Same as Figure A.2, but for correlations with integrated Br_2+HOBr in DC-8 flights (April 4, 5, 8, 9, 12, 16, and 17).

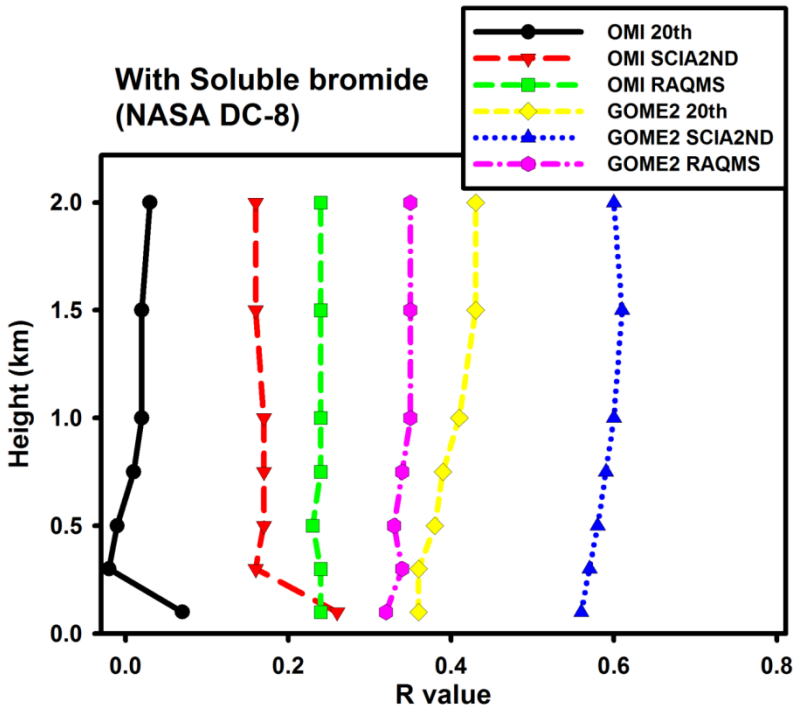

Figure A.3 Same as Figure A.1, but for correlations with integrated soluble bromide measured in DC-8 flights.

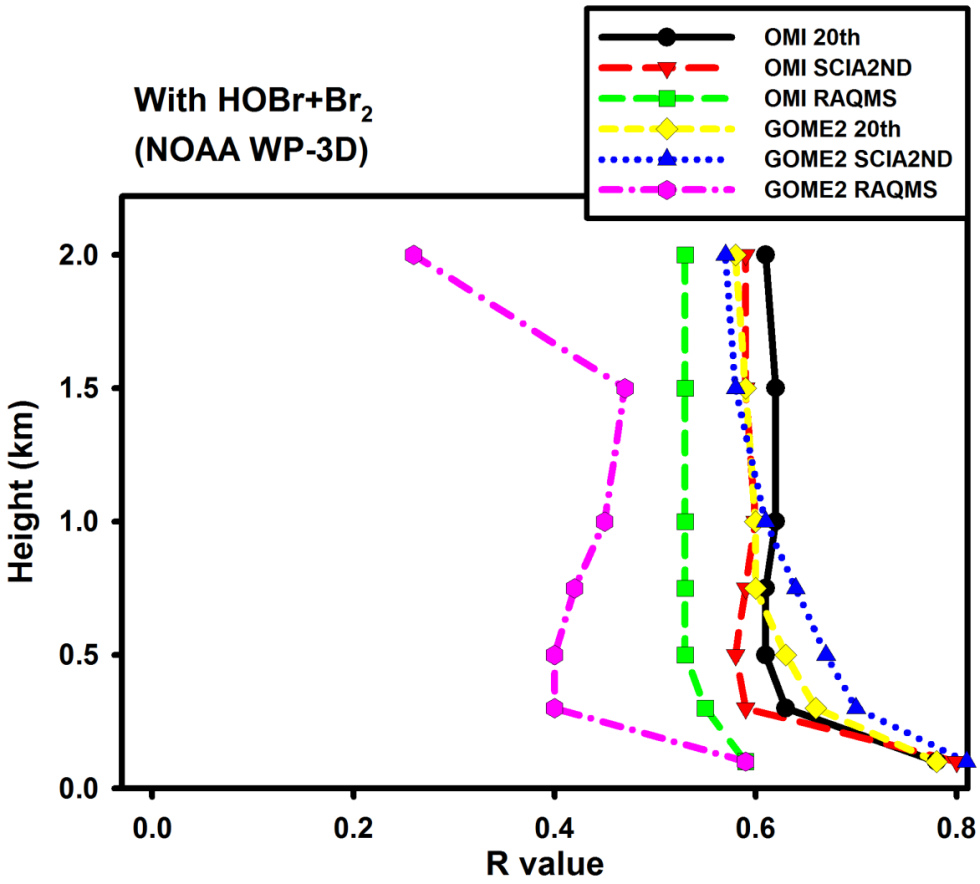

Figure A.4 Same as Figure A.1, but for correlations with integrated Br_2+HOBr in WP-3D flights (on April 12, 15, 18, 19, and 21). The more consistent correlation with Br_2+HOBr measurements during ARCPAC than ARCTAS (Figure A.2) reflects in part a smaller sampling region by WP-3D (to be shown in Figure 2.5). The smaller sampling region leads to a smaller variation of the estimated stratospheric column BrO during ARCPAC than ARCTAS. The variation of tropospheric column BrO is therefore more consistent among the different products during ARCPAC than ARCTAS.

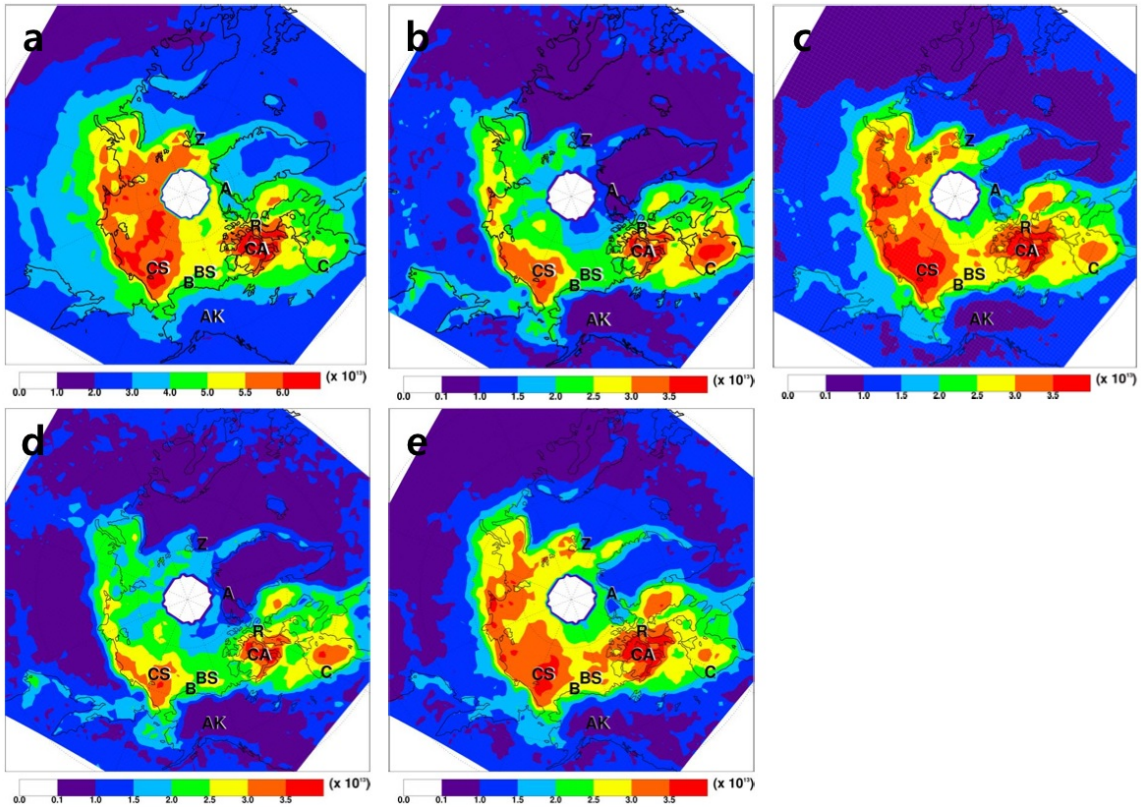

Figure A.5 Same as Figure 2.2, but for tropospheric BrO VCDs of (a) OMI-SCIA2ND, (b) GOME-2-20th, (c) OMI-20th, (d) GOME-2-RAQMS, and (e) OMI-RAQMS.

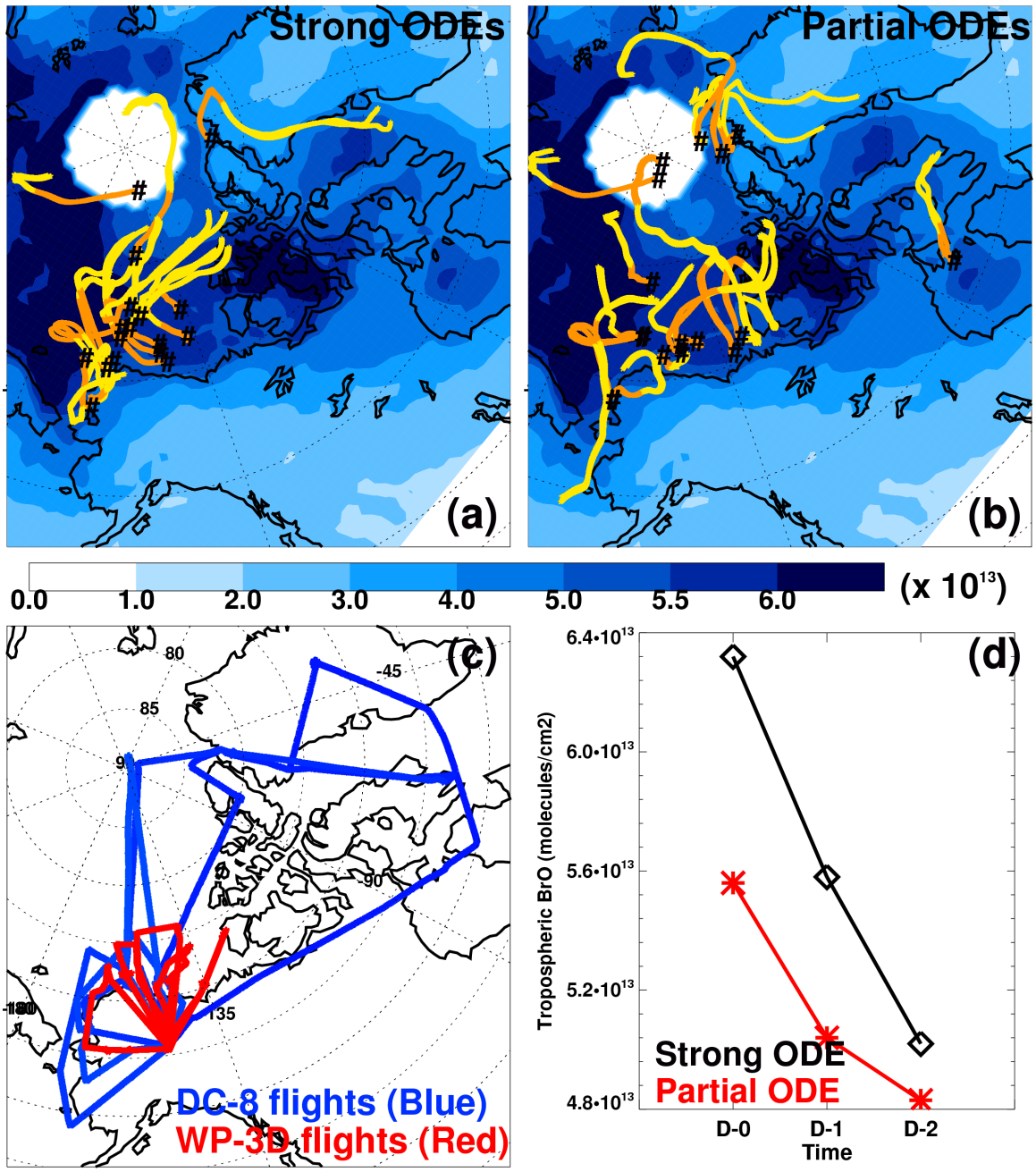

Figure A.6 Same as Figure 2.5, for tropospheric BrO VCDs of OMI-SCIA2ND.

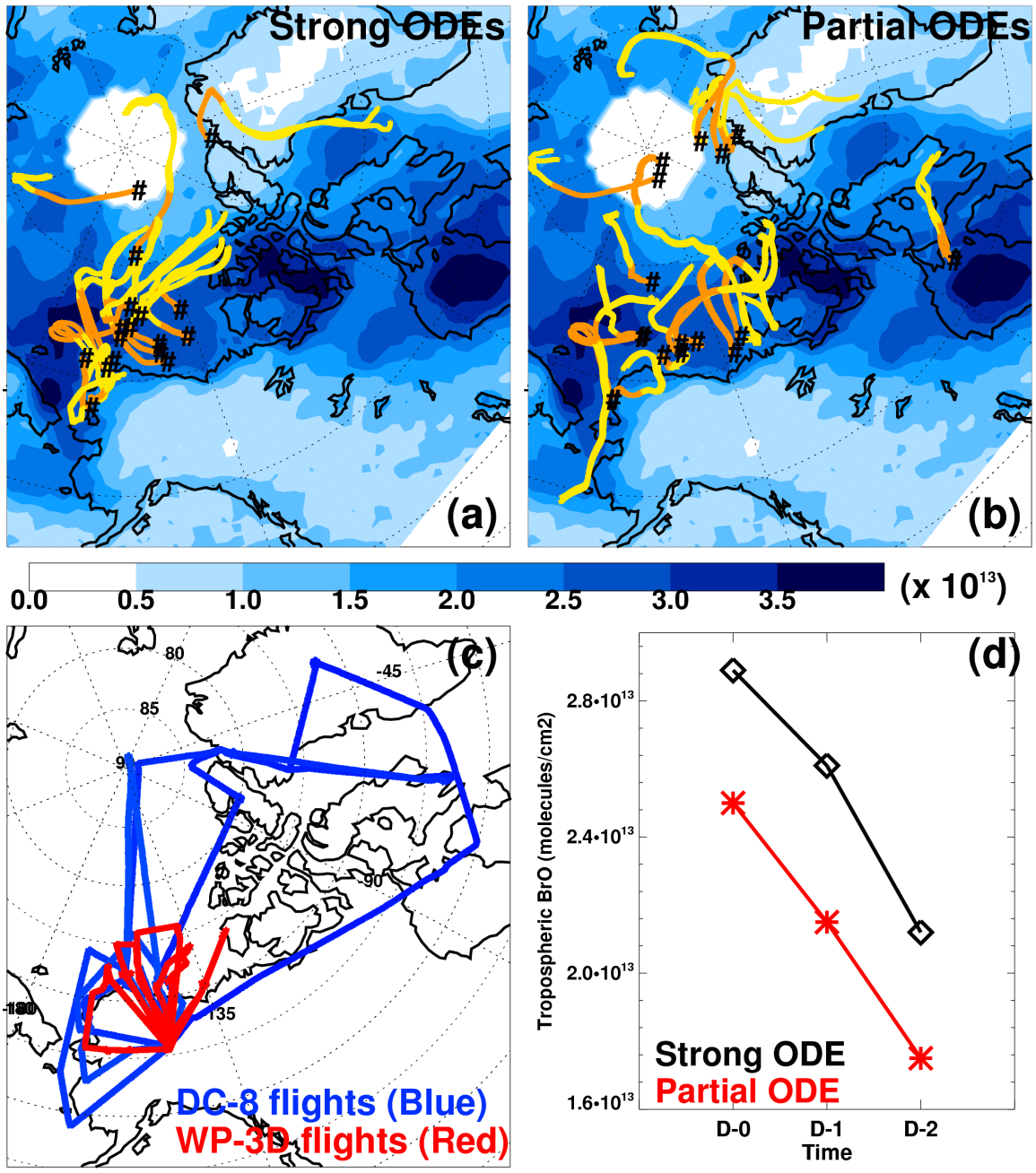

Figure A.7 Same as Figure 2.5, for tropospheric BrO VCDs of GOME-2-20th.

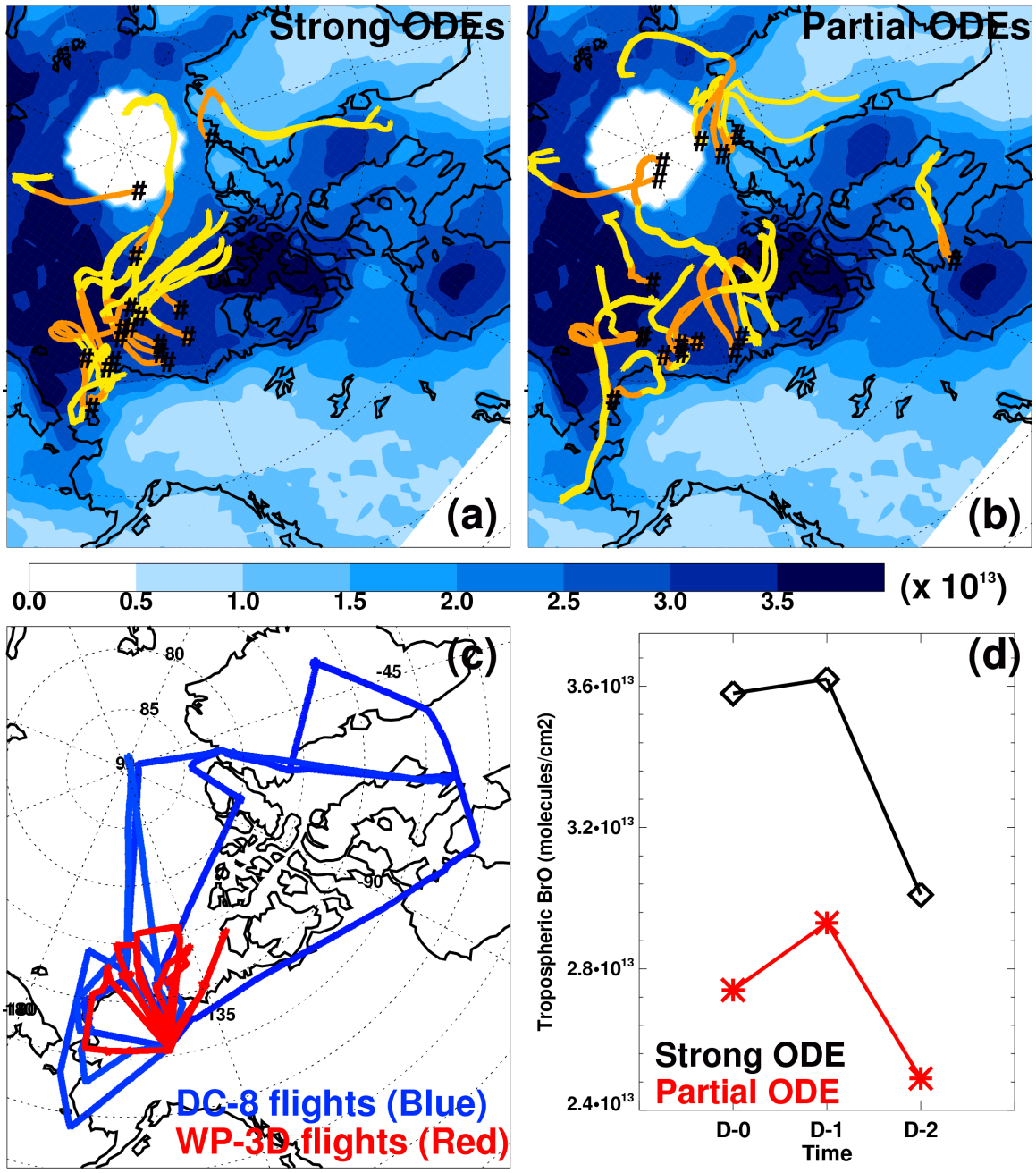

Figure A.8 Same as Figure 2.5, for tropospheric BrO VCDs of OMI-20th.

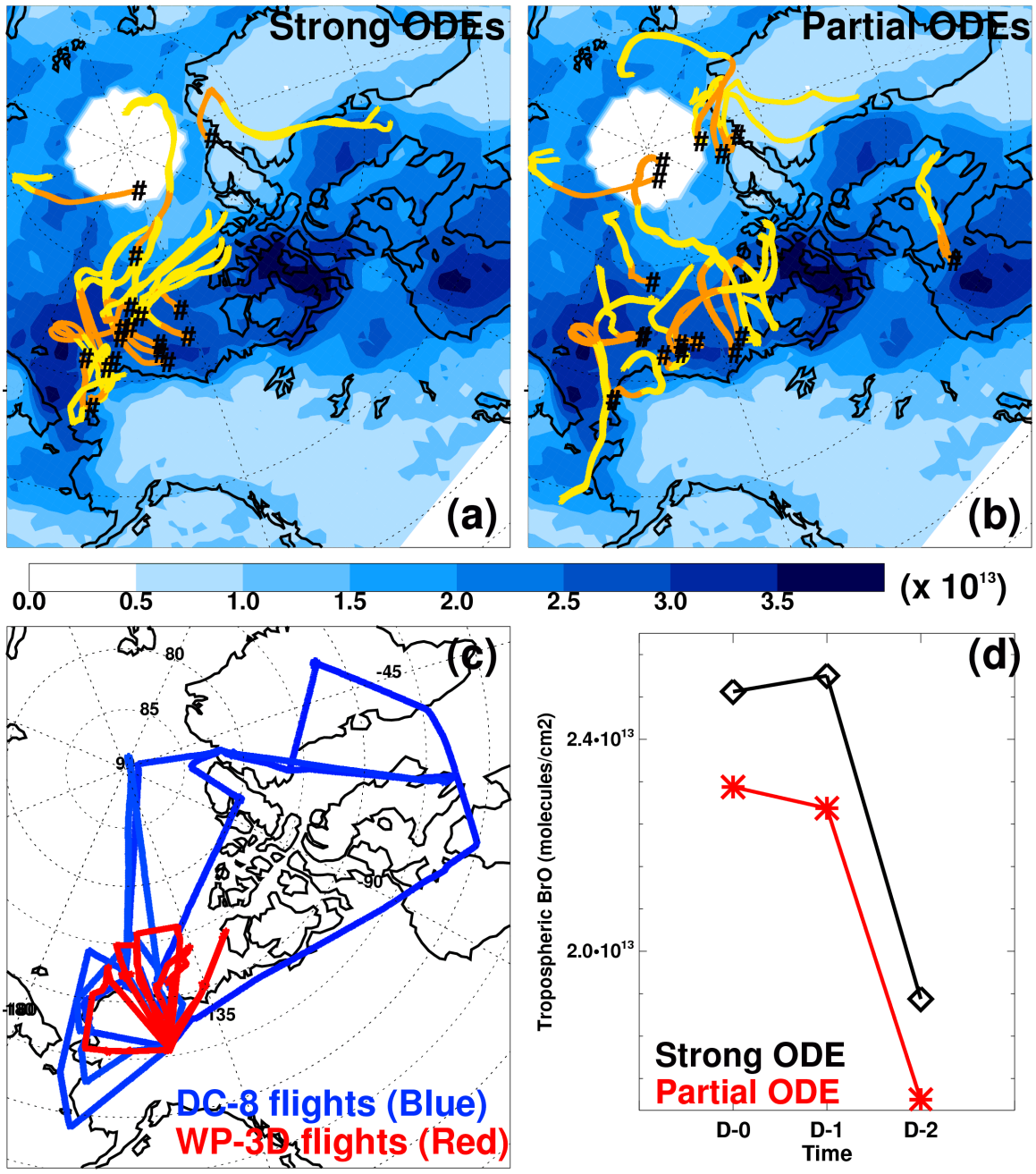

Figure A.9 Same as Figure 2.5, for tropospheric BrO VCDs of GOME-2-RAQMS.

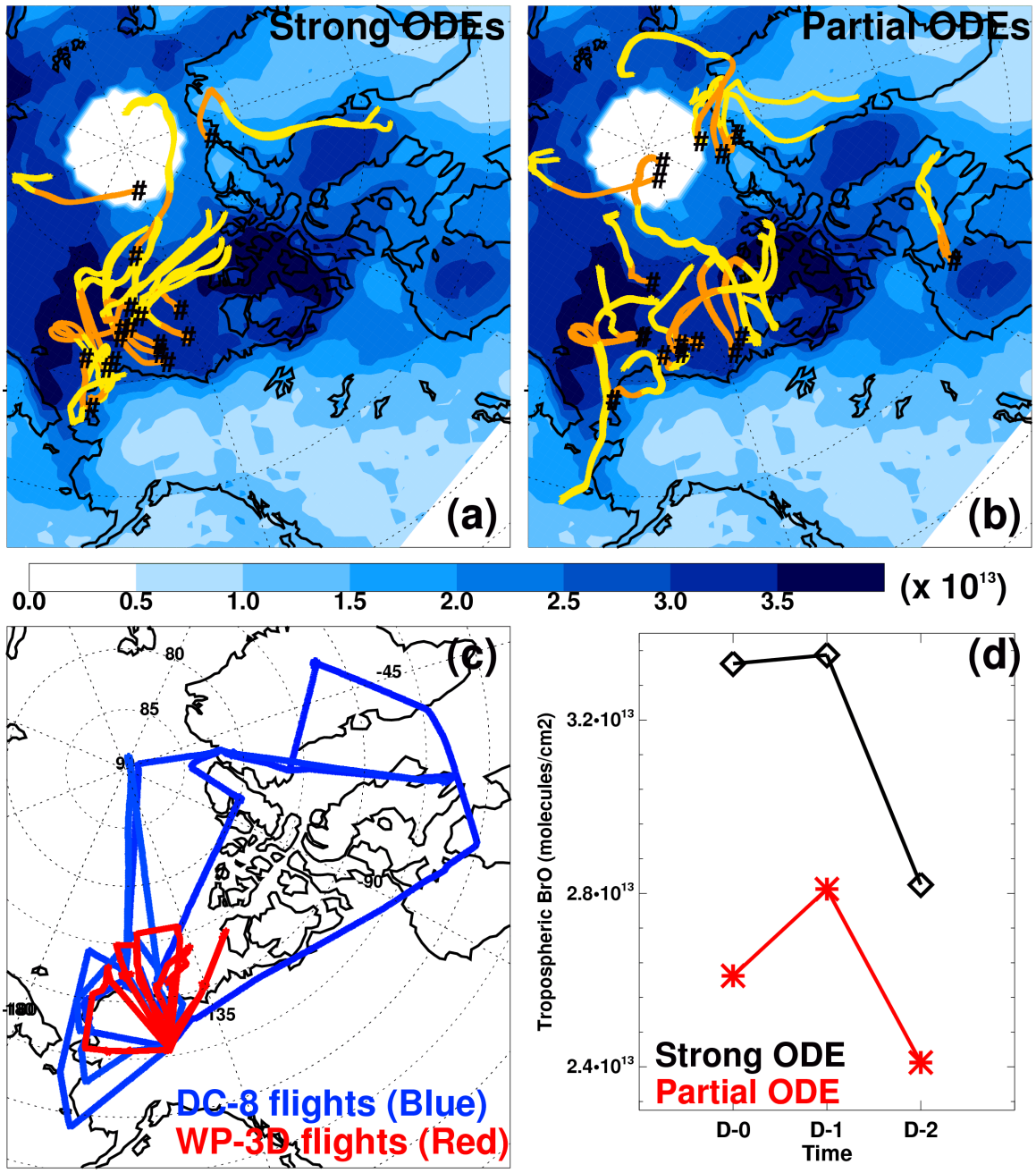

Figure A.10 Same as Figure 2.5, for tropospheric BrO VCDs of OMI-RAQMS.

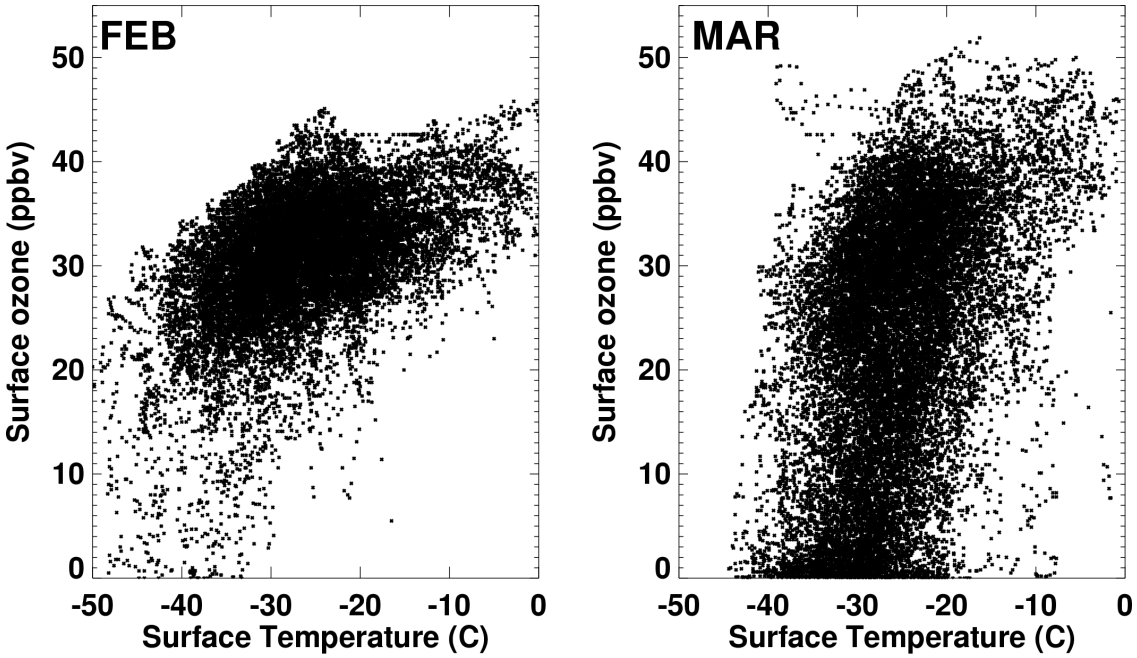

Figure A.11 Hourly surface ozone as a function of temperature at Barrow for February (left) and March (right). Ozone measurements from 1979 to 2008 were obtained from the NOAA Earth System Research Laboratory (ESRL) and the temperature dataset from the NOAA National Climate Data Center (NCDC).

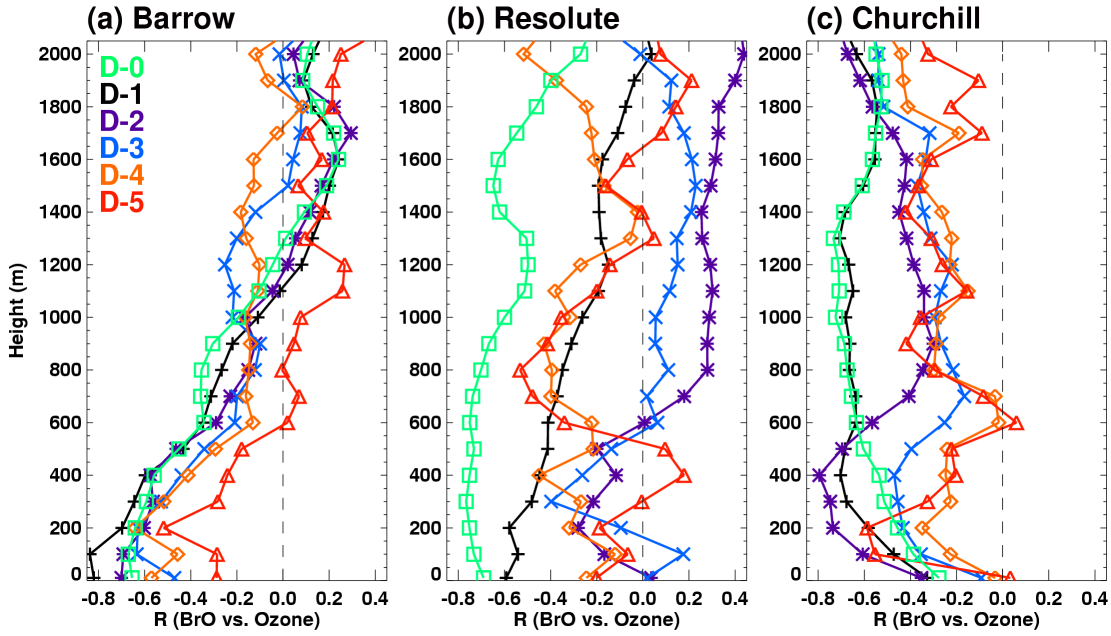

Figure A.12 Same as Figure 2.9, but for tropospheric BrO VCDs of OMI-SCIA2ND.

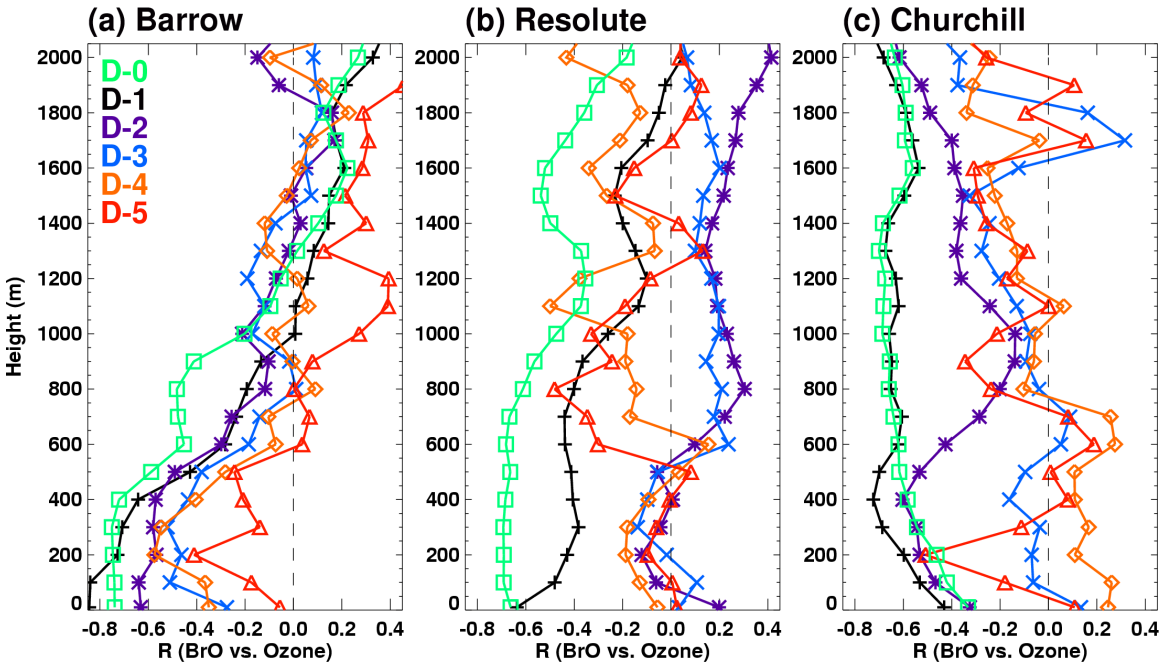

Figure A.13 Same as Figure 2.9, but for tropospheric BrO VCDs of GOME-2-20th.

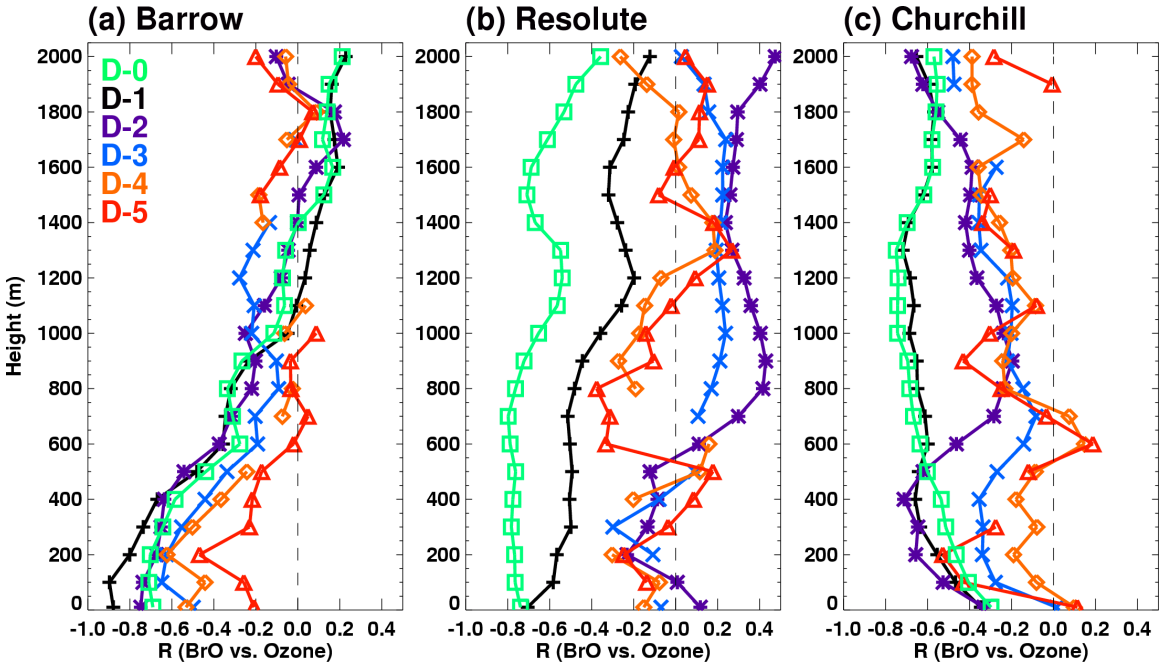

Figure A.14 Same as Figure 2.9, but for tropospheric BrO VCDs of OMI-20th.

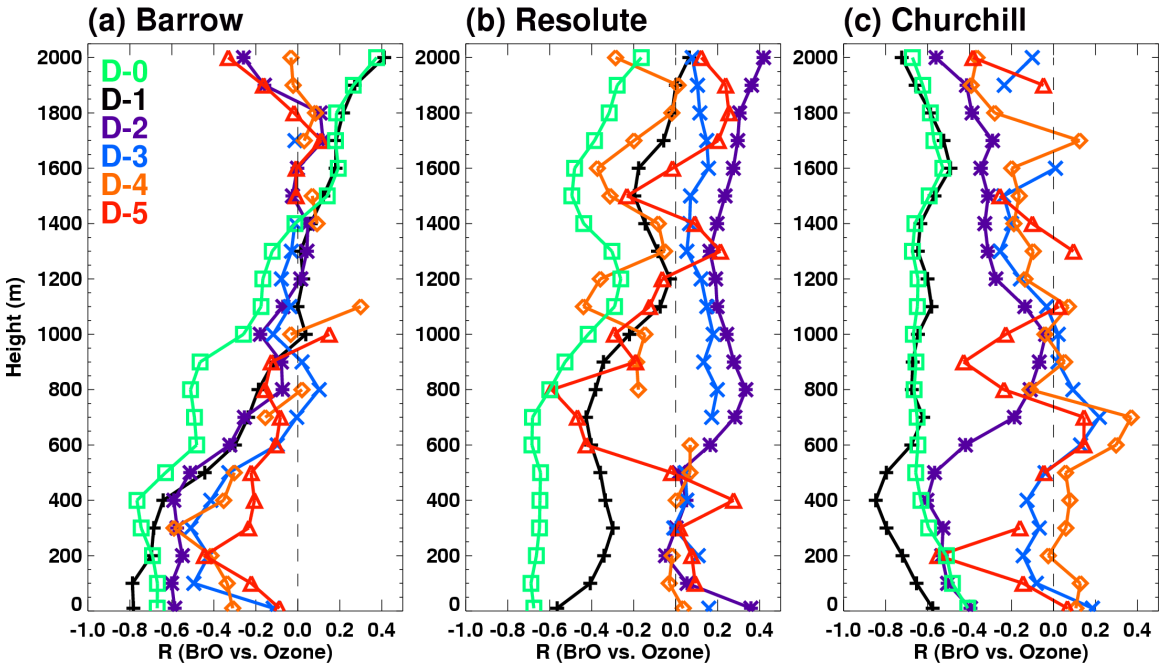

Figure A.15 Same as Figure 2.9, but for tropospheric BrO VCDs of GOME-2-RAQMS.

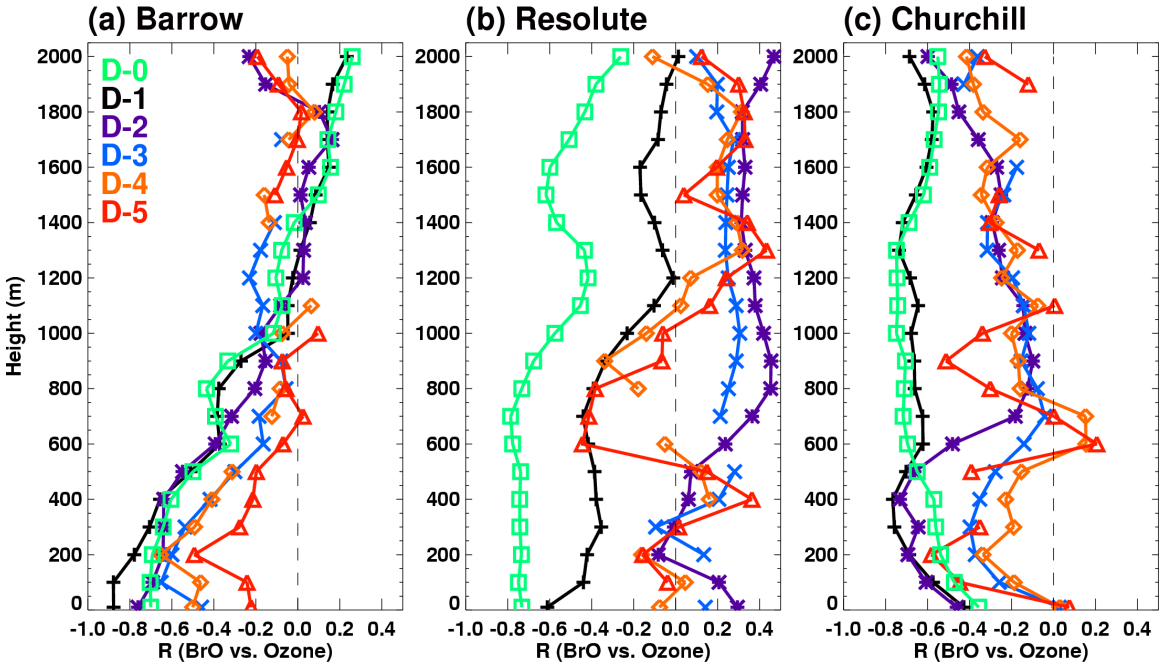

Figure A.16 Same as Figure 2.9, but for tropospheric BrO VCDs of OMI-RAQMS.

APPENDIX B

AUXILIARY MATERIALS FOR CHAPTER 5

The auxiliary materials are composed of the detail information for the measurements and estimation of surface NO_x at South Pole and the experiments based on global model simulations. The minor information (e.g., Antarctic topography) is also included.

The Antarctic topography: Antarctica is the large continental area located in the Southern Hemisphere, centered on the South Pole. About 95% of the whole region is covered by the ice and ice shelf. Due to its thickness, the highest altitude almost reaches about 5 km. Antarctica is composed of two large area, the east Antarctic plateau and the west Antarctica including the Antarctic peninsula. In this study, we define the east Antarctic plateau as the region where the altitude is higher than 3 km in the eastern part (0 to 180 °E) of Antarctic continent. The altitude distribution in Antarctic continent is shown in Figure B.1.

Vertical profile of ozone at South Pole: To see the chemical production of ozone at the surface, we calculated delta ozone1 using the vertical profile of ozone from ozonesonde measurements at the South Pole station. Owing to the small number of ozonesonde launching (4~5 times per month in general), it may not be appropriate to examine the year-to-year variation. Thus the vertical profile of ozone was compared for only seasonal

mean patterns during 20 years (1990-2010). As mentioned in the method section, delta ozone is calculated by subtracting the estimated background ozone from the real observed ozone. Considering the ozone in the mid-troposphere as the typical source of background ozone at the surface is a reasonable assumption. Then the background ozone level at the surface was estimated from the observed ozone profile, using the extrapolation from the each seasonal mean profile between 0.5 to 4.0 km heights above from the surface. Figure B.2 shows the estimated profile of ozone (0 to 0.5 km above) with real observed ozone profile (0.5 to 4.0 km) at each season.

The estimation of snow NO_x flux at the surface: Delta ozone estimated from the vertical profile of ozone is highly positive in the austral summertime (Figure 5.2), implying the local ozone production at the surface. It has been known that the NO_x emission from the snow surface can contributes to the surface ozone production in the east Antarctic plateau [Davis et al., 2008; Helmig et al., 2008]. Figure B.3 is snow NO_x measurements at South Pole showing the high concentration in the austral summer. We also calculated the local NO_x flux in the summer based on the simple equation of snow surface NO_x flux4. The equation of NO_x flux was derived from the 1-D model simulation with in situ measurements during the Antarctic Tropospheric Chemistry Investigation (ANTCI) in 2003 [Eisele et al., 2008]. First the 1-D model estimated the snow NO_x emission from the convergence between iterative simulations and in situ measurements. This estimated NO_x emission correlates with some of observed meteorology data, such as temperature and wind speed. Thus, snow NO_x emission was parameterized by the local wind speed and temperature as a polynomial form up to the second order4. This

estimation may include some uncertainty, but presumably shows the meaningful information qualitatively.

From the 1981 to 2010, the snow surface NO_x emission at the South Pole was calculated using the in situ measurements of temperature and wind speed obtained from the data archive of World Data Center for Greenhouse Gases (http://ds.data.jma.go.jp/gmd/wdcgg/). During the austral summer (November to January), snow surface NO_x emission has gradually increased (Figure 5.6), implying the increase of surface ozone production. Comparing to the increase trend of 90th percentile of surface ozone (Figure 5.1) and positive delta ozone in the austral summer (Figure 5.2), the increase of snow surface NO_x emission seems to contribute the ozone production at the surface.

30-year trends of 500-hpa potential temperatures: Same as Figure 5.3a, the trends of 500-hpa potential temperature were compared among four seasons (Figure 5.4). Potential temperatures were obtained from the National Centers for the Environmental Prediction – Department of Energy (NCEP-DOE) Reanalysis 2 dataset (NDR2) [Kanamitsu et al., 2002]. Similar to the trend of observed surface ozone at South Pole (Figure 5.1), 500-hpa potential temperatures show the consistent reversal trends for all seasons. Comparing trends of 5-year moving average between the surface ozone at South Pole and 500-hpa potential temperature over the east Antarctic plateau (Figure 5.5), correlation coefficient (R value) is 0.92, much higher than R=0.73 using just annual mean (Figure 5.3a), implying that the both reversal trends may be affected by the slow and steady low-frequent variations.

CAM5 model experiments: The NCAR Community Atmospheric Model version 5.0 (CAM5) [Neale et al., 2008] was used for our model experiments in this study. The common settings for all experiments are based on F component set, 1.9 × 2.5 resolution, and 30 vertical levels from the surface to the top of atmosphere. Prescribed meteorology in the model is obtained from the Atmospheric Model Intercomparison Project (AMIP), and natural surface emissions are from the fourth version of Model for Ozone and Related chemical Tracers (MOZART4).

To investigate the long-term influence of stratospheric ozone variation to the tropospheric atmosphere, both extensive tropospheric and stratospheric chemistry in CAM5 was used during 30 years (1981-2010). We executed two experiments, the model simulations using the variation of stratospheric ozone and climatology stratospheric ozone. These two simulations were setup in a same way except the prescribed ozone forcing in the stratosphere. To see the effect of stratospheric ozone change, we used the vertical profile of ozone data for 1981-2010 obtained from the Atmospheric Chemistry and Climate / Stratospheric Processes And their Role in Climate (AC&C/SPARC) ozone database, which consists of separate stratospheric and tropospheric data sources [Lamarque et al., 2010]. This data is interpolated from 0.5 × 0.5 grid to model grid of 1.9 × 2.5 and prescribed for only stratosphere (upper than 100-hpa level) in the model. This model experiment was compared with the simulation with climatology stratospheric ozone, which is average of AC&C/SPARC ozone at each layer in the stratosphere.

It has been known that global model shows large discrepancy of surface temperature trend with considering the stratospheric ozone pattern [Son et al., 2009]. Considering stratospheric ozone variation [Son et al., 2009] better captures the measured

temperature trend, which previous global did does not reproduce [Vaughan et al., 2001]. In this experiment, however, we do not find the clear difference of surface ozone trend between two simulations. Figure 5.7 shows the inter-annual variation of surface ozone difference at South Pole between two simulations. Positive difference means that the simulated ozone with AC&C/SPARC is larger than ozone with climatology stratospheric ozone. Ozone difference is positive in the 1980s but negative after. Since surface ozone photolysis depends on the amount of ultraviolet flux from the space, surface ozone could be more photolyzed when stratospheric ozone depletion is large [Schnell et al., 1991; Zhang et al., 2013]. Figure 5.7 probably reveals this effect of ultraviolet flux controlled by the thickness of stratospheric ozone layer. But the difference of simulated ozone is smaller than the scale of surface ozone trend during three decades, implying that the stratospheric ozone variation does not affect the surface ozone variation much.

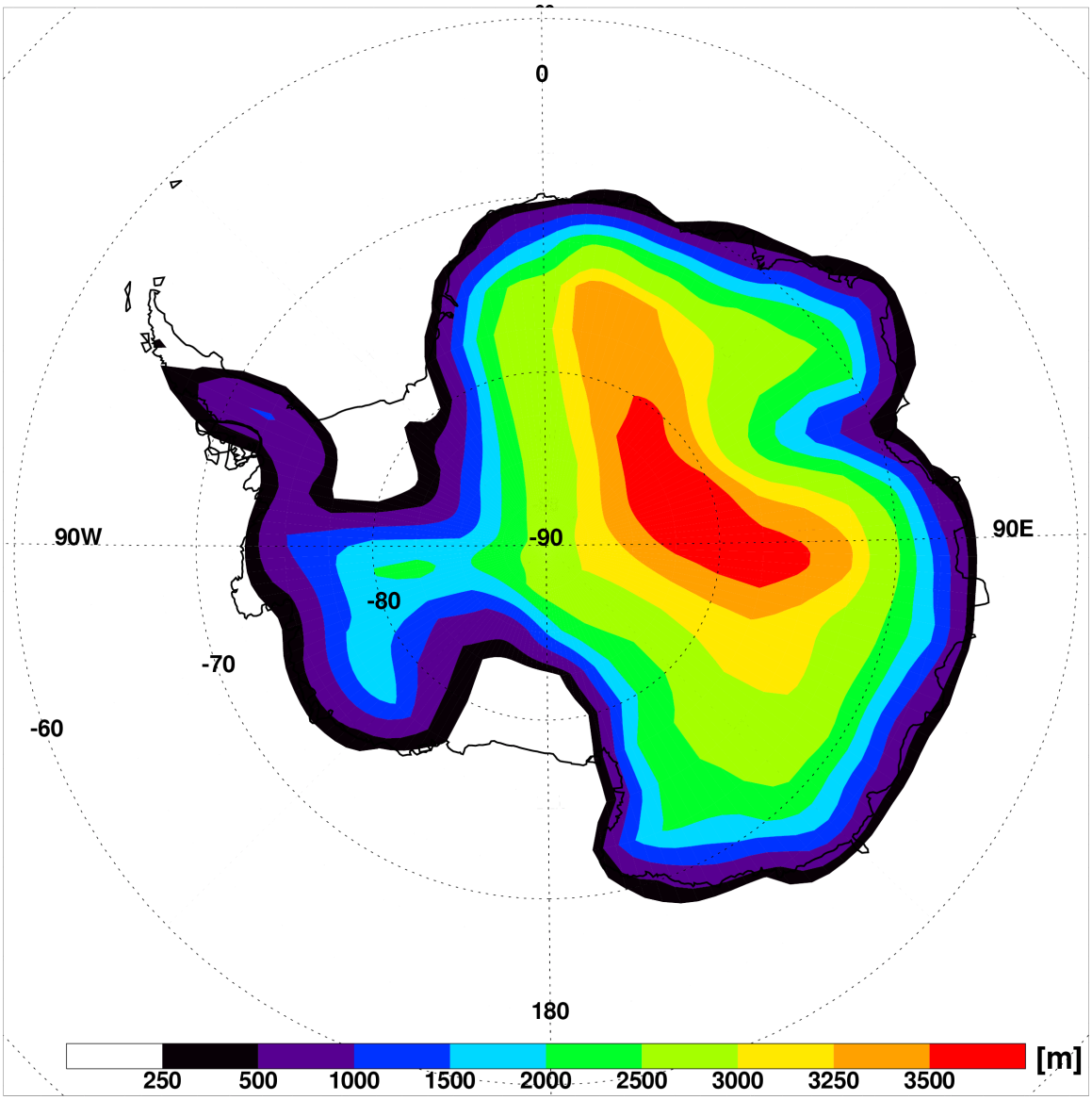

Figure B.1 The map of altitudes in the Antarctic continent.

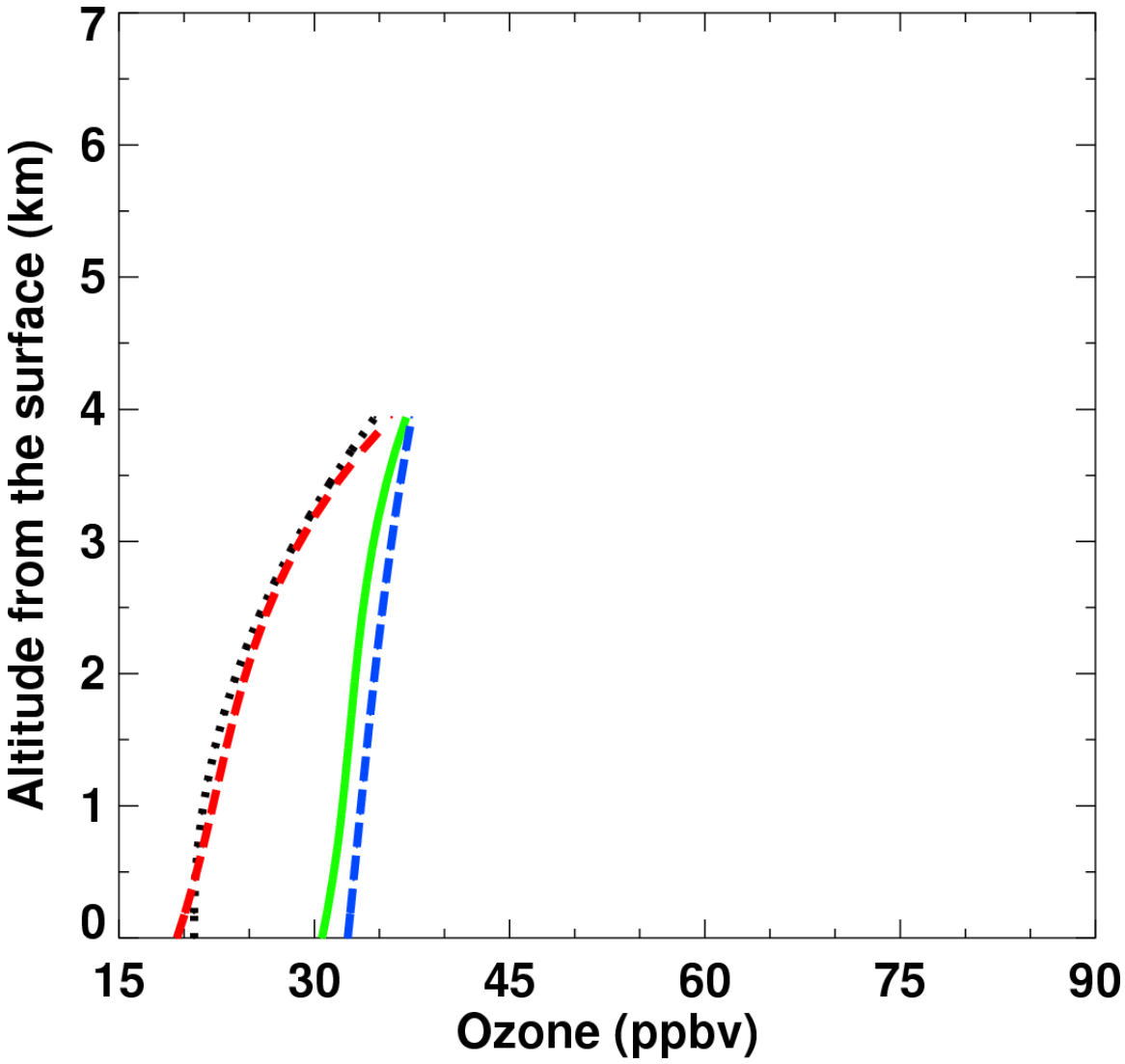

Figure B.2 The vertical profile of ozone combined the estimated ozone (0 to 0.5 km above) with real observed ozone profile (0.5 to 4.0 km) for the spring (blue dash-dot), summer (black dot), autumn (red dash), and winter (green solid line).

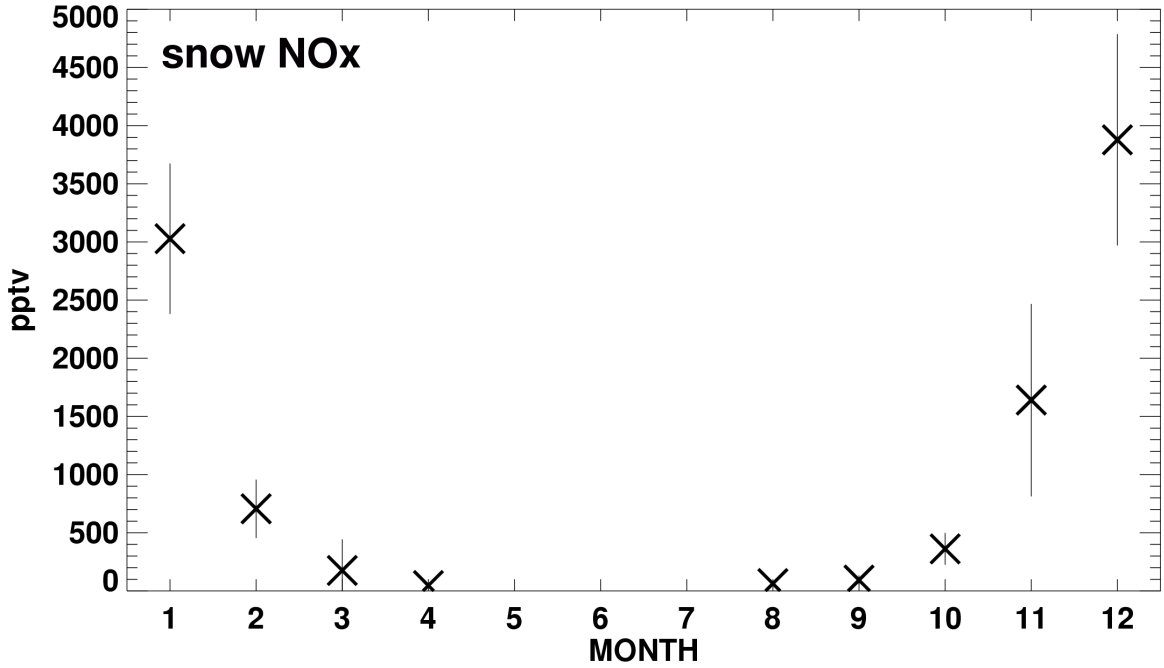

Figure B.3 Monthly mean variation of snow NO_x concentration, measured in the South Pole station from February 2006 to January 2007 (Data from Dr. D. Davis at Georgia Tech, private communication). Vertical bar indicates the 1-σ standard variation.

REFERENCES

Abbott, J. P. D., et al. (2012), Halogen activation via interactions with environmental ice and snow in the polar lower troposphere and other regions, *Atmos. Chem. Phys*., *12*, 6237-6271.

Anlauf, K. G., R. E. Mickle, N. B. A. Trivett (1994), Measurement of ozone during Polar Sunrise Experiment 1992, *J. Geophys. Res*., *99*, 25345-25353.

Arimoto, R., et al. (2004), Lead and mercury in aerosol particles collected over the South Pole during ISCAT-2000, *Atmos. Environ*., *38*, 5485-5491.

Arimoto, R., T. Zeng, D. Davis, Y. Wang, H. Khaing, C. Nesbit, and G. Huey (2008), Concentrations and sources of aerosol ions and trace elements during ANTCI-2003, *Atmos. Environ*., *42*, 2864-2876.

Barnston, A. G., and R. E. Livezey (1987), Classification, seasonality and persistence of low-frequency atmospheric circulation, *Mon. Weather Rev*., *115*, 1083-1126.

Barrie, L. A., J. W. Bottenheim, R. C. Schnell, P. J. Crutzen, and R. A. Rasmussen (1988), Ozone destruction and photochemical reactions at polar sunrise in the lower Arctic atmosphere, *Nature*, *334*, 138-141.

Barrie, L., and U. Platt (1997), Arctic tropospheric chemistry: an overview, *Tellus B*, *49*(5), 450-454.

Begoin, M., A. Richter, M. Weber, L. Kaleschke, X. Tian-Kunze, A. Stohl, N. Theys, and J. P. Burrows (2010), Satellite observations of long range transport of a large BrO plume in the Arctic, *Atmos. Chem. Phys*., *10*, 6515-6526.

Bintanja, R., G. J. van Oldenborgh, S. S. Drijfhout, B. Wouters, and C. A. Katsman (2013), Important role for ocean warming and increased ice-shelf melt in Antarctic sea-ice expansion, *Nature Geosci*., *6*, 376-379.

Bitz, C. M. and L. M. Polvani (2012), Antarctic climate response to stratospheric ozone depletion in a fine resolution ocean climate model, *Geophys. Res. Lett*., *39*, L20705.

Bottenheim, J. W., J. D. Fuentes, D. W. Tarasick, and K. G. Anlauf (2002), Ozone in the Arctic lower troposphere during winter and spring 2000 (ALERT2000), *Atmos. Environ*., *36*, 2535-2544.

Bottenheim, J. W., and E. Chan (2006), A trajectory study into the origin of spring time Arctic boundary layer ozone depletion, *J. Geophys. Res*., *111*, D19301, doi:10.1029/2006JD007055.

Bottenheim, J. W., S. Netcheva, S. Morin, and S. V. Nghiem (2009), Ozone in the boundary layer air over the Arctic Ocean: measurements during the TARA transpolar drift 2006-2008, *Atmos. Chem. Phys*., *9*, 4545-4557.

Brock, C. A., et al. (2011), Characteristics, sources, and transport of aerosols measured in spring 2008 during the aerosol, radiation, and cloud processes affecting Arctic Climate (ARCPAC) Project, *Atmos. Chem. Phys*., *11*, 2423-2453.

Bromwich, D. H., J. J. Cassano, T. Klein, G. Heinemann, K. M. Jines, K. Steffen, and J. E. Box (2001), Mesoscale modeling of katabatic winds over Greenland with the polar MM5, *Mon. Weather Rev*., *129*, 2290-2309.

Browell, E. V., et al. (2003), Ozone, aerosol, potential vorticity, and trace gas trends observed at high latitudes over North America from February to May 2000, *J. Geophys. Res*., 108(D4), 8369, doi:10.1029/2001JD001390.

Cavalieri, D. J., C. L. Parkinson, P. Gloersen, and H. Zwally. 1996, updated yearly. Sea Ice Concentrations from Nimbus-7 SMMR and DMSP SSM/I-SSMIS Passive Microwave Data. [2007-2008]. Boulder, Colorado USA: NASA DAAC at the National Snow and Ice Data Center, updated 2012.

Choi, S., et al. (2012), Analysis of satellite-derived Arctic tropospheric BrO columns in conjunction with aircraft measurements during ARCTAS and ARCPAC, *Atmos. Chem. Phys*., *12*, 1255-1285, doi:10.5194/acp-12-1255-2012.

Cole, A. S., and A. Steffen (2010), Trends in long-term gaseous mercury observations in the Arctic and effects of temperature and other atmospheric conditions, *Atmos. Chem. Phys*., *10*, 4661-4672.

Crawford, J. H., et al. (2001), Evidence for photochemical production of ozone at the South Pole surface, *Geophys. Res. Lett*., *28*, 3641-3644.

Cressman, G. P. (1959), An operational objective analysis system, *Mon. Weather Rev*., *87*, 367-374.

Davis, D., G. Chen, M. Buhr, J. Crawford, D. Lenschow, B. Lefer, R. Shetter, F. Eisele, L. Mauldin, and A. Hogan (2004), South Pole NO_x chemistry: an assessment of factors controlling variability and absolute levels, *Atmos. Environ*., *38*, 5375-5388.

Davis, D. D., et al. (2008), A reassessment of Antarctic plateau reactive nitrogen based on ANTCI 2003 airborne and ground based measurements, *Atmos. Environ*., *42*, 2831-2848.

Di Pierro M, L. Jaeglé, and T. L. Anderson (2011), Satellite observations of aerosol transport from East Asia to the Arctic: three case studies, *Atmos. Chem. Phys*., *11*, 2225-2243.

Dibb, J. E., L. D. Ziemba, J. Luxford, and P. Beckman (2010), Bromide and other ions in the snow, firn air, and atmospheric boundary layer at Summit during GSHOX, *Atmos. Chem. Phys*., *10*, 9931– 9942, doi:10.5194/acp-10-9931-2010.

Ding, Q., E. J. Steig, D. S. Battisti, and M. Küttel (2011), Winter warming in West Antarctica caused by central tropical Pacific warming, *Nature Geosci*., *4*, 398-403.

Dong, X., B. Xi, K. Crosby, C. N. Long, R. S. Stone, and M. D. Shupe (2010), A 10 year climatology of Arctic cloud fraction and radiative forcing at Barrow, Alaska, *J. Geophys. Res*., *115*, D17212, doi:10.1029/2009JD013489.

Draxler, R. R., and G. D. Hess (1998), An overview of the HYSPLIT_4 modeling system of trajectories, dispersion, and deposition, *Aust. Meteor. Mag*., *47*, 295-308.

Eckhardt, S., A. Stohl, S. Beirle, N. Spichtinger, P. James, C. Forster, C. Junker, T. Wagner, U. Platt, and S. G. Jennings (2003), The North Atlantic Oscillation controls air pollution transport to the Arctic, *Atmos. Chem. Phys*., *3*, 1769-1778.

Eisele, F., et al. (2008), Antarctic Tropospheric Chemistry Investigation (ANTCI) 2003 overview, *Atmos. Environ*., *42*, 2749-2761.

Evans, M. J., et al. (2003), Coupled evolution of BrO_x-ClO_x-HO_x-NO_x chemistry during bromine-catalyzed ozone depletion eventsin the arctic boundary layer, *J. Geophys. Res*., *108*(D4), 8368, doi:10.1029/2002JD002732.

Fan, S.-M., and D. J. Jacob (1992), Surface ozone depletion in Arctic spring sustained by bromine reactions on aerosols, *Nature*, *359*, 522-524.

Fenn, M. A., et al. (1999), Ozone and aerosol distributions and air mass characteristics over the South Pacific during the burning season, *J. Geophys. Res*., *104*(D13), 16197–16212, doi:10.1029/1999JD900065.

Foster, K. L., R. A. Plastridge, J. W. Bottenheim, P. B. Shepson, B. J. Finlayson-Pitts, and C. W. Spicer (2001), The role of Br2 and BrCl in surface ozone destruction at polar sunrise, *Science*, *291*, 471-474.

Frieß, U., H. Sihler, R. Sander, D. Pöhler, S. Yilmaz, and U. Platt (2011), The vertical distribution of BrO and aerosols in the Arctic: Measurements by active and passive differential optical absorption spectroscopy, *J. Geophys. Res*., *116*, D00R04, doi:10.1029/2011JD015938.

Gillert, N. P., and D. W. J. Thompson (2003), Simulation of recent Southern Hemisphere climate change, *Science*, *302*, 273-275.

Gillert, N. P., et al. (2008), Attribution of polar warming to human influence, *Nature Geosci*., *1*, 750-754.

Gilman, J.B., J. F. Burkhart, B. M. Lerner, E. J. Williams, W. C. Kuster, P. D. Goldan, P. C. Murphy, C. Warneke, C. Fowler, S. A. Montzka, B. R. Miller, L. Miller, S. J. Oltmans, T. B. Ryerson, O. R. Cooper, A. Stohl, and J. A. de Gouw (2010), Ozone variability and halogen oxidation within the Arctic and sub-Arctic springtime boundary layer, *Atmos. Chem. Phys*., *10*, 10223-10236.

Grannas, A. M., et al. (2007), An overview of snow photochemistry: evidence, mechanisms and impacts, *Atmos. Chem. Phys*., *7*, 4329-4373.

Halfacre, J. W., et al. (2013), Temporal and spatial characteristics of ozone depletion events from measurements in the Arctic, *Atmos. Chem. Phys. Discuss*., *13*, 30233-30285.

Hara, K., K. Osada, K. Matsunaga, Y. Iwasaka, T. Shibata, and K. Furuya (2002), Atmospheric inorganic chlorine and bromine species in Arctic boundary layer of the winter/spring, *J. Geophys. Res*., *107*(D18), 4361, doi:10.1029/2001JD001008.

Hausmann, M., and U. Platt (1994), Spectroscopic measurement of bromine oxide and ozone in the high Arctic during Polar Sunrise Experiment 1992, *J. Geophys. Res*., *99*(D12), 25399-25413.

Helmig, D., S. J. Oltmans, D. Carlson, J.-F. Lamarque, A. Jones, C. Labuschagne, K. Anlauf, and K. Hayden (2007), A review of surface ozone in the polar regions, *Atmos. Environ*., *41*, 5138-5161.

Helmig, D., et al. (2008), Nitric oxide in the boundary-layer at South Pole during the Antarctic Tropospheric Chemistry Investigation (ANTCI), *Atmos. Environ*., *42*, 2817-2830.

Hopper, J. F., L. A. Barrie, A. Silis, W. Hart, A. J. Gallant, and H. Dryfhout (1998), Ozone and meteorology during the 1994 Polar Sunrise Experiment, J. *Geophys. Res.*, *103*(D1), 1481-1492.

Hoskins, B. J., and K. I. Hodges (2002), New perspectives on the Northern Hemisphere winter storm tracks, *J. Atmos. Sci*., *59*, 1041-1061.

Howell, S. E. L., C. R. Duguay, and T. Markus (2009), Sea ice conditions and melt season duration variability within the Canadian Arctic Archipelago: 1979–2008, *Geophys. Res. Lett*., *36*, L10502, doi:10.1029/2009GL037681.

Hu, X.‐M., F. Zhang, G. Yu, J. D. Fuentes, and L. Wu (2011), Contribution of mixed‐phase boundary layer clouds to the termination of ozone depletion events in the Arctic, *Geophys. Res. Lett*., *38*, L21801, doi:10.1029/2011GL049229.

Hurrell, J. W. (1995), Decadal trends in the North Atlantic Oscillation and relationships to regional temperature and precipitation, *Science*, *269*, 676-679.

Intrieri, J. M., M. D. Shupe, T. Uttal, and B. J. McCarty (2002), An annual cycle of Arctic cloud characteristics observed by radar and lidar at SHEBA, *J. Geophys. Res*., *107*, 8030, doi:10.1029/2000JC000423.

Jacob, D. J., et al. (2010), The Arctic Research of the Composition of the Troposphere from Aircraft and Satellites (ARCTAS) mission: design, execution, and first results, *Atmos. Chem. Phys*., *10*, 5191-5212.

Jacobi, H.-W., L. Kaleschke, A. Richter, A. Rozanov, and J. P. Burrows (2006), Observation of a fast ozone loss in the marginal ice zone of the Arctic Ocean, *J. Geophys. Res.*, *111*, D15309, doi:10.1029/2005JD006715.

Jacobi, H.-W., S. Morin, and J. W. Bottenheim (2010), Observation of widespread depletion of ozone in the springtime boundary layer of the central Arctic linked to mesoscale synoptic conditions, *J. Geophys. Res*., *115*, D17302, doi:10.1029/2010JD013940.

Jones, A. E., P. S. Anderson, M. Begoin, N. Brough, M. A. Hutterli, G. Marchall, A. Richter, H. K. Roscoe, and E. W. Wolff (2009), BrO, blizzards, and drivers of polar tropospheric ozone depletion events, *Atmos. Chem. Phys*., *9*, 4639-4652.

Jones, A. E., P. S. Anderson, E. W. Wolff, H. K. Roscoe, G. J. Marshall, A. Richter, N. Brough, and S. R. Colwell (2010), Vertical structure of Antarctic tropospheric ozone depletion events: characteristics and broader implications, *Atmos. Chem. Phys*., *10*, 7775-7794.

Kalnay, E., M. Kanamitsu, R. Kistler, W. Collins, D. Deaven, L. Gandin, M. Iredell, S. Saha, G. White, J. Woollen, Y. Zhu, M. Chelliah, W. Ebisuzaki, W. Higgins, J. Janowiak, K. C. Mo, C. Ropelewski, J. Wang, A. Leetmaa, R. Reynolds, R. Jenne, and D. Joseph (1996), The NCEP/NCAR 40-year reanalysis project, *Bull. Am. Meteorol. Soc.*, *77*, 437-471.

Kaleschke, L., A. Richter, J. A. Burrows, O. Afe, G. Heygster, J. Notholt, A. M. Rankin, H. K. Roscoe, J. Hollwedel, T. Wagner, and H.-W. Jacobi (2004), Frost flowers on sea ice as a source of sea salt and their influence on tropospheric halogen chemistry, *Geophys. Res. Lett*., *31*, L16114, doi:10.1029/2004GL020655.

Kalnajs, L. E., and L. M. Avallone (2006), Frost flower influence on springtime boundary-layer ozone depletion events and atmospheric bromine levels, *Geophys. Res. Lett*., *33*, L10810, doi:10.1029/2006GL025809.

Kanamitsu, M., et al. (2002), NCEP-DOE AMIP-II reanalysis (R-2), *Bull. Am. Meterol. Soc.*, *91*, 1631–1643.

Keil A, D., and P. B. Shepson (2006), Chlorine and bromine atom ratios in the springtime Arctic troposphere as determined from measurements of halogenated volatile organic compounds, *J. Geophys. Res*., *111*, D17303, doi:10.1029/2006JD007119.

Koo, J.-H., Y. Wang, T. P. Kurosu, K. Chance, A. Rozonov, A. Richter, S. J. Oltmans, A. M. Thompson, J. W. Hair, M. A. Fenn, A. J. Weinheimer, T. B. Ryerson, S. Solberg, L. G. Huey, J. Liao, J. E. Dibb, J. A. Neuman, J. B. Nowak, P. B. Pierce, M. Natarajan, and J. Al-Saadi (2012), Characteristics of tropospheric ozone depletion events in the Arctic spring: analysis of the ARCTAS, ARCPAC, and ARCIONS measurements and satellite BrO observations, *Atmos. Chem. Phys*., *12*, 9909-9922.

Koo, J., Y. Wang, Y., T. Jiang, Y. Deng, S. J. Oltmans, and S. Solberg (2013), Occurence of near-surface ozone depletion in the Arctic spring strongly affected by northern-hemispheric climate variability, *presented at the Fall 2013 meeting of the American Geophysical Union*, San Francisco, California, USA.

Kurosu, T. and K. Chance (2011), OMBRO Readme file, https://www.cfa.harvard.edu/~tkurosu/SatelliteInstruments/OMI/PGEReleases/READMEs/OMBRO_v300_README.pdf.

Lamarque, J-F., et al. (2010), Historical (1850-2000) gridded anthropogenic and biomass burning emissions of reactive gases and aerosols: methodology and application, *Atmos. Chem. Phys*., *10*, 7017-7039.

Lau, N.-C. (1988), Variability of the observed midlatitude storm tracks in relation to low-frequency changes un the circulation pattern, *J. Atmos. Sci*., *45*, 2718-2743.

Leathers, D. J., and M. A. Palecki (1992), The Pacific/North American teleconnection pattern and United States climate II: Temporal characteristics and index specification, *J. Clim*., *5*, 707-716.

Lee, Y. Y., G.-H. Lim, and J.-S. Kug (2010), Influence of the East Asian winter monsoon on the storm track activity over the North Pacific, *J. Geophys. Res*., *115*, D09102, doi:10.1029/2009JD012813.

Lehrer, E., G. Hönninger, and U. Platt (2004), A one dimensional model study of the mechanism of halogen liberation and vertical transport in the polar troposphere, *Atmos. Chem. Phys*., *4*, 2427-2440.

Levy, H., II, M. D. Schwarzkopf, L. Horowitz, V. Ramaswamy, and K. L. Findell (2008), Strong sensitivity of late 21st century climate to projected changes in short-lived air pollutants, *J. Geophys. Res*., *113*, D06102, doi:10.1029/2007JD009176.

Liao, J., et al. (2012a), Observation of inorganic bromine species (HOBr, BrO, and Br_2) speciation at Barrow, Alaska in spring 2009, *J. Geophys. Res*., *117*, D00R16, doi:10.1029/2011JD016641.

Liao, J., L. G. Huey, E. Scheuer, J. E. Dibb, R. E. Stickel, D. J. Tanner, J. A. Neuman, J. B. Nowak, S. Choi, Y. Wang, R. J. Salawitch, T. Canty, K. Chance, T. Kurosu, R. Suleiman, A. J. Weinheimer, R. E. Shetter, A. Fried, W. Brune, B. Anderson, X. Zhang, G. Chen, J. Crawford, A. Hecobian, E. D. Ingall (2012b), Characterization of soluble bromide measurements and a case study of BrO observations during ARCTAS, *Atmos. Chem. Phys*., *12*, 1327-1338.

Liao, J., et al. (2014c), High levels of molecular chlorine in the Arctic atmosphere, *Nature Geosci*., advanced online publication, doi:10.1038/NGEO2046.

Linkin, M. E., and S. Nigam (2008), The north Pacific oscillation-west Pacific teleconnection pattern: mature-phase structure and winter impacts, *J. Clim*., *21*, 1979-1997.

Liou, K. N, (2002), *An Introduction to Atmospheric radiation, the second edition*, Academic press, Los Angeles, California, USA, pp. 41-60.

Mahajan, A. S., et al. (2010), Evidence of reactive iodine chemistry in the Arctic boundary layer, *J. Geophys. Res*., *115*, D20303, doi:10.1029/2009JD013665.

Manney, G. L., et al. (2011), Unprecedented Arctic ozone loss in 2011, *Nature*, *478*, 469-475.

Mantua, N. J., S. R. Hare, Y. Zhang, J. M. Wallace, and R. C. Francis (1997), A Pacific interdecadal climate oscillation with impacts on salmon production, *Bull. Am. Meteorol. Soc*., *78*, 1069-1079.

McElroy, C. T., C. A. McLinden, and J. C. McConnell (1999), Evidence for bromine monoxide in the free tropospheric during the Arctic polar sunrise, *Nature*, *397*, 338-341.

McLandress, C., et al. (2011), Separating the dynamical effects of climate change and ozone depletion: Part 2. Southern Hemisphere troposphere, *J. Clim*., *24*, 1850–1868.

Michalowski, B. A., J. S. Francisco, S.-M. Li, L. A. Barrie, J. W. Bottenheim, and P. B. Shepson (2000), A computer model study of multiphase chemistry in the Arctic boundary layer during polar sunrise, *J. Geophys. Res*., *105*(D12), 15131-15545.

Min, S.-K., X. Zhang, and F. Zwiers (2008), Human-induced Arctic moistening, *Science*, *320*, 518-520.

Morin, S., G. Hönninger, R. M. Staebler, and J. W. Bottenheim (2005), A high time resolution study of boundary layer ozone chemistry and dynamics over the Arctic Ocean near Alert, Nunavut, *Geophys. Res. Lett*., *32*, L08809, doi:10.1029/2004GL022098.

Morin, S., G. M. Marion, R. von Glasow, D. Voisin, J. Bouchez, and J. Savarino (2008), Precipitation of salts in freezing seawater and ozone depletion events: a status report, *Atmos. Chem, Phys*., *8*, 7317-7324.

Murayama, S., S. Taguchi, and K. Higuchi (2004), Interannual variation in the atmospheric CO2 growth rate: Role of atmospheric transport in the northern hemisphere, *J. Geophys. Res*., *109*, D02305, doi:10.1029/2003JD003729.

Myoung B, and Y. Deng (2009), Interannual variability of the cyclonic activity along the U.S. Pacific coast: influences on the characteristics of winter precipitation in the western United States, *J. Clim*. *22*, 5732-5747.

Neale, R. B., et al. (2008), Description of the NCAR community atmosphere model (CAM 5.0), NCAR Tech. Note NCAR/TN-486+STR.

Neuman, J. A., J. B. Nowak, L. G. Huey, J. B. Burkholder, J. E. Dibb, J. S. Holloway, J. Liao, J. Peischl, J. M. Roberts, T. B. Ryerson, E. Scheuer, H. Stark, R. E. Stickel, D. J. Tanner, and A. Weinheimer (2010), Bromine measurements in ozone depleted air over the Arctic Ocean, *Atmos. Chem, Phys*., *10*, 6503-6514.

Nghiem, S. V., I. G. Rigor, D. K. Perovich, P. Clemente-Colón, J. W. Weatherly, and G. Neumann (2007), Rapid reduction of Arctic perennial sea ice, *Geophys. Res. Lett*., *34*, L19504, doi:10.1029/2007GL031138.

Nghiem, S. V., et al. (2012), Field and satellite observations of the formation and distribution of Arctic atmospheric bromine above a rejuvenated sea ice cover, *J. Geophys. Res*., *117*, D00S05, doi:10.1029/2011JD016268.

Oltmans, S. J. (1981), Surface ozone measurements in clean air, *J. Geophys. Res*., *86*(C2), 1174-1180.

Oltmans, S. J., and H. Levy II (1994), Surface ozone measurements from a global network, *Atmos. Environ*., *28*, 9-24.

Oltmans S. J., et al. (2006), Long-term changes in tropospheric ozone, *Atmos. Environ*., *40*, 3156-3173.

Oltmans, S. J., B. J. Johnson, and J. M. Harris (2012), Springtime boundary layer ozone depletion at Barrow, Alaska: Meteorological influence, year to year variation, and long-term change, *J. Geophys. Res*., *117*, D00R18, doi:10.1029/2011JD016889.

Oltmans S. J., et al. (2013), Recent tropospheric ozone changes – A pattern dominated by slow or no growth, *Atmos. Environ*., *67*, 331-351.

Oum, K. W., M. J. Lakin, and B. J. Finlayson-Pitts (1998), Bromine activation in the troposphere by the dark reaction of O_3 with seawater ice, *Geophys. Res. Lett*., *25*(21), 3923-3926.

Parrish, D. D., K. C. Aikin, S. J. Oltmans, B. J. Johnson, M. Ives, and C. Sweeny (2010), Impact of transported background ozone inflow on summertime air quality in a California ozone exceedance area, *Atmos. Chem. Phys*., *10*, 10093–10109.

Piot, M., and R. von Glasow (2008), The potential importance of frost flowers, recycling on snow, and open leads for ozone depletion events, *Atmos. Chem. Phys*., *8*, 2437-2467.

Piot, M., and R. von Glasow (2009), Modelling the multiphase near-surface chemistry related to ozone depletions in polar spring, *J. Atmos. Chem*., *64*, 77-105.

Polvani, L. M. and K. L. Smith (2013), Can natural variability explain observed Antarctic sea ice trends? New modeling evidence from CMIP5, *Geophys. Res. Lett*., *40*, 3195-3199.

Pöhler, D., L. Vogel, U. Frieβ, and U. Platt (2010), Observation of halogen species in the Amundsen Gulf, Arctic, by active long-path differential optical absorption spectroscopy, *Proc. Natl. Acad. Sci*., *107*, 6582-6587.

Pratt, K. A., et al. (2013), Photochemical production of molecular bromine in Arctic surface snowpacks, *Nature Geosci*., *6*, 351-356.

Proshutinsky, A., R. Krishfield, and D. Barber (2009), Preface to special section on Beaufort Gyre Climate System Exploration Studies: Documenting key parameters to understand environmental variability, *J. Geophys. Res*., *114*, C00A08, doi:10.1029/2008JC005162.

Quinn, P. K., T. S. Bates, K. Schulz, and G. E. Shaw (2009), Decadal trends in aerosol chemical composition at Barrow, Alaska: 1976-2008, *Atmos. Chem. Phys*., *9*, 8883-8888.

Reynolds, R.W., N. A. Rayner, T. M. Smith, D. C. Stokes, and W. Wang (2002), An improved in situ and satellite SST analysis for climate, *J. Clim*., *15*, 1609-1625.

Richter, A., F. Wittrock, M. Eisinger, and J. P. Burrows (1998), GOME observations of tropospheric BrO in northern hemispheric spring and summer 1997, *Geophys. Res. Lett*., *25*, 2683-2686.

Ridley, B. A., et al. (2003), Ozone depletion events observed in the high latitude surface layer during the TOPSE aircraft program, *J. Geophys. Res*., *108*, 8356, doi:10.1029/2001JD001507.

Rivière, G. (2010), Role of Rossby wave breaking in the west Pacific teleconnection, *Geophys. Res. Lett*., 37, L11802, doi:10.1029/GL043309.

Rozanov, A., et al. (2011), BrO vertical distributions from SCIAMACHY limb measurements: comparison of algorithms and retrieval results, *Atmos. Meas. Tech*., *4*, 1319-1359, doi:10.5194/amt-4-1319-2011.

Sander, R., and P. J. Crutzen (1996), Model study indicating halogen activation and ozone destruction in polluted air masses transported to the sea, *J. Geophys. Res*., *101*, 9121-9138.

Sander, R., Y. Rudich, R. von Glasow, and P. J. Crutzen (1999), The role of $BrNO_3$ in marine tropospheric chemistry: A model study, *Geophys. Res. Lett.*, *26*(18), 2857-2860.

Sander, R., J. P. Burrows, and L. Kaleschke (2006), Carbonate precipita- tion in brine – a potential trigger for tropospheric ozone depletion events, *Atmos. Chem. Phys*., *6*, 4653–4658.

Schneider, D. P., E. J. Steig, and J. C. Comiso (2004), Recent climate variability in Antarctica from satellite-derived temperature data, *J. Clim*., *17*, 1569-1583.

Schnell, R. C. et al (1991), Decrease of summer tropospheric ozone concentrations in Antarctica, *Nature*, *351*, 726-729.

Schroeder, W. H., K. G. Anlauf, L. A. Barrie, J. Y. Lu, A. Steffen, D. R. Schneeberger, and T. Berg (1998), Arctic springtime depletion of mercury, *Nature*, *394*, 331-332.

Screen, J. A., and I. Simmonds (2012), Half-century air temperature change above Antarctica: Observed trends and spatial reconstructions, *J. Geophys. Res*., *117*, D16108.

Seabrook, J. A., J. Whiteway, R. M. Staebler, J. W. Bottenheim, L. Komguem, L. H. Gray, D. Barber, and M. Asplin (2011), LIDAR measurements of Arctic boundary layer ozone depletion events over the frozen Arctic Ocean, *J. Geophys. Res*., *116*, D00S02, doi:10.1029/2011JD016335.

Seabrook, J. A., J. A. Whiteway, L. H. Gray, R. Staebler, and A. Herber (2013), Airborne lidar measurements of surface ozone depletion over Arctic sea ice, *Atmos. Chem. Phys*., *13,* 6023-6029.

Seinfeld, J. H., and S. N. Pandis (1998), *Atmoshpheric chemistry and physics from air pollution to climate change*, *the first edition*, Wiley-interscience, USA, pp. 601-605.

Serreze, M. C., and A. P. Barrett (2011), Characteristics of the Beaufort sea high, J. *Clim*., *24*, 159-182.

Shaw, G. E. (1995), The arctic haze phenomenon, *Bull. Am. Meteorol. Soc.*, *76*, 2403-2414..

Shindell, D. T., and G. A. Schmidt (2004), Southern Hemisphere climate response to ozone changes and greenhouse gas increases, *Geophys. Res. Lett*., *31*, L18209.

Sigmond, M. and J. C. Fyfe (2010), Has the ozone hole contributed to increased Antarctic sea ice extent?, *Geophys. Res. Lett*., *37*, L18502.

Simpson, W. R., L. Alvarez-Aviles, T. A. Douglas, M. Sturn, and F. Domine (2005), Halogens in the coastal snow pack near Barrow, Alaska: Evidence for active bromine air-snow chemistry during springtime, *Geophys. Res. Lett*., *32*, L04811, doi:10.1029/2004GL021748.

Simpson, W. R., R. von Glasow, K. Riedel, P Anderson, P. Ariya, J. Bottenheim, J. Burrow, L. J. Carpenter, U. Frieß, M. E. Goodsite, D. Heard, M. Hutterli, H.-W. Jacobi, L. Kaleschke, B. Neff, J. Plane, U. Platt, A. Richter, H. Roscoe, R. Sander, P. Shepson, J. Sodeau, A. Steffen, T. Wagner, and E. Wolff (2007a), Halogens and their role in polar boundary-layer ozone depletion, *Atmos. Chem. Phys*., *7*, 4375-4418.

Simpson, W. R., D. Carlson, G. Hönninger, T. A. Douglas, M. Sturn, D. Perovich, and U. Platt (2007b), First-year sea-ice contact predicts bromine monoxide (BrO) levels at Barrow, Alaska better than potential frost flower contact, *Atmos. Chem. Phys*., *7*, 621-627.

Sinnhuber, B.-M., A. Rozanov, N. Sheode, O. T. Afe, A. Richter, M. Sinnhuber, F. Wittrock, and J. P. Burrows (2005), Global observations of stratospheric bromine monoxide from SCIAMACHY, *Geophys. Res. Lett*., *32*, L20810, doi:10.1029/2005GL023839.

Slusher, D. L., et al. (2002), Measurements of pernitric acid at the South Pole during ISCAT 2000, *Geophys. Res. Lett*., *29*(21), 2011, doi:10.1029/2002GL015703.

Solberg, S., N. Schmidbauer, A. Semb, and F. Stordal (1996), Boundary layer ozone depletion as seen in the Norwegian Arctic in spring, *J. Atmos. Chem*., *23*, 301-332.

Solomon, S., R. W. Portmann, T. Sasaki, D. J. Hofmann, and D. W. J. Thompson (2005), Four decades of ozonesonde measurements over Antarctica, *J. Geophys. Res*., *110*, D21311.

Solomon, S., D. Qin, M. Manning, Z. Chen, M. Marquis, K. Averyt, M. Tignor, and H. Miller (Eds.) (2007), *Climate Change 2007: The Physical Science Basis.*

Contribution of Working Group I to the Fourth Assessment Report of the Intergovernmental Panel on Climate Change, Cambridge Univ. Press, Cambridge, U. K.

Son, S.-W., N. F. Tandon, L. M. Polvani, and D. W. Waugh (2009), Ozone hole and southern hemisphere climate change, *Geophys. Res. Lett*., *36*, L15705.

Son, S-W., et al. (2010), Impact of stratospheric ozone on Southern Hemisphere circulation change: A multimodel assessment, *J. Geophys. Res*., *115*, D00M07.

Spicer, C. W., R. A. Plastridge, K. L. Foster, B. J. Finlayson-Pitts, J. W. Bottenheim, A. M. Grannas, and P. B. Shepson (2002), Molecular halogens before and during ozone depletion events in the Arctic at polar sunrise: concentrations and sources, *Atmos. Environ.*, *36*, 2721-2731.

Steffen, A., T. Douglas, M. Amyot, P. Ariya, K. Aspmo, T. Berg, J. Bottenheim, G. Brooks, F. Cobbett, A. Dastoor, A. Dommergue, R. Ebinghaus, C. Ferrari, K. Gardfeldt, M. E. Goodsite, D. Lean, A. J. Poulain, C. Scherz, H. Skov, J. Sommer, and C. Temme (2008), A synthesis of atmospheric mercury depletion event chemistry in the atmosphere and snow. *Atmos. Chem. Phys*., *8*, 1445-1482.

Steig, E. J., et al. (2009), Warming of the Antarctic ice-sheet surface since the 1957 International Geophysical Year, *Nature*, *457*, 459-462.

Streets, D. G., D. T. Shindell, Z. Lu, and G. Faluvegi (2013), Radiative forcing due to major aerosol emitting sectors in China and India, *Geophys. Res. Lett*., *40*, 4409-4414, doi:10.1002/grl.50805.

Strong, C., J. D. Fuentes, R. E. Davis, and J. W. Bottenheim (2002), Thermodynamic attributes of Arctic boundary layer ozone depletion, *Atmos. Environ*., *36*, 2641-2652.

Tackett, P. J., A. E. Cavender, A. D. Keil, P. B. Shepson, J. W. Bottenheim, S. Morin, J. Deary, A. Steffen, and C. Doerge (2007), A study of the vertical scale of halogen chemistry in the Arctic troposphere during Polar Sunrise at Barrow, Alaska, *J. Geophys. Res*., *112*, D07306, doi:10.1029/2006JD007785.

Tang, T., and J. C. McConnell (1996), Autocatalytic release of bromine from Arctic snow pack during polar sunrise, *Geophys. Res. Lett*., *23*(19), 2633-2636.

Tarasick, D. W. and J. W. Bottenheim (2002), Surface ozone depletion episodes in the Arctic and Antarctic from historical ozonesonde records, *Atmos. Chem. Phys*., *2*, 197-205.

Theys, N., M. Van Roozendael, F. Hendrick, X. Yang, I. De Smedt, A. Richter, M. Begoin, Q. Errera, P. V. Johnston, K. Kreher, and M. De Mazie`re (2011), Global observations of tropospheric BrO columns using GOME-2 satellite data, *Atmos. Chem. Phys*., *11*, 1791–1811, doi:10.5194/acp-11-1791-2011.

Thompson, D. W. J., and J. M. Wallace (1998), The Arctic oscillation signature in the wintertime geopotential height and temperature fields, *Geophys. Res. Lett*., *25*, 1297-1300.

Thompson, D. W. J. and S. Solomon (2002), Interpretation of recent Southern Hemisphere climate change, *Science*, *296*, 895–899.

Thompson, D. W. J., M. P. Baldwin, and S. Solomon (2005), Stratosphere–troposphere coupling in the Southern Hemisphere, *J. Atmos. Sci*., *62*, 708–715.

Thompson, D. W. J., S. Solomon, P. J. Kushner, M. H. England, K. M. Grise, and D. J. Karoly (2011), Signatures of the Antarctic ozone hole in Southern Hemisphere surface climate change, *Nature Geosci*., *4*, 741-749.

Thompson, A. M., S. J. Oltmans, D. W. Tarasick, P. Von der Gathen, H. G. J. Smit, and J. C. Witte (2011), Strategic ozone sounding networks: Review of design and accomplishments, *Atmos. Environ*., *45*, 2145-2163.

Toyota, K., J. C. McConnell, A. Lupu, L. Neary, C. A. McLinden, A. Richter, R. Kwok, K. Semeniuk, J. W. Kaminski, S.-L. Gong, J. Jarosz, M. P. Chipperfield, and C. E. Sioris (2011), Analysis of reactive bromine production and ozone depletion in the Arctic boundary layer using 3-D simulations with GEM-AQ: inference from synoptic-scale patterns, *Atmos. Chem. Phys*., *11*, 3949-3979.

Turner, J., et al. (2005), Antarctic climate change during the last 50 years, *Int. J. Climatol*., *25*, 279-294.

Turner, J., et al. (2009), Non-annular atmospheric circulation change induced by stratospheric ozone depletion and its role in the recent increase of Antarctic sea ice extent, *Geophys. Res. Lett*., *36*, L08502.

Vaughan, D. G., G. J. Marshall, W. M. Connolley, J. C. King, and R. Mulvaney (2001), Devil in the detail, *Science*, *293*, 1777-1779.

Vogt, R., P. J. Crutzen, and R. Sander (1996), A mechanism for halogen release from sea-salt aerosol in the remote marine boundary layer, *Nature*, *383*, 327-330.

Van Dam, B., D. Helmig, J. F. Burkhart, D. Obrist, and S. J. Oltmans (2013), Springtime boundary layer O3 and GEM depletion at Toolik Lake, Alaska, *J. Geophys. Res*., *118*, 3382–3391, doi:10.1002/jgrd.50213.

von Glasow, R., and P. J. Crutzen (2004), Model study of multiphase DMS oxidation with a focus on halogens, *Atmos. Chem. Phys*., *4*, 589-608.

Wallace, J. M., and D. S. Gutzler (1981), Teleconnections in the geopotential height field during the Northern Hemisphere winter, *Mon. Weather Rev*., *109*, 784-812.

Wang, T. X., M. D. Kelley, J. N. Cooper, R. C. Beckwith, and D. W. Margerum (1994), Equilibrium, Kinetic, and UV-spectral characteristics of aqueous bromine chloride, bromine, and chlorine species, *Inorg. Chem*., *33*, 5872-5878.

Wang, Y., B. Ridley, A. Fried, C. Cantrell, D. Davis, G. Chen, J. Snow, B. Heikes, R. Talbot, J. Dibb, F. Flocke, A. Weinheimer, N. Blake, D. Blake, R. Shetter, B. Lefer, E. Atlas, M. Coffey, J. Walega, and B. Wert (2003), Springtime photochemistry at northern mid and high latitudes, *J. Geophys. Res*., *108*, 8358.

Wang, Y., et al. (2008), Assessing the photochemical impact of snow NO_x emissions over Antarctica during ANTCI 2003, *Atmos. Environ*., *42*, 2849-2863.

Wennberg, P. (1999), Atmospheric chemistry: Bromine explosion, *Nature*, *397*, 299-301.

Xie, Z. Q., R. Sander, U. Pöschl, and F. Slemr (2008), Simulation of atmospheric mercury depletion events (AMDEs) during polar springtime using the MECCA box model, *Atmos. Chem. Phys*., *8*, 7165-7180.

Yang X, J. A. Pyle, and R. A. Cox (2008), Sea salt production and bromine release: Role of snow on sea ice, *Geophys. Res. Lett*., *35*, L16815, doi:10.1029/2008GL034536.

Yang, X., J. A. Pyle, R. A. Cox, N. Theys, and M. Van Roozendael (2010), Snow-sourced bromine and its implications for polar tropospheric ozone, *Atmos. Chem. Phys.*, *10*, 7763-7773.

Yeh, S.-W., B. P. Kirtman (2004), The North Pacific Oscillation-ENSO and internal atmospheric variability, *Geophys. Res. Lett*., *31*, L13206, doi:10.1029/2004GL019983.

Zhang, H., S. Wu, and Y. Wang (2013), Effects of stratospheric ozone recovery on tropospheric chemistry and air quality, *Atmos. Chem. Phys. Discuss*., *13*, 21427-21453.

Zhang, J. (2007), Increasing Antarctic sea ice under warming atmospheric and oceanic conditions, *J. Clim*., *20*, 2515–2529.

Zeng, G., O. Morgenstern, P. Braesicke, and J. A. Pyle (2010), Impact of stratospheric ozone recovery on tropospheric ozone and its budget, *Geophys. Res. Lett*., *37*, L09805.

Zeng, T., Y. Wang, K. Chance, E. V. Browell, B. A. Ridley, and E. L. Atlas (2003), Widespread persistent near-surface ozone depletion at northern high latitudes in spring, *Geophys. Res. Lett*., *30*, 2298, doi:10.1029/2003GL018587.

Zeng, T., Y. Wang, K. Chance, N. Blake, D. Blake, and B. Ridley (2006), Halogen-driven low-altitude O3 and hydrocarbon losses in spring at northern high latitudes, *J. Geophys. Res.*, *111*, D17313, doi:10.1029/2005JD006706.

Zhao, T. L., S. L. Gong, J. W. Bottenheim, J. C. McConnell, R. Sander, L. Kaleschke, A. Richter, A. Kergweg, K. Toyota, and L. A. Barrie (2008), A three-dimensional model study on the production of BrO and Arctic boundary layer ozone depletion, *J. Geophys. Res*., *113*, D24304, doi:10.1029/2008JD010631.

VITA

Ja-Ho Koo

Ja-Ho Koo was born in Daegu, South Korea. He received a B.S. in the Atmospheric Science and Chemistry from Yonsei University, Seoul, Korea in 2006 and a M.S. in the Atmospheric science from Yonsei University, Seoul Korea in 2008. After a half of year experience as a research associate in the Global Environmental Laboratory at Yonsei University, he came to Georgia Institute of Technology for the doctoral course in the School of Earth and Atmospheric Sciences. He used to enjoy listening to music all days and likes to swim, walk around his town, and do hiking during holidays.